

**IDENTIFICATION OF METAL-ORGANIC FRAMEWORK
MATERIALS FOR ADSORPTIVE SEPARATION OF THE RARE
GASES: APPLICABILITY OF IAST AND EFFECTS OF
INACCESSIBLE REGIONS**

A Thesis
Presented to
The Academic Faculty

By

Timothy Milner Van Heest

In Partial fulfillment
Of the Requirements for the Degree
Master of Science in Chemical and Biomolecular Engineering

Georgia Institute of Technology

May, 2012

Identification of Metal Organic Framework Materials for Adsorptive Separation of the
Rare Gases: Applicability of IAST and the Effect of Inaccessible Regions

Approved by:

Dr. David Sholl, Advisor
School of Chemical and Biomolecular
Engineering
Georgia Institute of Technology

Dr. Krista Walton
School of Chemical and Biomolecular
Engineering
Georgia Institute of Technology

Dr. Sankar Nair
School of Chemical and Biomolecular
Engineering
Georgia Institute of Technology

Dr. Peter Hesketh
School of Mechanical Engineering
Georgia Institute of Technology

Date Approved: March 15, 2011

PREFACE

Metal organic framework chemistry has taken the academic chemistry community by storm since they first debuted in 1998 at the hands of Omar Yaghi. Since that time, thousands of open framework MOFs have been synthesized. The properties of these MOFs range dramatically across the diverse set of synthesized materials, as do the prospective applications for these materials.

Still, there is not yet any economically viable application for these materials. Significant barriers to entry include difficulty in scaling synthesis and stability issues. Problems with scaling production are currently being addressed in other research programs, but the problem of stability can be approached from two directions. It is possible to either attempt to make a material more stable, or to find an application in which stability is not as much of an issue. Towards the second goal, I offer the opportunity of low temperature separations of the rare gases.

The rare gases, or noble gases, are known for their non reactive chemistry. Combining this with the low temperature conditions necessary for separations of these gases, and the conditions are ideal for sensitive materials.

In addition to its role as an entry point for MOFs into the world market, this separation is also of significant scientific value. The rare gases are excellent test case studies due to their simplicity. Any models which become inaccurate for the rare gases will be much more likely to fail for more chemically complex mixtures of gases and fluids. To understand the limits of our models in the general case, it is thus worthwhile to start with the rare gases to get an upper bound on the capabilities of our methods.

From all the research that has been performed, it certainly seems MOFs have a role to play in the future of advanced separation and advanced materials applications. Perhaps this thesis will convince the reader that low temperature rare gas separations are a good starting point for these applications.

ACKNOWLEDGEMENTS

I would like to thank my advisor, Professor David Sholl, for his patience and understanding as I sought direction in my research. Your drive, intelligence, and focus are truly inspiring. I would also like to thank our collaborators at Sandia National Laboratory for their discussion, input, and guidance, and my committee members for their time and guidance.

Fellow members of the Sholl group also deserve considerable thanks. I am especially appreciative of the conversations with Emmanuel Haldoupis and Dr. Taku Watanabe. MOF lunch was always something I looked forward to.

I would like to thank the engineers who pushed me toward advanced studies in the sciences, in particular my uncle Dr. Drew Hoffmann and my grandfather Jim Hoffmann. Your achievements and your wealth of knowledge are continual inspirations to me.

To my parents, I offer thanks for guidance and support. Thank you for guiding me towards a rewarding and challenging career, and thank you for your support of my difficult decision to leave graduate school early instead of staying to finish a doctorate. Most of all, thank you for guiding me toward a saving faith in Jesus Christ, in whom all of my best decisions and actions have their foundation.

Lastly, I thank my wife, Carley. Your understanding, patience, and trust have made all of this so much more enjoyable.

TABLE OF CONTENTS

PREFACE	iii
ACKNOWLEDGEMENTS	v
LIST OF TABLES	vii
LIST OF FIGURES	viii
LIST OF SYMBOLS AND ABBREVIATIONS	x
SUMMARY	xi
CHAPTER 1: INTRODUCTION	1
CHAPTER 2: COMPUTATIONAL METHODS	5
CHAPTER 3: RESULTS	8
3.1 Screening Procedure	8
3.2 Accessibility Analysis	14
3.3 Ideal Adsorbed Solution Theory (IAST)	20
3.4 Reverse Selectivity	30
3.5 Temperature Effects	38
CHAPTER 4: CONCLUSIONS	41
APPENDIX A: ACCESSIBILITY BOUNDS FOR FOUR NOBLE GASES	43
APPENDIX B: ADDITIONAL EVIDENCE FOR THE ACCURACY OF IAST	46
APPENDIX C: PARAMETERIZING THE SURFACE AREA CORRECTION	50
APPENDIX D: SCREENING DATA SUMMARY	51
APPENDIX E: BINARY GCMC DATA	54
APPENDIX F: PROOF IAST IS EXACT AT LOW LOADING	61
REFERENCES	63

LIST OF TABLES

Table 1	Lennard-Jones potential parameters for adsorbates.	7
Table 2	The six classes of candidate materials identified in the screening procedure.	14
Table 3	The 25 materials in which inaccessible regions could occur.	18
Table 4	The screening data for all 70 candidate structures	51
Table 5a	Data for GCMC isotherm calculations using a 50:50 binary mixture of Ar and Kr.	54
Table 5b	Data for GCMC isotherm calculations using a 50:50 binary mixture of Kr and Xe.	56
Table 5c	Data for GCMC isotherm calculations using a 50:50 binary mixture of Xe and Rn.	58

LIST OF FIGURES

Figure 1	Comparison of the diffusivities of noble gases in selected MOFs calculated using MD and TST using a value of $\nu = 1.3 \times 10^{10}$ Hz for TST.	10
Figure 2	Comparison of the diffusivities of noble gases in selected MOFs calculated using MD and TST using a value of $\nu = 3 \times 10^{10}$ Hz for TST.	11
Figure 3	Correlation between pore limiting diameter and the energy barrier for diffusion of Ar.	16
Figure 4	Maximum and minimum diameters estimated to prevent movement between material cavities for each of the four adsorbates.	17
Figure 5	The top materials for the Ar-Kr separation with selectivities calculated via IAST for equimolar bulk phase mixtures.	21
Figure 6	The top materials for the Kr-Xe separation with selectivities calculated via IAST for equimolar bulk phase mixtures.	22
Figure 7	The top materials for the Xe-Rn separation with selectivities calculated via IAST for equimolar bulk phase mixtures.	23
Figure 8a	Isotherms from both the binary GCMC simulation and the IAST calculation for an 80:20 mixture of Kr to Xe.	26
Figure 8b	Selectivity for Xe over Kr in an 80:20 mixture of Kr to Xe.	26
Figure 9	Single component isotherms for Kr and Xe in HKUST-1 and their Dual-site Langmuir isotherm fits obtained after constraining a correct fit in the low pressure limit.	27
Figure 10	Comparison of binary isotherm data generated by binary GCMC, traditional IAST with curve fitting, and IAST without curve fitting.	28
Figure 11	Comparison between IAST and binary GCMC values of selectivity for the 70 candidate materials at 5 fugacities.	29
Figure 12	The distribution of observed ratios of Henry's constants for Kr and Xe for the 3432 materials analyzed in our screening calculations.	31
Figure 13	Configuration in which the energy of interaction between an adsorbate and 6 carbon atoms is exactly enough to offset the unfavorable interaction energy between the adsorbate and the two closer framework	33

carbon atoms.

Figure 14	Correlation between accessible surface area ratios (the exact value is defined in the text) and selectivities for the Kr/Xe separation.	35
Figure 15	The selectivity for the Xe-Kr separation as a function of the fractal dimension in the size range between Kr and Xe.	36
Figure 16	The difference between interaction potential energy with a carbon atom for Kr and Xe and Rn and Xe.	37
Figure 17	Effect of temperature on the adsorptive selectivity for Kr/Xe on GUPJEG01 at low loading.	39
Figure 18	Effect of temperature on the adsorptive selectivity as a function of loading for Xe/Kr on YAPXIX.	40
Figure 19a	Correlation between pore limiting diameter and the energy barrier for diffusion for Ar.	43
Figure 19b	Correlation between pore limiting diameter and the energy barrier for diffusion for Kr.	44
Figure 19c	Correlation between pore limiting diameter and the energy barrier for diffusion for Xe.	44
Figure 19d	Correlation between pore limiting diameter and the energy barrier for diffusion for Rn.	45
Figure 20	Comparison between the Henry's constant calculated in the screening calculations and Henry's constants calculated by fitting single component isotherm data.	47
Figure 21	CDFs describing the probability of achieving IAST results with a given percent deviation from binary GCMC data.	48
Figure 22	Correlation between the number of IAST results and the difference between IAST and binary GCMC for three cases.	49
Figure 23	Correlation between the favorability measure and normalized surface area for the MOFs	50

LIST OF SYMBOLS AND ABBREVIATIONS

GCMC = grand canonical Monte Carlo

IAST = ideal adsorbed solution theory

MD = molecular dynamics

MOF = metal organic framework

ZIF = zeolitic imidazolate framework

SUMMARY

A collection of >3000 MOFs with experimentally confirmed structures were screened for performance in three binary separations: Ar/Kr, Kr/Xe, and Xe/Rn. 70 materials were selected for further analysis, and calculations were performed to account for inaccessible regions. Single component GCMC calculations were performed to parameterize IAST calculations on these 70 materials, and the curve fitting problem in IAST was discussed. IAST calculations were confirmed with extensive binary GCMC calculations. For each binary separation, materials were identified with predicted performance that surpasses the state of the art. “Reverse selective” materials, for which a smaller gas species is preferably adsorbed over a larger species, were explained on the basis of surface fractal geometry, computed via a corrected surface area calculation. The effect of temperature on separation performance was also examined.

CHAPTER 1: INTRODUCTION

The rare (or noble) gases have a variety of industrial applications in areas as diverse as lasers,¹ chemical analysis,² and medicine.³ The gases are most often produced via fractional distillation of air at cryogenic temperatures. While this method is an effective and mature technology, the high pressures and low temperatures required also make this approach expensive, resulting in noble gas prices that can rival precious metals on a mass basis.⁴ Opportunities to move the operation of this separation into a regime with higher temperatures and lower pressures have spurred research into alternative methods of separation.

Adsorptive separations of noble gases are one effective approach to these separations. Much of the literature concerning adsorptive separation of noble gases utilizes carbon molecular sieves (CMS) or zeolites as the adsorbate with noble gases used either as a proxy for understanding the behavior of more complex gas species or as a probe to investigate material properties. Studies utilizing noble gases in this way have examined adsorption kinetic selectivity,⁵ material characterization methodology,⁶ adsorption model analysis,⁷ and other topics.

A smaller body of work focuses on adsorptive separations of noble gases. These generally target either the removal of noble gases from nuclear off gas streams, or the purification of Xe for use as an anesthetic. Manukata *et al.*⁸ compared the performance of zeolite 5A with activated charcoal for the separation of Xe and Kr from N₂. They found that the presence of Xe, or the presence of large amounts of N₂, competitively inhibited the adsorption of Kr from mixtures involving all three gases. Similarly,

Ianovski *et al.*⁹ compared the adsorption of Kr and Xe on H-mordenite with adsorption on several carbon-based adsorbates, and found that the traditional carbon-based adsorbents slightly outperformed the H-mordenite. Underhill¹⁰ used the Dubinin-Radushkevich theory of adsorption in the design of activated charcoal adsorption beds for the separation of mixtures of Ar, Kr, and Xe, finding that the theory worked well for these gas species. Bazan *et al.*⁴ compared the efficacy of B3 activated carbon with zeolite molecular sieves 4AK and 13X-K2 for separation of Ar, Kr, O₂, and Xe at 303 K. Their results showed that in all cases Xe was the most strongly adsorbed species, as would be expected from the relative polarizability of these species.

In recent years, metal organic framework (MOF) materials have been considered as candidates for noble gas separations. The very high surface area of these materials¹¹ are an excellent fit for the physisorption processes that drive separations of the rare gases.¹² Thus far, attempts to develop industrially relevant applications for MOFs have been stymied by the poor stability of MOFs under industrially relevant conditions.¹³ Aside from the remarkably stable ZIF family of materials,¹⁴ a number of MOFs have been shown to be very sensitive to the presence of trace solvents (such as water) and high temperatures.¹⁵ Application of these materials to low or ambient temperature processes involving inert gases (i.e., industrial conditions for noble gas separation by adsorption) would provide a path forward through operating conditions that promote material stability.

The literature covering adsorptive separations of noble gases by MOFs is limited but promising. Mueller *et al.*^{13b} examined the gas storage capabilities of MOF-5 for Xe, Kr, and Ar, finding that the Xe was favored to a large extent over the other two gas species.

They also analyzed the MOF CuBTC, finding that the adsorption capacity of this material was almost twice as high as a popular CMS, and the gas molecule mobility inside this structure was two to three orders of magnitude higher than current CMSs and zeolites. Both of these properties make these materials good candidates for adsorptive separation via pressure swing or temperature swing processes.¹⁶ Greathouse *et al.*¹² used both static and flexible force field models in Grand Canonical Monte Carlo (GCMC) calculations to examine the adsorption and separation of noble gases by IRMOF-1. They found that at both low temperature and room temperature MOF structural flexibility did not have an appreciable effect on the amount of gas adsorbed. Also using GCMC, Ryan *et al.*¹⁷ examined eight MOFs for their performance in Xe/Kr separations, with the goal of identifying a viable candidate for Kr/Xe separations of nuclear off gas streams.¹⁸ By performing calculations with binary mixtures, they found that Pd-MOF is a good candidate for this separation, providing a predicted selectivity >18 for this separation for binary GCMC data at 0.01, 0.1, and 1 MPa. This is notably larger than the maximum selectivity of ~10 found by Bazan *et al.*⁴ for the same separation on CMS B3, or the selectivity of 4 for zeolite NaA found by Jameson *et al.*¹⁹ Most recently, Thallapally *et al.*²⁰ found that the metal organic framework NiDOBDC achieved an adsorption selectivity similar to activated carbon in experiments at room temperature. The authors hypothesized that the polarizability of the noble gas when interacting with the open metal sites of NiDOBDC was responsible for the increased selectivity of this material when compared with MOF-5.

In this paper, we build upon previous research into the potential of MOFs for noble gas separations. In particular, we examine adsorption of Ar, Kr, Xe, and Rn. We provide

a more extensive survey of the noble gas separation potential of known MOFs than has been presented in the literature thus far by screening a library of over 3000 materials whose synthesis has been reported previously. In Section 3.1 we explain the methods utilized in these screening results and highlight some interesting findings from these calculations. Section 3.2 addresses the issue of cavity accessibility in metal organic frameworks and its important effects on the accuracy of various calculation methods. In Section 3.3 we provide an extensive analysis of the accuracy of IAST for predictions of the efficacy of materials for separation of binary mixtures of noble gases in MOFs. Section 3.4 analyzes a phenomenon we call “reverse selectivity” and explains why it occurs, and how the concept of local fractal dimension can be used to quantify its importance. In Section 3.5 we discuss the effect of temperature on separation effectiveness, and in Chapter 4 we provide our conclusions.

CHAPTER 2: COMPUTATIONAL METHODS

In this work, Grand Canonical Monte Carlo (GCMC) simulations²¹ were performed to calculate both single and multi-component isotherm data for Ar, Kr, Xe, and Rn in each selected material. MOF frameworks were assumed to be rigid in their experimentally reported structures. Framework-adsorbate interactions were calculated using interpolation from a pre-computed grid with grid points spaced every 0.2 Å. Attempt probabilities for MC moves were 0.3 for canonical moves and 0.7 for insertion/deletion in single component isotherms, and 0.3 for canonical moves, 0.6 for insertion/deletion, and 0.1 for exchange moves in binary isotherms.

For single component isotherm calculations, 5 million equilibration steps and 5 million data production steps were used. To test for equilibration, several points on each isotherm were re-computed with 50 million equilibration steps and 50 million data production steps. The location of these points varied based on the characteristics of each individual isotherm. For cases where there was a greater than 5% difference in values, the isotherms were re-computed with the larger number of steps. As an additional check on convergence, the variance of the adsorbed amount during the production phase was recorded, and this was typically found to be less than 1% of the adsorbed amount. For cases where the variance was larger than 1%, values were re-computed using 500 million steps. In these cases, there was consistently less than a 2% difference in isotherm values at any point when comparing results at 50 million and 500 million steps. For binary calculations, the same procedure of incrementing the number of iterations to insure

convergence was followed, starting again at 50 million equilibration steps and 50 million data production steps.

Single component isotherms were computed for fugacities from 1×10^{-6} to 1×10^6 bar with data collection points evenly spaced, 7 per order of magnitude. This range of conditions was chosen primarily to probe the entire adsorption isotherm and to allow for accurate Ideal Adsorbed Solution Theory calculations, not because practical applications occur across this entire range. For some isotherms this range was extended lower or higher to capture the Henry's regime or the maximum loading regime for adsorption.

Diffusion of noble gases in MOFs was examined using molecular dynamics (MD) simulations²¹. All MD calculations were performed in the NVT ensemble using an Andersen thermostat at infinite dilution (i.e., ignoring adsorbate-adsorbate interactions) with 5 adsorbate molecules per unit cell. Starting configurations were initialized with 15 million Monte Carlo steps followed by 15 million MD steps. The step size used was 1 fs and the total simulation time for data collection was 20 ns per trajectory. Diffusivities were calculated by averaging the results of 20 independent trajectories. For both molecular dynamics and Monte Carlo calculations, all simulations were performed in a $2 \times 2 \times 2$ unit cell. All calculations were performed at 298 K unless otherwise specified. As mentioned above, MOF frameworks were assumed to be rigid throughout our calculations.

Both adsorbate-adsorbate and adsorbate-framework interactions were modeled with a 12-6 Lennard-Jones interaction potential. The adsorbate-adsorbate interaction parameters used are provided in Table 1. The values for Ar, Kr, and Xe were chosen from a single source²² for self-consistency. The values for Rn were from a separate

source.²³ The universal force field,²⁴ with Lorentz-Berthelot mixing rules,²⁵ was used to define framework-adsorbate interactions. These interaction potentials were also used in the screening procedures detailed below. In all calculations, the real-space cutoff for interactions was 17 Å.

Table 1: Lennard-Jones potential parameters for adsorbates.

Species	σ (Å)	ϵ (K)
Ar	3.405	120
Kr	3.69	170
Xe	4.10	211
Rn	4.17	300

CHAPTER 3: RESULTS

3.1 Screening Procedure

One goal of this work was to extend the analysis of the capabilities of MOFs for noble gas separations to a large number of materials for which synthetic routes already exist. We followed the methods of Haldoupis *et al.*²⁶ to develop a database of MOF materials from the Cambridge Structural Database (CSD).²⁷ This led to a collection of 3432 MOFs with well-defined crystal structures. This collection did not include MOFs that have a significant degree of disorder within their reported crystal structure or materials for which some atomic species were not defined in the reported structure. Solvent molecules were removed from each structure prior to use in our calculations. In the following subsections, first, the calculations performed on this set of materials are explained. Second, the decision process leading to material requirements is described and the results of the screening calculations are examined.

3.1.1 Screening Calculations

For each MOF considered, a set of screening calculations were performed to calculate several parameters including pore limiting diameters, Henry's constants, and diffusivity for each of the four adsorbate species. The pore limiting diameter (PLD) is defined as the minimum diameter along the largest interconnected path through a periodic material. This value is used to understand barriers to diffusion, and is calculated using van der Waals radii for the framework atoms in accordance with the procedure developed by Haldoupis *et al.*²⁶ Henry's constants were calculated via Monte Carlo integration using the method described by Goodbody *et al.*²⁸ Extensive comparisons with Henry's

constants calculated from the low loading regime of isotherms obtained from GCMC showed excellent agreement between the more efficient calculations based on direct MC integration.

Calculating diffusivities for all of the materials in the screening database via molecular dynamics would require a large computational effort. Nonetheless, estimates of the diffusivity were needed for the screening procedure. To meet this need, the method described by Haldoupis *et al.* for calculating energy barriers for spherical adsorbates in porous crystalline materials²⁶ was used in a transition state theory (TST) estimate of the diffusivity. This method gives

$$D_s = \frac{1}{2} \nu \ell^2 e^{-\Delta E/RT} \quad 1$$

where D_s is the self-diffusivity of the adsorbate in the MOF, ν is a vibrational frequency, ℓ is the hop length, ΔE is the energy barrier to diffusion, R is the gas constant, and T is the temperature. For simplicity in applying this result to a large number of materials, the hop length was estimated using the shortest dimension of each material's unit cell. The variable which is most uncertain in this equation is the vibrational frequency. To achieve a better estimate from TST, this value was fit by minimizing the error between the TST estimate and a collection of diffusivities calculated by MD. The MOFs used in this fitting procedure were identified in an early iteration of the screening process, and any MD diffusivities values less than 1×10^{-10} cm²/s were not considered in the fit because for diffusivities below this value a statistically significant number of inter-cage hop movements were not observed. The result of this fit is show in Figure 1. The vibrational constant used by Haldoupis *et al.* was 1×10^{12} Hz, while the value calculated via this fitting procedure is 1.3×10^{10} Hz.

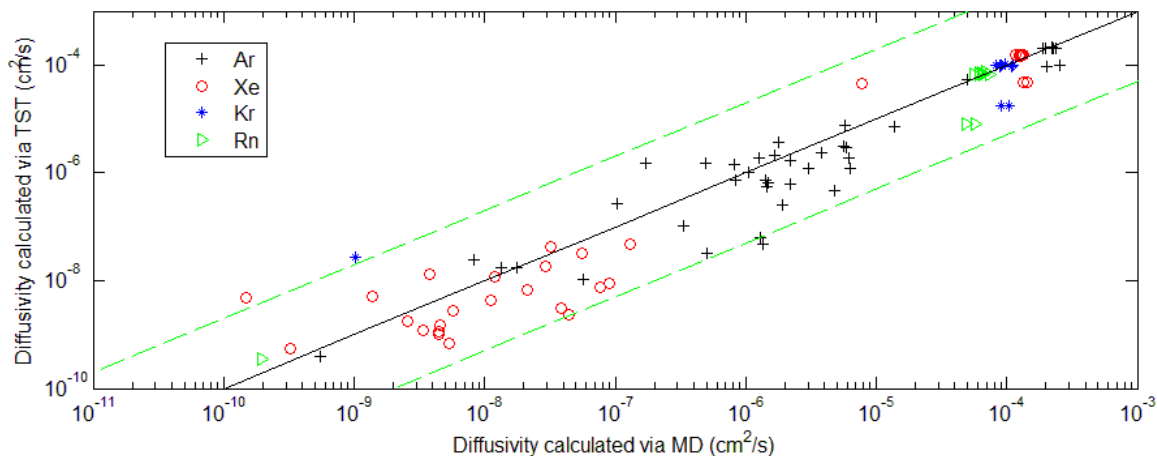


Figure 1: Comparison of the diffusivities of noble gases in selected MOFs calculated using MD and TST using a value of $\nu = 1.3 \times 10^{10}$ Hz for TST. The solid black line represents equivalence between the two values, and the green dashed lines are approximate upper and lower bounds on the fit added to guide the eye at $\nu = 2.6 \times 10^{11}$ Hz and 6.5×10^8 Hz.

Once a refined set of materials was identified by the screening approach defined below, we revisited the definition of the vibrational frequency in TST. To this end, MD calculations were performed on these materials, and the fitting of the TST vibrational frequency constant was repeated with the MD data for this final set of materials. Instead of 1.3×10^{10} Hz, the new data set better matched the MD data when a value of 3×10^{10} Hz was used. Figure 2 illustrates that the relationship between MD and TST data has considerably more scatter than the first data set used to obtain an estimate for the vibrational frequency constant. This is a result of the greater amount of structural variability in this set of materials compared to the first set used. Although the agreement between MD and TST is not excellent for either case, we found it to be sufficient for the purposes of the material screening to which it is applied.

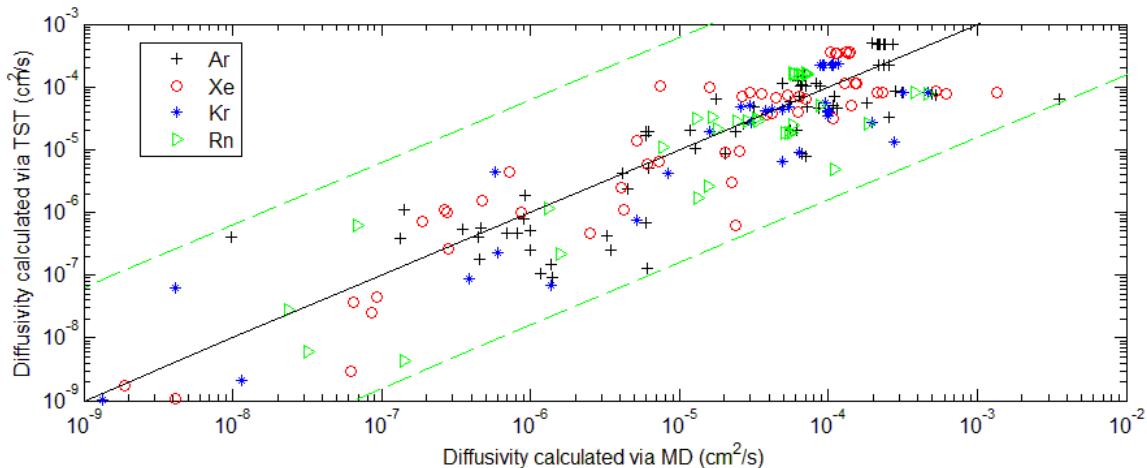


Figure 2: Comparison of the diffusivities of noble gases in selected MOFs calculated using MD and TST using a value of $\nu = 3 \times 10^{10}$ Hz for TST. The solid black line represents equivalence between the two values, and the green dashed lines are approximate upper and lower bounds on the fit added to guide the eye at $\nu = 1.9 \times 10^{12}$ Hz and 4.8×10^8 Hz.

3.1.2 Material Requirements

The targeted application of the MOFs in the screening set (i.e., the separation of noble gas pairs) guided the selection of a collection of requirements for prospective materials. First, because noble gases that are closest in size are the most difficult to separate, we only considered Ar/Kr, Kr/Xe, and Xe/Rn selectivity. Second, to be useful in separations the material must be highly selective for one rare gas over another. This selectivity for adsorptive separation is

$$S = \frac{x_1/x_2}{y_1/y_2} \quad 2$$

where x_i is the adsorbed phase mole fraction for adsorbate i , and y_i is the gas phase mole fraction for adsorbate i . In the limit of dilute adsorbate loadings, the selectivity reduces to the ratio of the Henry's constants for the adsorbates.²⁹

Since membrane applications for MOFs can potentially broaden the scope of separations that are possible beyond those based on adsorption alone,²⁹⁻³⁰ we also examined permselectivity as a predictor of membrane effectiveness. The permselectivity of species 1 over species 2 in a binary system is defined as³¹

$$\alpha_{perm, \frac{1}{2}} = q_1/q_2 \times D_1/D_2 \quad 3$$

where q_i is loading of adsorbate i in the membrane and D_i is the diffusivity of species i in the membrane. In the limit of zero adsorbate loading the ratio of the adsorbed amounts reduces to the ratio of the Henry's constants, and the diffusivities simplify to the self diffusivities,³² so in this limit

$$\alpha_{perm, \frac{1}{2}} = H_1/H_2 \times D_{s,1}/D_{s,2} \quad 4$$

where H_i is the Henry's constant for species i and $D_{s,i}$ is the self-diffusivity of species i . In our screening calculations, self diffusivities calculated via TST were used for all permselectivity estimates.

In membranes, high selectivity values can either be achieved kinetically (by one gas moving through the material much faster than another) or via adsorption (with one species adsorbing much more strongly than another), while in pure adsorption separations the diffusion matters much less. Still, it is worthwhile to consider diffusivity in materials for adsorptive separations. Thus an additional requirement for candidate materials for separations was that, regardless of the selectivity, to be useful, gas must be able to enter and leave the material at an appreciable rate. This requirement suggests that useful materials should be required to surpass lower bounds for the Henry's constants and

adsorbate diffusivities. The minimum Henry's constant was chosen to be 0.05 mmol/g-atm; this is slightly larger than the value for an ideal gas in an empty volume (0.0409 mmol/cm³-atm) when a framework density of 1 g/cm³ is assumed. To limit attention to materials allowing rapid diffusion, at least one adsorbing species was required to have a diffusivity larger than 1×10^{-8} cm²/s. This value was chosen because, as mentioned previously, it is difficult to accurately measure diffusivities lower than this with standard MD simulations. When estimating permselectivities, the diffusivity for species with a calculated diffusivity less than 1×10^{-10} cm²/s was increased to be equal to 1×10^{-10} cm²/s to avoid biasing our material selection towards materials with extraordinarily low diffusivities where framework flexibility could significantly impact the true diffusivity.

Once materials that met these minimum requirements had been identified, the large number of MOFs available were ranked in terms of their adsorption selectivity and permselectivity. The requirement for high kinetic or adsorption selectivity was handled by setting minimum values for the ratio of the Henry's constants (for adsorption selectivity) or the estimated permselectivity (for kinetic selectivity). These minimum values were modified for each separation case to identify the desired number of candidates for that case.

This full set of material requirements leads to six possible categories of candidate materials. Many of the candidates selected from the original set of 3432 materials fell into multiple categories. These categories are summarized in Table 2. A category for kinetic separations of Rn and Xe was not included, because no candidates meeting the requirements for diffusivity and Henry's constant were found with a predicted permselectivity greater than 10. The values for the "Other Criteria" were chosen to bias

towards candidates for adsorption-based separations. The value of 30 for the Henry's constant ratios was chosen because it yielded 50 candidate materials for each separation. The cutoffs for the permselectivities were chosen because they yielded 20 candidates each. The value of 5 for the case where Kr was favored over Xe was chosen because it yielded 5 candidate materials. In all, 70 distinct MOFs were found that met at least one of these six set of criteria. These criteria are summarized in Table 2, and the materials themselves are listed in Table 4 of Appendix D.

Table 2: The six classes of candidate materials identified in the screening procedure.

Class	Separation	Kinetic requirement	Adsorption requirement	Other criteria
1	Kr/Ar adsorption	$D_{Kr} > 1 \times 10^{-8} \text{ cm}^2/\text{s}$	$H_{Kr} > 0.05 \text{ mmol/g-atm}$	$H_{Kr}/H_{Ar} > 30$
2	Xe/Kr adsorption	$D_{Xe} > 1 \times 10^{-8} \text{ cm}^2/\text{s}$	$H_{Xe} > 0.05 \text{ mmol/g-atm}$	$H_{Xe}/H_{Kr} > 30$
3	Rn/Xe adsorption	$D_{Rn} > 1 \times 10^{-8} \text{ cm}^2/\text{s}$	$H_{Rn} > 0.05 \text{ mmol/g-atm}$	$H_{Rn}/H_{Xe} > 30$
4	Ar/Kr kinetic	$D_{Ar} > 1 \times 10^{-8} \text{ cm}^2/\text{s}$	$H_{Ar} > 0.05 \text{ mmol/g-atm}$	$P_{Ar}/P_{Kr} > 180$
5	Kr/Xe kinetic	$D_{Kr} > 1 \times 10^{-8} \text{ cm}^2/\text{s}$	$H_{Kr} > 0.05 \text{ mmol/g-atm}$	$P_{Kr}/P_{Xe} > 410$
6	Kr/Xe adsorption	$D_{Kr} > 1 \times 10^{-8} \text{ cm}^2/\text{s}$	$H_{Kr} > 0.05 \text{ mmol/g-atm}$	$H_{Kr}/H_{Xe} > 5$

3.2 Accessibility Analysis

In the pore structure of MOFs, channels of various sizes connect cavities which also vary in size. In some structures, a cavity may be large enough to contain an adsorbate, but the channel connecting that cavity to the rest of the structure is too small to allow the adsorbate to move into the cavity. In these cases, treating all regions of the structure as equally accessible (as during a typical GCMC simulation) gives a qualitatively incorrect picture of adsorption in the material. This issue has been described previously in simulations of zeolites.³³

To ensure that these adsorbates are not allowed to access these regions during GCMC simulations, a computational tool was developed to analyze the size of each pore leading to each cavity of a structure (henceforth, sub-pores). If a sub-pore diameter (i.e., the smallest diameter in a pore leading to a cavity) is smaller than the pore limiting diameter of the entire structure, that cavity is identified as possibly inaccessible. Of the 70 materials identified as described above, 25 were found to contain regions matching this description.

By correlating pore limiting diameters (PLDs) to diffusion energy barriers for each of the 3432 MOFs examined it was possible to approximate the energy barrier resulting from a given sub-pore diameter. The activation energy for Ar diffusion in these 3432 MOFs is shown as a function of the PLD in Figure 3. Similar figures for the remaining three adsorbates are provided in Figures 19a-d in Appendix A. As illustrated in Figure 3, this data makes it possible to identify an upper and lower bound on the PLD values that lead to a diffusion activation energy of 100 kJ/mol. We assumed that a 100 kJ/mol energy barrier would restrict passage of adsorbate molecules through a pore to a rate where cavities accessed through such a pore are effectively inaccessible. This rather high value was selected because of recent studies of flexibility effects in ZIF-8³⁴ which indicate that intra-molecular motion of the framework atoms may significantly reduce barriers for diffusing species in some MOFs. In Figure 3, a small number of outliers exist that are associated with small energy barriers in pores that are small but are energetically smooth. These points were ignored when determining bounds.

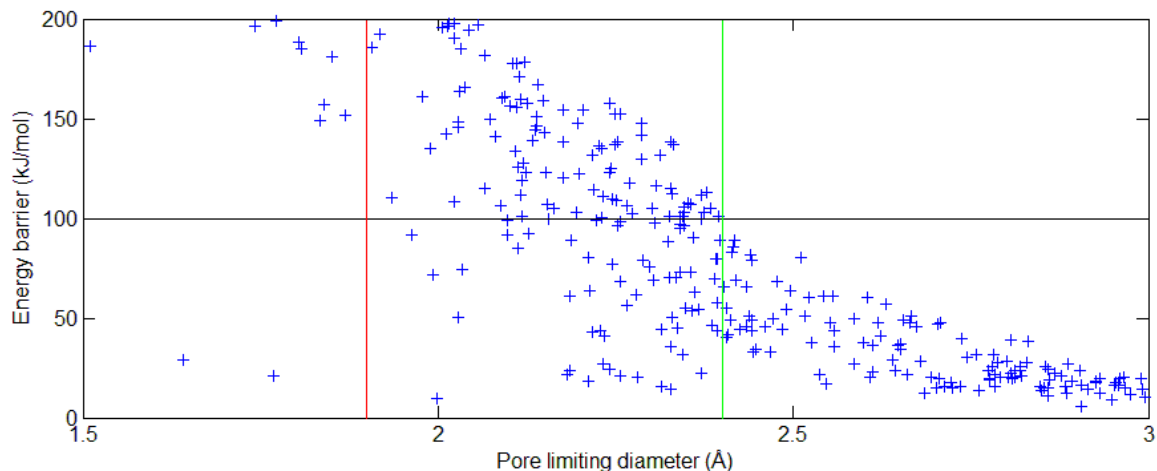


Figure 3: Correlation between pore limiting diameter and the energy barrier for diffusion of Ar. Red and green lines provide upper and lower bounds, respectively, for the size of a pore yielding a 100 kJ/mol barrier.

A summary of this analysis for all four adsorbates is shown in Figure 4. For each adsorbate, there is a ~ 0.5 Å gap between the smallest estimated accessible pore (the lower bound illustrated in Figure 3) and largest estimated inaccessible pore (the upper bound illustrated in Figure 3). As expected, the minimum size of the PLD required to allow access to a material cavity increases with the size of the adsorbate.

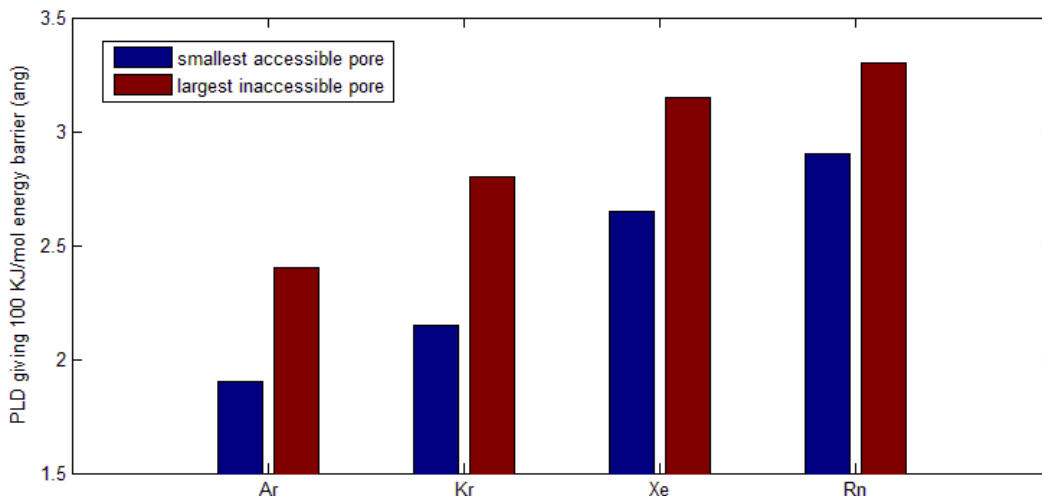


Figure 4: Maximum and minimum diameters estimated to prevent movement between material cavities for each of the four adsorbates examined.

This data was used by comparing the sub-pore diameter for each sub-cavity to the values shown in Figure 4. If the diameter was smaller than the smallest accessible pore, the associated sub-cavity was classified as inaccessible. If the diameter was larger than the largest inaccessible pore, the sub-cavity was classified as accessible. If the diameter fell between these two values, it was classified as ambiguous. For the purpose of our study, these ambiguous diameters were also defined as accessible to simplify analysis. Table 3 provides the results of this analysis for the 25 materials determined to have possible inaccessible regions. The sub-pore limiting diameters in this table that are <0.5 Å were rounded down to 0. The accessibility code for each adsorbate uses 1 to indicate all sub-cavities are inaccessible, 2 to indicate all sub-cavities are accessible, 3 to indicate accessibility is ambiguous for all sub-cavities, and 4 for materials with sub-cavities which fall into different classifications. Materials for which all cavities are accessible (blocked)

for all four adsorbates are denoted open (blocked), while materials that give different results for different adsorbates are denoted mixed.

Table 3: The 25 materials in which inaccessible regions could occur. An explanation of the meaning of each column is provided in the text.

REFCODE	Radii of inaccessible regions	Accessibility code				Summary
		Ar	Kr	Xe	Rd	
CAZGIT	3.38	2	2	2	2	Open
GIYSAJ	3.12 / 2.92	2	2	3	3	Open
HEGNAJ	3.99 / 4.19 / 4.39 / 3.79	2	2	2	2	Open
HEGNIR	4.33 / 4.13	2	2	2	2	Open
HEGNOX	4.33	2	2	2	2	Open
HEGNUD	4.19 / 3.99 / 4.39 / 3.79	2	2	2	2	Open
HEGPAL	4.40 / 4.20 / 4.00	2	2	2	2	Open
HITYEP	1.15	1	1	1	1	Blocked
KAHMOW	2.89	2	2	3	1	Mix
KAHQUG	0 / 1.11	1	1	1	1	Blocked
KAHRAN	1.02	1	1	1	1	Blocked
KAHSES	0	1	1	1	1	Blocked
KAHSIW	0	1	1	1	1	Blocked
KAHSOC	1.09	1	1	1	1	Blocked
KAHSUI	1.07	1	1	1	1	Blocked
MIKJAR	4.43 / 4.03 / 4.23 / 3.83	2	2	2	2	Open
MOXNUJ	2.77 / 2.97	2	4	3	4	Mix
NAJVUQ	0	1	1	1	1	Blocked
ODOXEK	1.44	1	1	1	1	Blocked
PAZBOH	0	1	1	1	1	Blocked
PAZBUN	0	1	1	1	1	Blocked
WOCVUG	2.66	2	3	3	1	Mix
XALDIY	1.68	1	1	1	1	Blocked
XEQNIQ	0	1	1	1	1	Blocked
YAPXIX	2.88	2	2	3	1	Mix

Of the 25 materials identified to have possible inaccessible regions, 8 (13) were determined to be open (blocked). The four remaining materials present the interesting case of the sub-cavities only being accessible to some of the adsorbates. The materials with CSD (Cambridge Structural Database)²⁷ reference codes KAHMOW, YAPXIX, MOXNUJ, and WOCVUG have all sub-cavities defined as accessible to every adsorbate except Rn. The material MOXNUJ is a particularly interesting case. In this material there were two systems of sub-pores of different sizes, one with a diameter of 2.77 Å, and one with a diameter of 2.97 Å. Both of these systems were accessible to Ar. For Kr, one of the systems of cavities was accessible while the other was ambiguous, so in our analysis the entire structure was defined as accessible. For Xe, both systems of sub-cavities were ambiguous, so the entire structure was again defined as accessible. For Rn, one of the systems was ambiguous while the other was inaccessible. For this case we broke from our previous convention of defining ambiguous regions as accessible and instead defined both systems of cavities inaccessible. This choice was made to simplify our analysis. To completely resolve complex situations like this one, a detailed analysis of the hopping rates between cavities that accurately incorporated the effect of framework flexibility would be required, a task that is beyond the scope of our current work.

To perform GCMC calculations for a material that includes blocked regions, the adsorbate-framework interaction potential energy was set to a large positive value for all locations within each blocked region. Test calculations showed that calculations that neglected pore blocking overestimated Henry's constants by factors as large as several orders of magnitude (see Figure 20). This problem was noted for several materials found through the screening calculation, and several of these materials identified as excellent

candidates were later determined to be poor to average performers once blocked regions were taken into account. Still, these materials were kept in the analyzed set of candidates for the sake of completeness. In what follows, all GCMC results presented use region blocking to define accessibility.

3.3 Ideal Adsorbed Solution Theory (IAST)

Although single component isotherms are valuable for an initial consideration of a material's potential for adsorptive separation applications, binary isotherm data is essential for fully evaluating a material. Ideal adsorbed solution theory (IAST)³⁵ is a useful approach to make predictions about binary adsorption using only single component isotherms. Many examples of applying IAST to MOFs exist in the literature, and the agreement between experimental and computational binary isotherm data and IAST predictions has been excellent for most cases.³⁶ To gain further insight into the separation potential of the 70 materials identified, IAST was used to predict adsorption selectivities for binary mixtures of Ar/Kr, Kr/Xe, and Xe/Rd.

Figures 5 through 7 illustrate the selectivities calculated at 298 K for the top candidate materials for each separation. Values were calculated at five different total fugacities for the gas phase and three different mole fractions for the first component in the gas phase ($y = 0.01, 0.5, \text{ and } 0.99$). Only the data for equimolar gas mixtures ($y = 0.50$) is displayed here because it was found that the selectivities were insensitive to the gas phase mole fractions. The selectivities shown in these plots are the larger of either the selectivity for species 1 over species 2 or the selectivity for species 2 over species 1. The larger of these values is displayed to ease comparison of performance across materials. The top candidates for each separation were identified by ranking the

materials by the average of their selectivities for the fifteen conditions examined (five fugacities with three molar concentrations each).

Figure 5 shows the top candidate materials found for the adsorptive separation of Ar and Kr. All of the 16 materials shown in this figure adsorb Kr more strongly than Ar. The strongest separation observed was at a fugacity of 0.01 bar for the MOF with CSD reference code ECAVIO with a selectivity of 22.

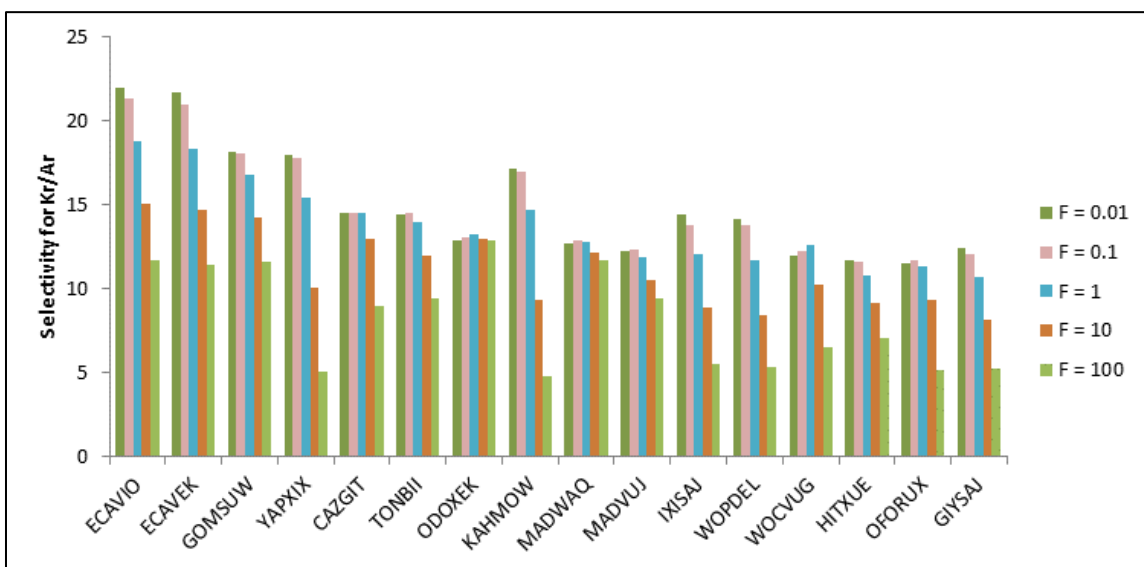


Figure 5: The top materials for the Ar-Kr separation with selectivities calculated via IAST for equimolar bulk phase mixtures. Materials are identified by their Refcodes.

Figure 6 shows the top candidate materials found for the adsorption separation of Kr and Xe. Of the 19 materials shown, 13 adsorbed Kr more strongly than Xe, while 6 adsorbed Xe more strongly than Kr. This behavior of adsorbing the smaller over the larger species was unexpected, and the reason for this is examined in more detail in Section 3.5. The strongest separation observed was at 0.1 bar for the MOF with CSD reference code GUPJEG01 with a selectivity of 12,500.

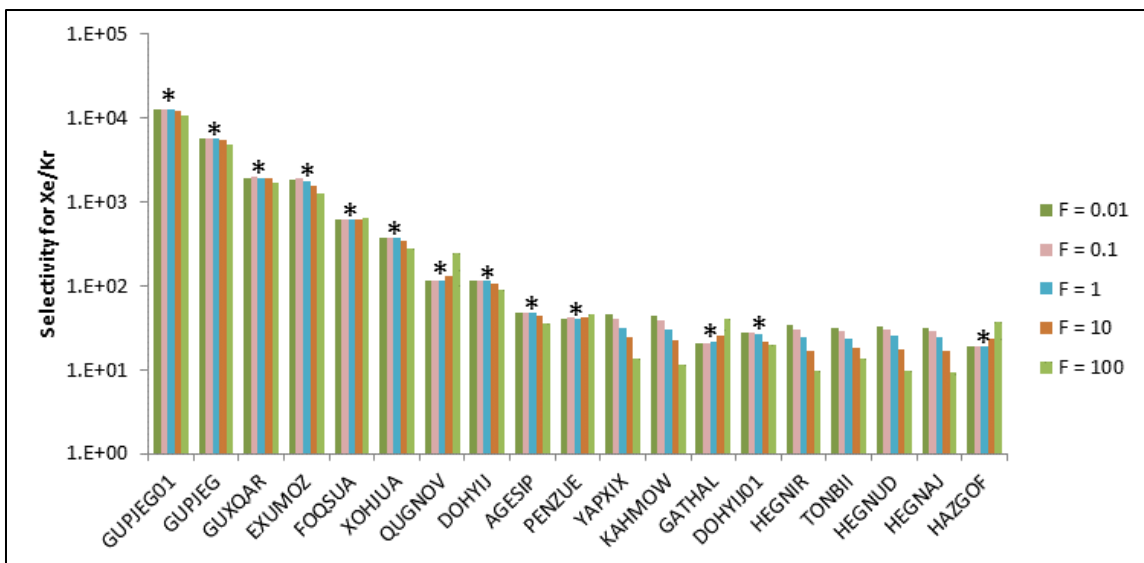


Figure 6: The top materials for the Kr-Xe separation with selectivities calculated via IAST for equimolar bulk phase mixtures. Stars indicate materials that exhibit reverse selectivity, that is, preferential adsorption of Kr relative to Xe.

Figure 7 shows the top candidate materials found for adsorption separation of Xe and Rn. Of the 18 materials shown, only 2 adsorbed Xe more strongly than Rn, however, these were the top two candidates. For these two structures, Rn was excluded from parts of the material that were accessible to the other four gas species. The strongest separation observed was at 0.1 bar for the MOF with CSD reference code YAPXIX with a selectivity of nearly 4 million. Among the materials that adsorbed Rn preferentially, the largest selectivity was for ECAVEK with a value of 46.67.

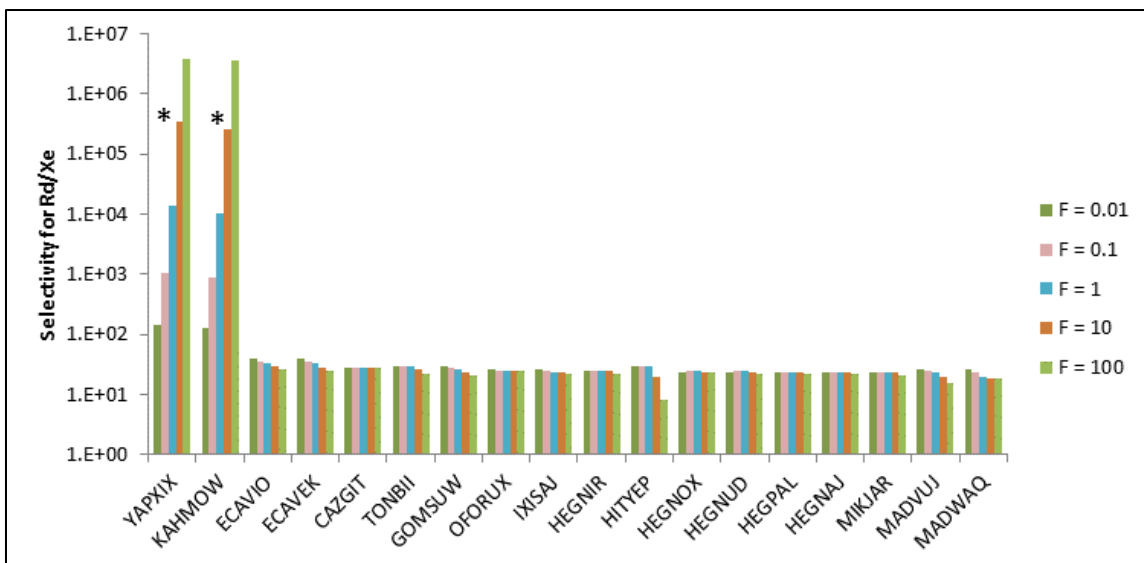


Figure 7: The top materials for the Xe-Rn separation with selectivities calculated via IAST for equimolar bulk phase mixtures. Stars indicate materials that exhibit reverse selectivity, that is, preferential adsorption of Xe relative to Rn.

3.3.1 Comparison to previous results

As mentioned above, several previous studies have elaborated on the applicability of IAST to computing binary isotherms in MOFs for simple gas mixtures,^{36a, 36c, 36e, f, 36h} with most finding excellent agreement between IAST predictions and binary GCMC calculations. However, recently Ryan *et al.*¹⁷ analyzed several MOFs for their performance in the Kr/Xe separation and found that for one common MOF, HKUST-1 (CuBTC), binary isotherm results were poorly predicted by IAST. The agreement between IAST and binary isotherms was particularly poor in the low loading regime of the isotherms. The rationale given for this effect was the failure of IAST to capture competitive adsorption in small pockets of the pore structure. If this observation is correct, it implies that IAST cannot be used to when highly competitive adsorption exists. This problem is particularly acute for our application as these cases are the most

interesting when looking for a material for adsorptive separations. We show below, however, that the failure of IAST in the calculations of Ryan *et al.* stemmed not from the precision of IAST for the system of interest, but rather from a subtle problem in the curve fitting used in their analysis.

The pitfalls associated with curve fitting in the application of IAST have been discussed elsewhere.³⁷ Not surprisingly, if the fitted single-component isotherms used in IAST do not precisely represent the isotherms, then the resulting IAST predictions can be inaccurate. In the limit of infinite dilution, molecules of any adsorbing species experience no adsorbate-adsorbate interactions. As a result, the Henry's constant for adsorption of a species is identical in both single component and binary adsorption, provided both species in the binary mixture are in the Henry's law limit. Thus, the adsorption selectivity in this limit can be defined without invoking IAST or any other approximation: it is exactly the ratio of the single component Henry's constants.³⁸ If the fitted single component isotherms used in an IAST calculation do not correctly reproduce the Henry's law limit, the selectivity predicted by IAST in the limit of low pressures will also be incorrect.

The example that Ryan *et al.* examined was Kr and Xe in HKUST-1. In their analysis of selectivity as a function of pressure, they found IAST predicted that HKUST-1 was selective for Kr at low pressures, while binary simulations showed the opposite low pressure selectivity, with the material demonstrating a strong preference for Xe at low pressures. In contrast, Figures 8a and 8b show that our IAST calculations are consistent with our binary GCMC calculations, and that our binary GCMC calculations are consistent with those of Ryan *et al.* We found that as long as the single component

isotherm data was extended to include the Henry's Law regime for both adsorbates, then IAST predictions were accurate for this system in the low pressure limit. It appears that the unusual inaccuracy of IAST described by Ryan *et al.* for this system was associated with incomplete fitting of their single component data, not any unusual physical property of the MOF. Figures 8a and 8b summarize these findings for this system. Both figures show the excellent agreement between IAST and binary GCMC data, and the second also compares IAST results to ideal selectivity. The ideal selectivity is the ratio of amounts adsorbed at the same fugacity value from single component isotherms. It is clear that IAST provides a significant improvement over ideal selectivity as a predictor for binary selectivity.

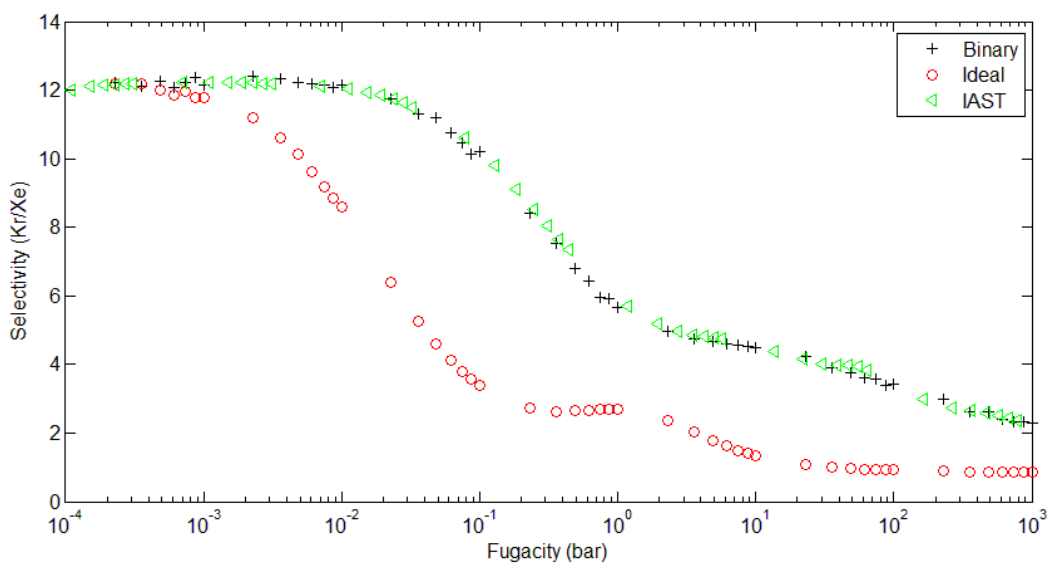
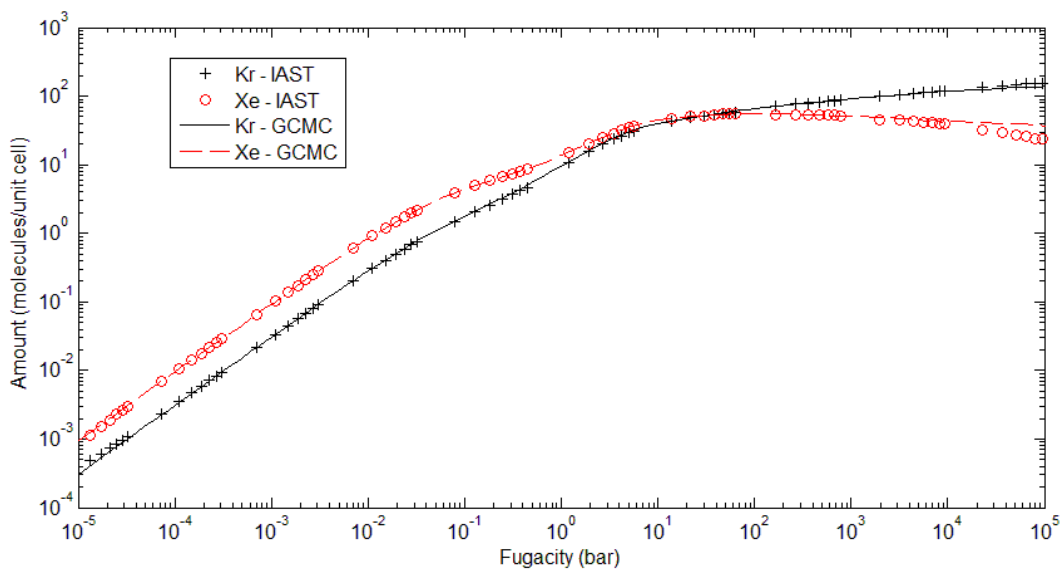


Figure 8: a) Isotherms from both the binary GCMC simulation and the IAST calculation for an 80:20 mixture of Kr to Xe. b) Selectivity for Xe over Kr in an 80:20 mixture of Kr to Xe. Ideal selectivity (the ratio of amounts adsorbed at the same fugacity value from single component isotherms) is shown along with binary (from binary GCMC) and IAST selectivity.

3.3.2 IAST without curve fitting

Obtaining an accurate fit to the single component isotherms is critical to obtaining good IAST results. Again examining the case of Kr and Xe in HKUST-1, Figure 9 illustrates the best fit obtained to single component isotherm data. Dual-site Langmuir (DSL) models were used for the isotherms and the fit to these equations were constrained to produce the correct Henry's constant. The remaining 3 degrees of freedom were optimized through an iterative procedure coupling Monte Carlo optimization with an enhanced Newton's method solver.³⁹ Despite taking careful steps to optimize this fit, the fitted equations leave much to be desired.

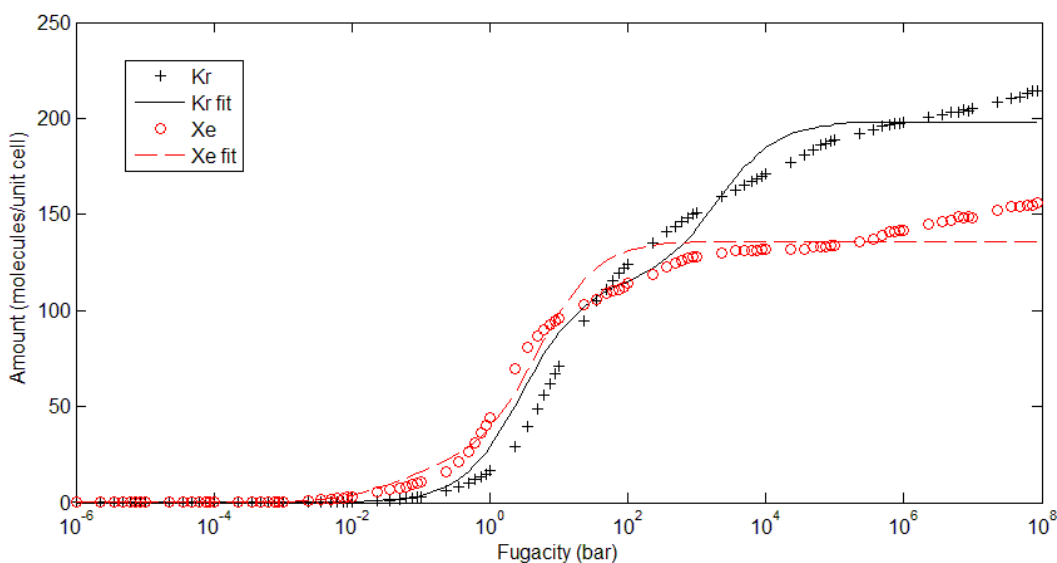


Figure 9: Single component isotherms for Kr and Xe in HKUST-1 and their Dual-site Langmuir isotherm fits obtained after constraining a correct fit in the low pressure limit.

To sidestep these problems in curve fitting, for all of the IAST calculations presented here the integrals that must be calculated to apply IAST³⁵ were performed using a simple trapezoidal-rule integration technique on the isotherm data itself.³⁹

Because of the quality of our GCMC data and the fact that it spans a broad range of loadings, this method gave very good results when compared to binary GCMC data. Figure 10 compares the result of performing IAST calculations with traditional curve fitting and with the numerical integration technique for the case of Xe and Kr in HKUST-1. The calculation that forgoes curve fitting provides a much improved agreement with binary GCMC calculations. With the use of this simplified method, IAST can be applied to a wide variety of systems while avoiding curve fitting errors. This method was used for all IAST calculations presented in this work unless otherwise noted.

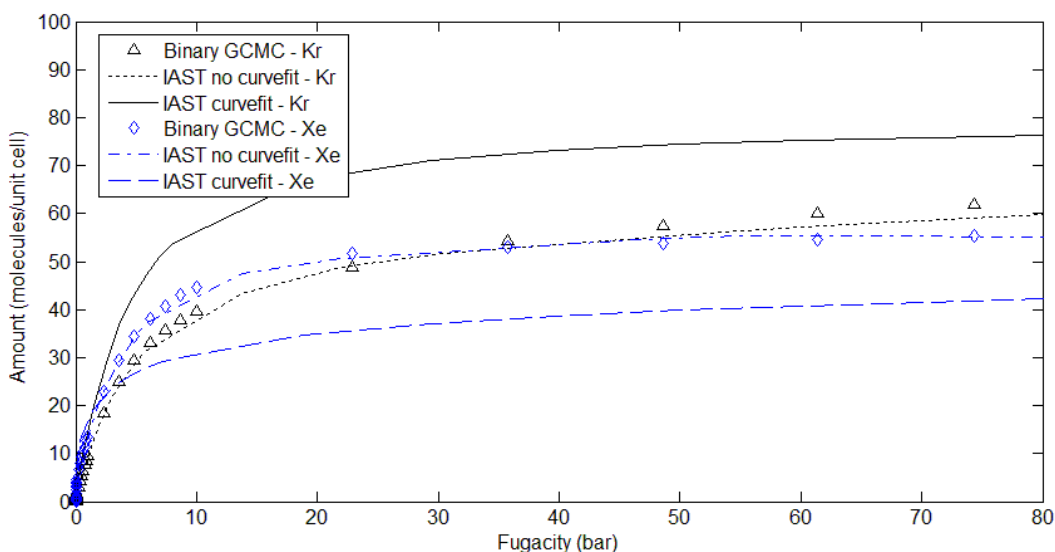


Figure 10: Comparison of binary isotherm data generated by binary GCMC, traditional IAST with curve fitting, and IAST without curve fitting.

3.3.3 Large scale comparison of IAST to binary data

To further quantify the applicability of IAST to adsorption of noble gases in MOFs, binary calculations were performed for each gas pair (i.e., Ar/Kr, Kr/Xe, and Xe/Rn) in each of the 70 materials examined. Binary calculations were performed with

an 80:20 mixture, with the larger portion of the mixture consisting of the smaller of the two species. Calculations were performed at 5 state points, with fugacity ranging from 0.01 to 100 bar. Convergence at each pressure point was confirmed by increasing the number of iterations used until the calculated values stopped changing. Figure 11 compares these binary calculations with IAST calculations performed using the IAST-without-curve-fitting method described above.

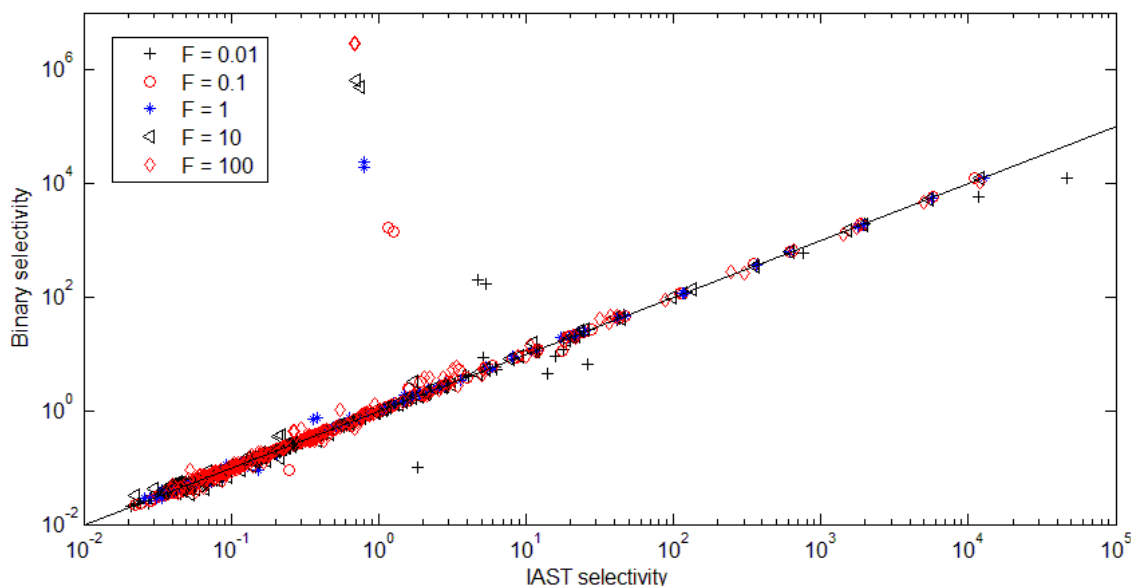


Figure 11: Comparison between IAST and binary GCMC values of selectivity for the 70 candidate materials at 5 fugacities (F). The fugacities range from 0.01 to 100 bar.

Figure 11 illustrates that the agreement between IAST calculations and binary results are generally very good for the materials tested. There are a few cases, however, where the deviation with binary data is very significant. Similar to the differences in Henry's constants calculated by GCMC and direct integral Monte Carlo illustrated in Figure 20, the differences between IAST and binary selectivities shown here can be explained due to

the way inaccessible regions are handled. All cases where there is a large deviation between IAST and binary data involve blocked regions. More specifically, all these cases involve a case where a region is blocked to just 1 of the 2 materials involved in the separation (those materials identified as type “mix” in Table 3). In these cases, unsurprisingly, IAST fails to accurately predict selectivity. In principle, this limitation of IAST can be overcome by using an approach that applies IAST separately to distinct volumes within the material,⁴⁰ but we have not performed calculations of this kind. If these “mixed type” materials are excluded from consideration, over 90% (97%) of the examples we examined showed a deviation of less than 10% (30%) between the IAST-predicted selectivity and the selectivity determined from binary GCMC.

3.4 Reverse selectivity

During screening calculations, we found that many MOFs had a higher Henry’s constant for a smaller gas species than for a larger species, a phenomenon that can be termed “reverse selectivity”. This was surprising, since the strength of a van der Waals interaction generally scales with the size of an adsorbate. This is illustrated in Figure 12, which shows the distribution of the ratios of Henry’s constants for Kr and Xe for all of the 3432 MOFs we considered. As mentioned previously, in the limit of dilute loading this ratio is equal to the adsorption selectivity for a binary mixture. In Figure 12, this ratio is defined so that it is larger than 1 for all materials. Specifically, for normally selective materials (blue bars), the Henry’s constant ratio is defined as H_{Xe}/H_{Kr} , while for the reverse selective materials case (red bars) it is defined as H_{Kr}/H_{Xe} . Figure 12 shows that, for the case of Kr and Xe, reverse selectivity is quite common, and also that the reverse selective MOFs display some of the highest predicted selectivities for adsorptive

separations. This figure was produced using screening calculation data where blocked regions were not considered, thus the trivial cases in which regions of a material are physically blocked from one of two materials is not considered here.

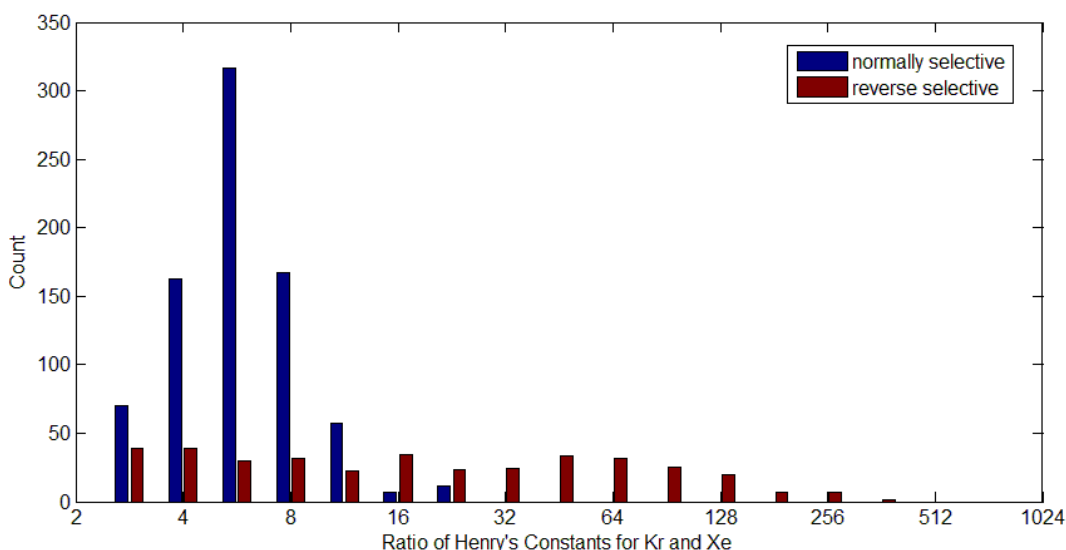


Figure 12: The distribution of observed ratios of Henry's constants for Kr and Xe for the 3432 materials analyzed in our screening calculations. The convention used to define this ratio is described in the text.

We hypothesized that in these “reverse selective” materials the mechanism for the reverse selectivity was a lack of accessible surface for adsorption for the larger species. To test this assumption, surface area calculations were performed on the set of 70 candidate materials found from the screening calculations using a slightly modified version of the method developed by Düren *et al.*⁴¹ In this method, the surface area is calculated by “rolling” a spherical probe molecule over the surface of a material. The resulting surface area is a function of the size of the probe molecule. In many cases, the size of the probe molecule is chosen to be close to the size of nitrogen, so resulting

surface areas can be compared with results from BET analysis of experimental data.⁴² In our application, however, a different probe size was used to calculate the effective surface area for each adsorbate. This results in four values of the surface area for each material. We also quantified the favorability of interaction for each MOF-adsorbate pair using the ratio of the Henry's constant to the effective Henry's constant for an ideal gas in an empty box. Values of this ratio greater than 1 indicate that adsorption in the MOF framework is favorable (i.e., more favorable than adsorption in an empty box).

Initially, surface areas were calculated using a probe size equal to σ from the adsorbate-adsorbate Lennard-Jones potentials. With this definition, 48 of the 288 MOF-adsorbate pairs examined gave a calculated surface area of zero, even though a favorable MOF-adsorbate interaction was observed. Because framework atom sizes are defined by their Lennard-Jones σ parameters, using this value for the probe molecule corresponds to rolling the probe molecule over a surface where the interaction energy with the closest framework atom is always zero. While this assures a favorable interaction at all points on the surface, this method does not include sites where interaction with the closest framework atom is unfavorable but interactions with other nearby framework atoms are favorable, resulting in a net interaction that is energetically favorable.

To represent the regions with net favorable interactions more reliably, we developed an adjusted definition of the probe size of each adsorbate. This correction was applied by first considering the magnitude of the energy of favorable interactions. We found that using a value that accounts for the energy of six strongly favorable interactions between the adsorbate and framework carbon atoms works well. More information justifying this choice is given in Appendix C. Assuming, as we did in our calculations,

standard mixing rules for the Lennard-Jones interactions between adsorbates and the MOF atoms, this energy is

$$E = 6\varepsilon_{mix} = 6\sqrt{\varepsilon_{adsorbate}\varepsilon_{carbon}} \quad 5$$

The corrected probe molecule size was then calculated by computing the distance at which the unfavorable interaction with two framework carbon atoms completely offsets this favorable contribution. This scenario is illustrated in Figure 13. The interaction is with two carbon atoms because the probe molecule is rolled on a surface (at a fixed distance from framework atoms), and overlap with a second framework atom is checked to determine if a “rolling move” is valid.⁴¹

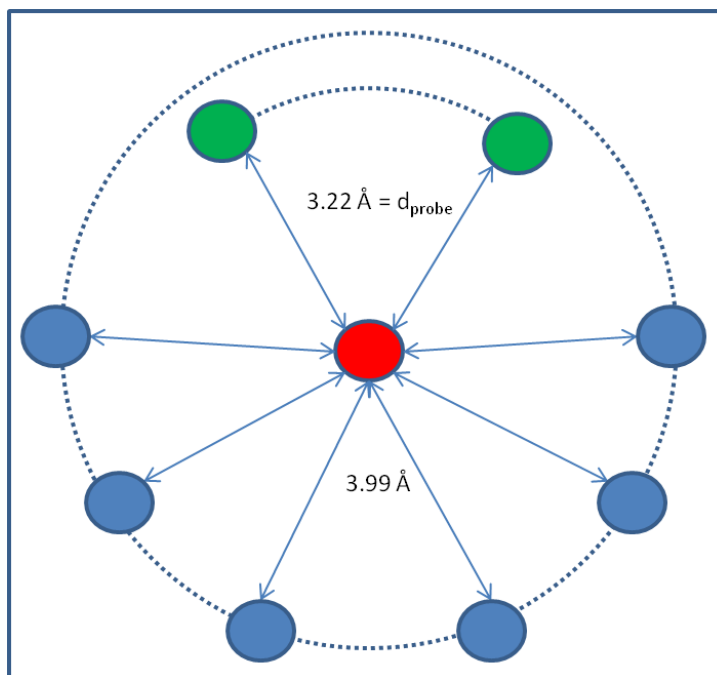


Figure 13: Configuration in which the energy of interaction between an adsorbate (red, center) and 6 carbon atoms (blue, bottom) is exactly enough to offset the unfavorable interaction energy between the adsorbate and the two closer framework carbon atoms (green, top).

The corrected probe diameter is thus

$$d_{probe} = 2\sigma_{carbon} - \left(\frac{4\epsilon_{mix}\sigma_{mix}^6 + \sqrt{16\epsilon_{mix}^2\sigma_{mix}^6 + 8\epsilon_{mix}\sigma_{mix}^{12}E}}{8\epsilon_{mix}\sigma_{mix}^{12}} \right)^{-1/6} \quad 6$$

where ϵ_{mix} and σ_{mix} are the values for the Lennard-Jones interaction between carbon and the adsorbate, calculated via Lorenz-Berthelot mixing rules, E is the energetic contribution of favorable interaction defined above, and σ_{carbon} is the Lennard-Jones size parameter for carbon. The probe molecule sizes calculated using Equation 6 are approximately 0.5 Å smaller than the corresponding Lennard-Jones sigma parameters. The sizes calculated are 2.96, 3.22, 3.61, and 3.67 Å, for Ar, Kr, Xe, and Rn, respectively.

Figure 14 displays the strong correlation between the accessible surface area and selectivity for the Kr/Xe separation for the 70 candidate materials. Here, the accessible surface area is represented by the ratio of the normalized surface areas (nSA, the accessible surface area divided by the surface area of the spherical probe molecule) for the two adsorbates. When this value is 0.1, for example, Xe can access only ~10% of the surface area available to Kr. The selectivities in the figure were calculated for a mixture of 80% Kr and 20% Xe at five pressures using IAST. This figure illustrates that for this particular separation, surface area is an excellent predictor of selectivity.

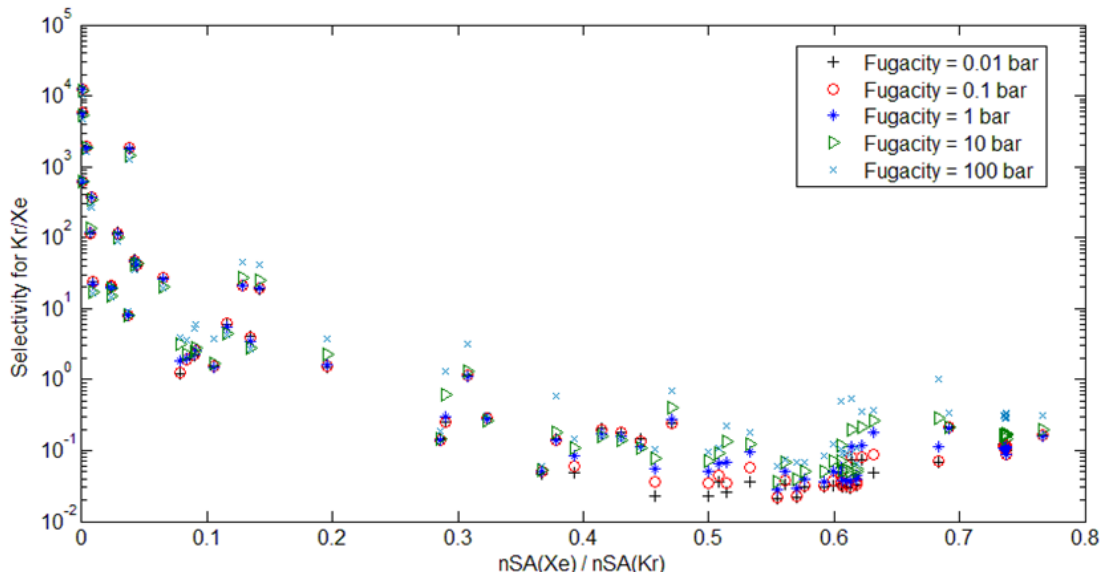


Figure 14: Correlation between accessible surface area ratios (the exact value is defined in the text) and selectivities for the Kr/Xe separation.

An alternative way to view the change in accessible adsorption sites as probe molecule size changes is by invoking the concept of fractal dimension. Fractal dimension has been used in the past to describe the change in adsorption capacity of zeolites as adsorbate size changes.⁴³ The Pfeifer-Avniir equation for determining fractal surface dimension is⁴⁴

$$S = fV^{-D+1}a \quad 7$$

where S is the surface area, a is the cross sectional area of the adsorbate, f is a constant, V is the molar volume of the adsorbate, and D is the fractal dimension. For the metal organic frameworks analyzed, it was found that the fractal dimension was highly variable within the range of adsorbate sizes examined. To examine whether the fractal dimension of the MOFs could explain selectivity for Kr over Xe, the fractal dimension was calculated in the range of probe sizes between the two adsorbates, with sizes defined by

Equation 6. Figure 15 shows the result of this analysis. In this figure, the ordinate remains the same as in Figure 14 and the abscissa changes to the fractal dimension of each material in the range of probe sizes between 3.22 (Kr) and 3.61 (Xe) Å. The results reveal that for a fractal dimension above 5 the material will selectively adsorb the smaller over the larger species.

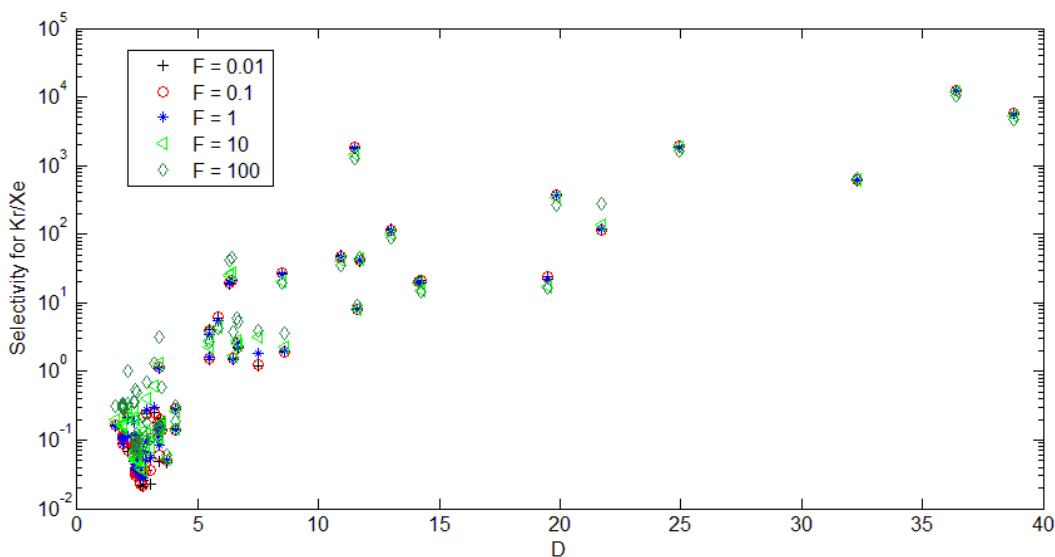


Figure 15: The selectivity (calculated using IAST for and 80% Kr and 20% Xe mixture using IAST, on the abscissa) for the Xe-Kr separation as a function of the fractal dimension in the size range between Kr and Xe.

Although surface area is a useful tool for understanding reverse selectivity, not all trends in selectivity can be explained by surface area. We found several materials for which Kr is favored over Xe, but Rn is also favored over Xe. In these cases, the Kr/Xe selectivity can be explained with the geometric argument above, while the Xe/Rn selectivity cannot. The reason for this situation can be understood by examining the relative magnitude of the difference in size (σ) and energy (ε) terms between the Lennard-

Jones potentials for Kr, Xe, and Rn. When the adsorbate changes from Kr to Xe, σ increases 11% while ϵ changes 24%. From Xe to Rn, σ changes 1.7% and ϵ changes 42%. The relative change in the size term (relative to the change in the energy term) is more than 10 times larger for the Kr - Xe case, indicating the much more significant impact of size effects for this separation. This is illustrated in Figure 16. Here, the interaction energies of each adsorbate with a carbon atom was defined using the Lennard-Jones potential and Lorentz-Berthelot mixing rules. The figure shows the difference in the energies for each gas pair. For distances between 3.92 and 4.03 Å, the interaction energy with carbon is more favorable for Kr than for Xe and also more favorable for Rn than for Xe. If a material has many regions where interactions at this distance occur, the material will be more selective for Kr than Xe, and more selective for Rn than Xe.

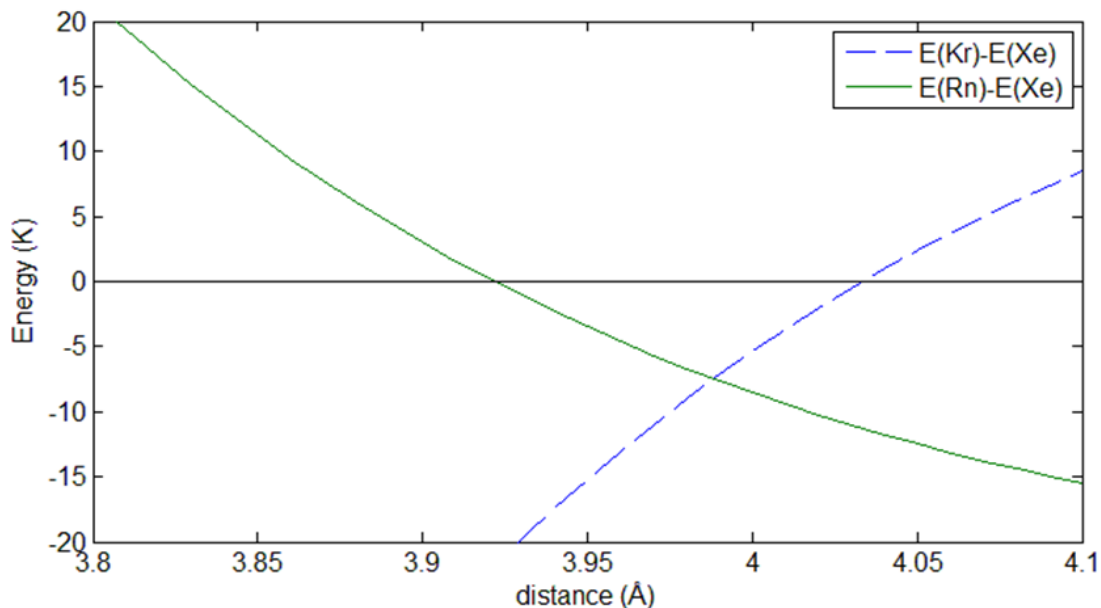


Figure 16: The difference between interaction potential energy with a carbon atom for Kr and Xe and Rn and Xe.

3.5 Temperature Effects

To illustrate the impact of temperature on selective adsorption in MOFs, the effect of temperature on separation performance was investigated for two sample materials. One material (CSD reference code GUPJEG01) was chosen because of its performance as a reverse selective material for the Kr-Xe separation, and the other was chosen as a typical example of a normal strongly selective material (CSD reference code YAPXIX). Reverse selective materials work well in separations because the larger species is excluded due to unfavorable interactions in the tight confines of the MOF structure. This effect is strongly magnified at lower temperatures. Figure 17 shows this effect for the case of the first MOF, GUPJEG01. The predicted low loading selectivity (calculated via binary GCMC for an 80% Kr, 20% Xe mixture) for this material increases by more than 2 orders of magnitude when the temperature is decreased from room temperature (298 K) to dry ice temperatures (194 K). Although not shown on the figure, when the temperature was further decreased to 77 K, the simulation (using a fugacity range from 1×10^{-6} to 100 bar) did not record any Xe being adsorbed at all, indicating nearly perfect selectivity.

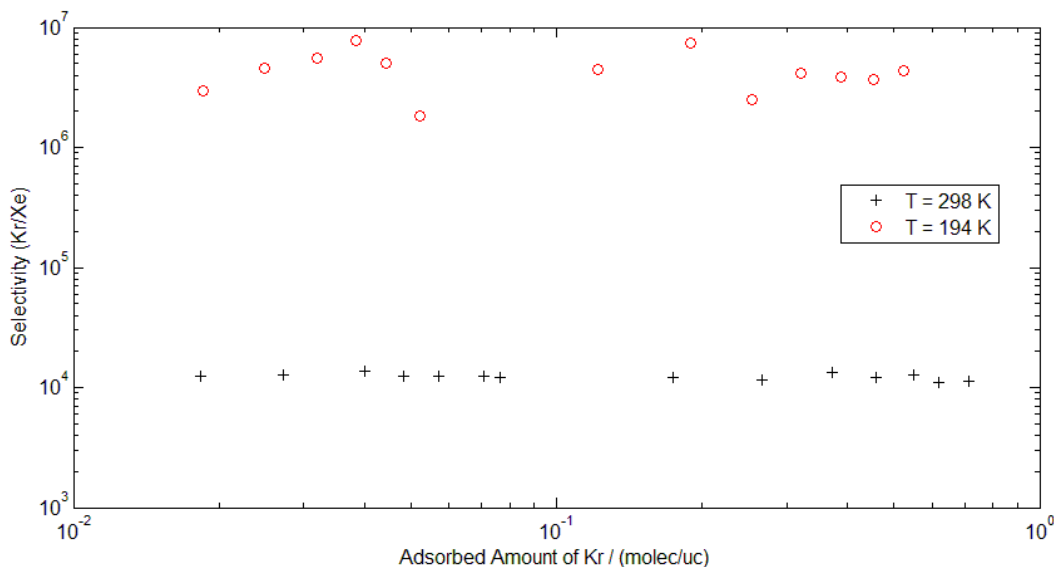


Figure 17: Effect of temperature on the adsorptive selectivity for Kr/Xe on GUPJEG01 at low loading.

The second case studied was that of a more normally selective material, selective for Xe over Kr. In this case, the adsorptive selectivity does not respond to changes in temperature by simply increasing at all loadings. At low loadings the adsorbed amount is dominated by enthalpic effects. As a result, the selectivity increases at lower temperatures in this regime. This situation is illustrated by the data at 298 and 194 K in Figure 18. At high loadings, however, selectivity is dominated by entropic effects which allow the smaller species to adsorb preferentially. At the lowest temperature shown in Figure 18, all of the fugacities probed in our calculations (1×10^{-6} to 100 bar) gave results in the high loading regime, resulting in a separation which is slightly selective for adsorption of Kr over Xe.

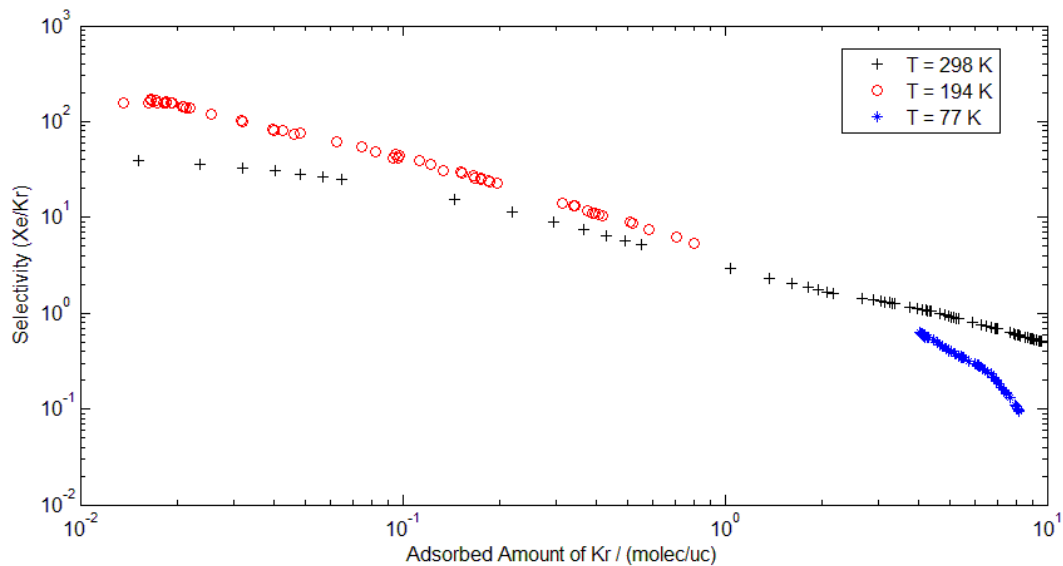


Figure 18: Effect of temperature on the adsorptive selectivity as a function of loading for Xe/Kr on YAPXIX.

CHAPTER 4: CONCLUSIONS

We have performed GCMC simulations and IAST calculations for four noble gas species and three noble gas pairs in a large number of metal organic framework materials. The aims of these calculations were to: first, identify interesting candidates for separating noble gas pairs; second, to examine the applicability of IAST to binary calculations; and third, to elucidate the mechanisms of separation for the best performing materials, both to further enhance conceptual understanding of adsorption separations and to guide in the identification of additional candidates through further screening calculations.

Towards our first goal, a set of screening calculations were performed on a set of over 3,400 materials using crystal structures of materials reported previously in the literature. Screening criteria were developed that yielded 70 candidates for 7 different separations. Materials were identified for both kinetic and adsorptive separation. Although subsequent analysis of these materials focused on adsorptive separation abilities, the kinetic separation candidates were included in this analysis because several of these materials exhibited strong reverse selectivity. Several interesting materials were found in this work that have excellent properties for each of the three separations studied. In particular, the material GUPJEG01 (Mn(dcbp))⁴⁵ is predicted to be an excellent candidate for further research into its applicability to Kr/Xe separations. Experimental verification of these findings would be a significant step toward the use of these materials in practical applications.

For the second goal, calculations were performed on each of the 70 candidate materials to determine accessibility of the adsorbate to all areas of the framework, and

portions of each framework physically inaccessible to each adsorbate were blocked.

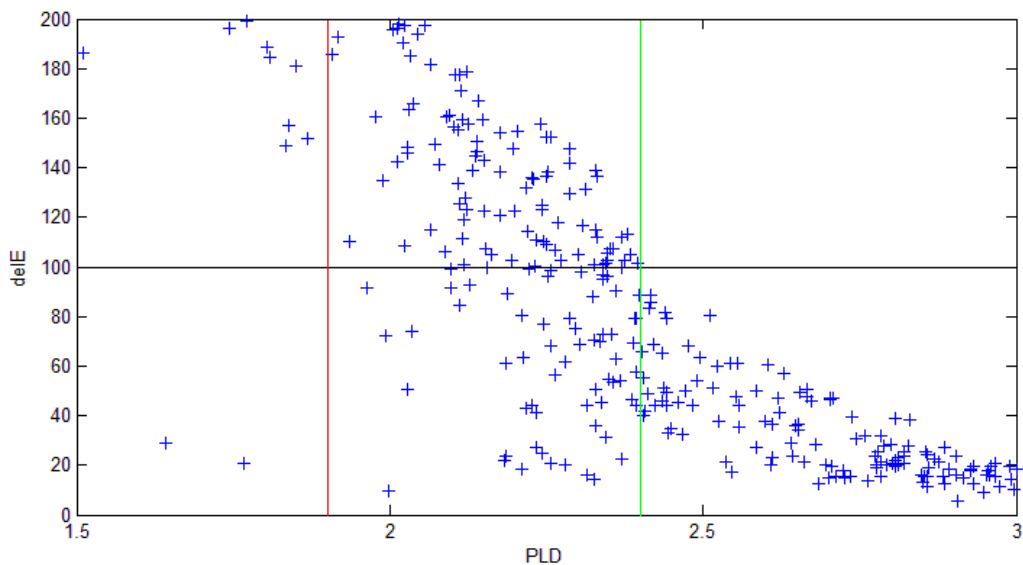
Next, single component GCMC calculations were performed using the information about blocked regions, and this data was used in IAST predictions of binary selectivity. We showed that IAST is in almost all cases an excellent method for calculating binary selectivity. The only cases in which IAST did not give excellent results were materials where, due to pore blocking effects, some volume within a material is completely inaccessible to one of the two adsorbing species.

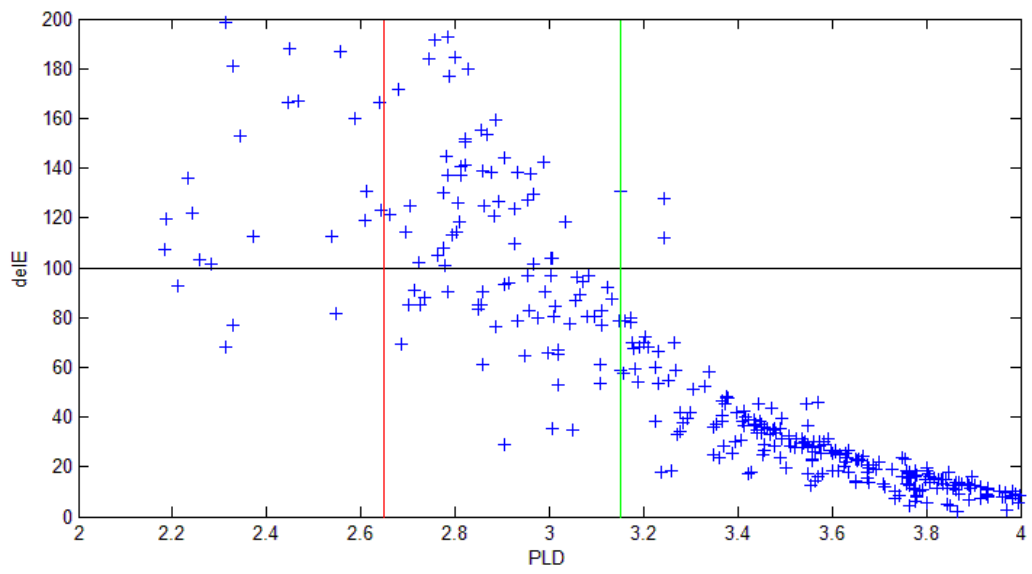
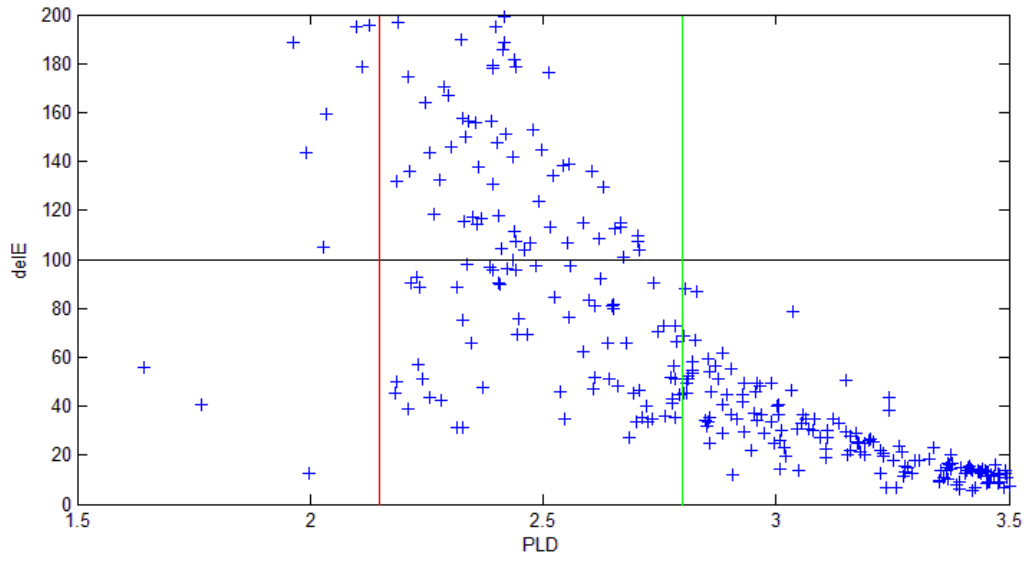
An unexpected feature of our results was the existence of many materials that were “reverse selective”, that is, where adsorption does not favor the larger of two adsorbing species. We explored the reverse selectivity observed in the Kr/Xe separation to better understand the mechanism of this phenomenon. We found that surface area trends in general, and surface fractal dimension in particular, are excellent predictors of this effect. The method we presented for performing corrected adsorbate-specific surface area calculations will be valuable in future material screening procedures, especially as the size of existing material libraries continue to grow.⁴⁶ We also explored the effect of temperature on adsorptive separation, and showed that reverse selective materials are especially interesting for the way separation performance increased with decreasing temperature.

This work focused on the specific case of non-polar spherical adsorbates in MOFs. Non-spherical and polar adsorbates add additional complexity to the problem, and the applicability of the methods discussed here is uncertain. For the materials identified, physical experiments must be performed to verify predicted performance.

APPENDIX A: ACCESSIBILITY BOUNDS FOR FOUR NOBLE GASES

The upper and lower bounds for accessible pore sizes for each adsorbate were determined by visually fitting the data. The red line marks the lower bound on the size, the minimum pore size likely to give an energy barrier of 100 KJ/mol or less. The green line marks the upper bound, the maximum pore diameter that may have an energy barrier of at least 100 KJ/mol. The three figures below are for Ar, Kr, Xe, and Rn, respectively. The figure for Ar is also provided in the text.





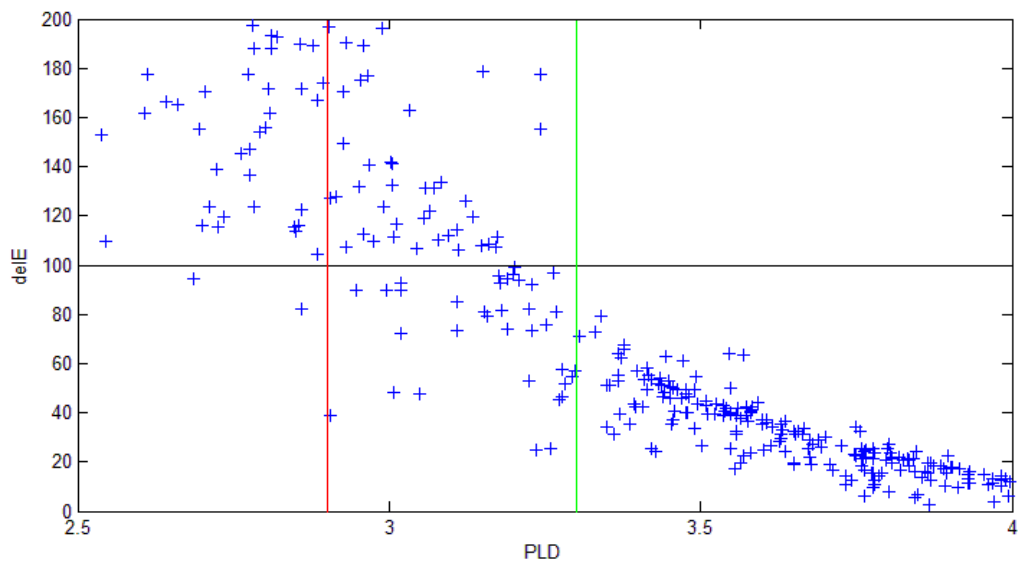


Figure 19a-d: Correlation between pore limiting diameter and the energy barrier for diffusion for Kr, Xe, and Rn, calculated via the TST approximation mentioned in Section 3.1.1. The vertical lines indicate the selected bounds for values of pore limiting diameter giving a 100 kJ/mol energy barrier to passage.

APPENDIX B: ADDITIONAL EVIDENCE FOR THE ACCURACY OF IAST

After identifying the inaccessible regions as described above, we repeated the calculation of the Henry's constants in each material to understand the effect of not considering inaccessible regions during the material screening procedure.

In these calculations, gridpoints associated with blocked regions were assigned an arbitrary high (unfavorable) energy value. The effect of correcting for blocked regions is seen clearly when comparing the value of the Henry's constant calculated in the screening calculations (a method which does not consider cavity accessibility) and the value calculated by fitting in the dilute regime of single component isotherms (which do consider cavity accessibility). Figure 20 illustrates that the agreement between these values is very good for most cases, and any significant deviation between the values can be attributed to the fact that the method for calculating Henry's constants used in the screening calculation does not account for blocked regions.

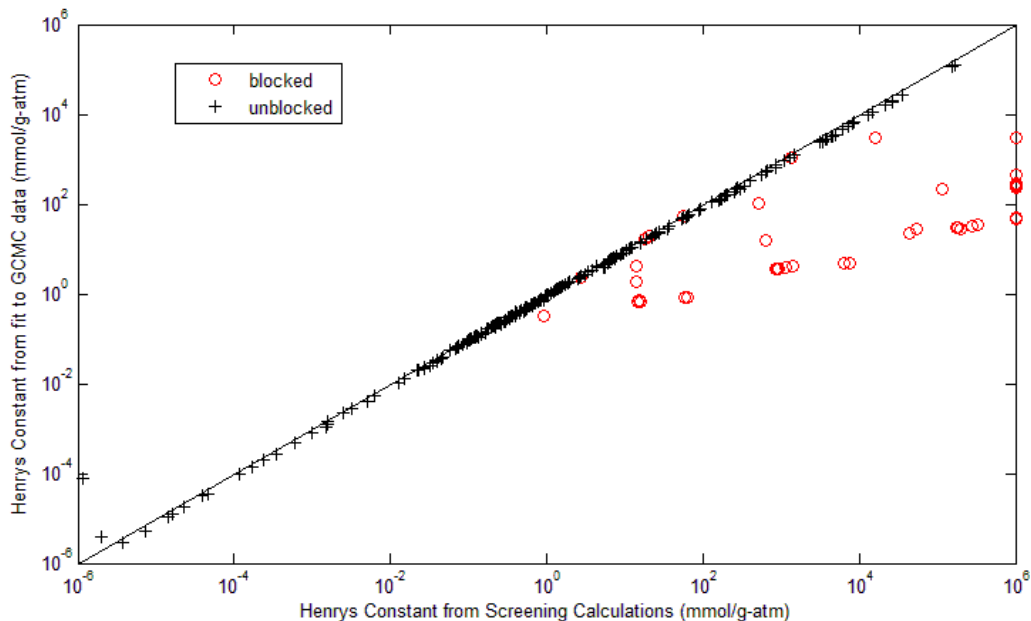


Figure 20: Comparison between the Henry's constant calculated in the screening calculations (not accounting for sub-cavity accessibility, labeled "unblocked") and Henry's constants calculated by fitting single component isotherm data (accounting for sub-cavity accessibility, labeled "blocked"). The black line represents equivalence between the two values and is included to guide the eye.

Figure 21 compares the cumulative distribution function (CDF) for the probability of achieving agreement between IAST and binary calculations to within a given percent for two classes of materials. The first class, represented by the black line, includes all materials in which just one of the two single component isotherms used in the IAST calculation uses region blocking to exclude a species (the "mix" materials). The red curve represents all other materials. This plot shows that there is a greater than 90% chance that the agreement between IAST and binary GCMC will be within 20% when the entire material is treated consistently for blocked regions for the case of noble gas adsorption.

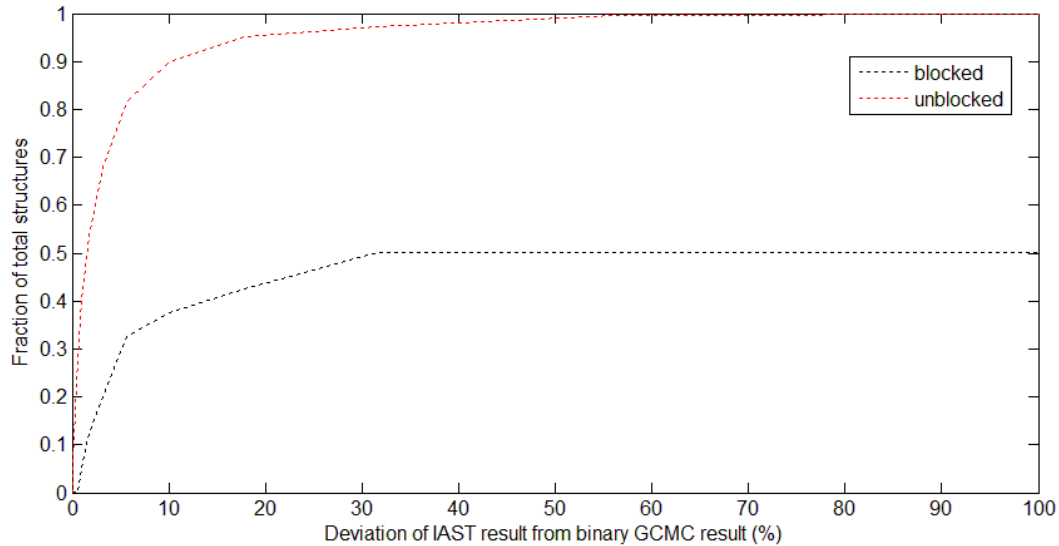


Figure 21: CDFs describing the probability of achieving IAST results with a given percent deviation from binary GCMC data. The “blocked” curve represents structures where only some of the sub-cavities are blocked, while the “unblocked” curve is for all other materials.

The agreement between IAST and binary GCMC was excellent for most cases. The cases where the fit were poor all have the same characteristic. For these cases, the materials had blocked regions. Specifically, in these materials, a portion of the material was inaccessible to Rn while remaining accessible to Xe. The figure below illustrates this with a histogram depicting the number of IAST results falling within a given range of the binary GCMC result for materials without any blocked regions, for all materials with any blocked regions, and for the specific case where portions of the material were blocked to only one of the two adsorbates. For all cases where the fractional difference between the IAST and the binary GCMC values (defined as the absolute value of the difference divided by the GCMC result) was greater than 1, the large deviation between binary GCMC and IAST results can be explained by the way blocked regions are handled.

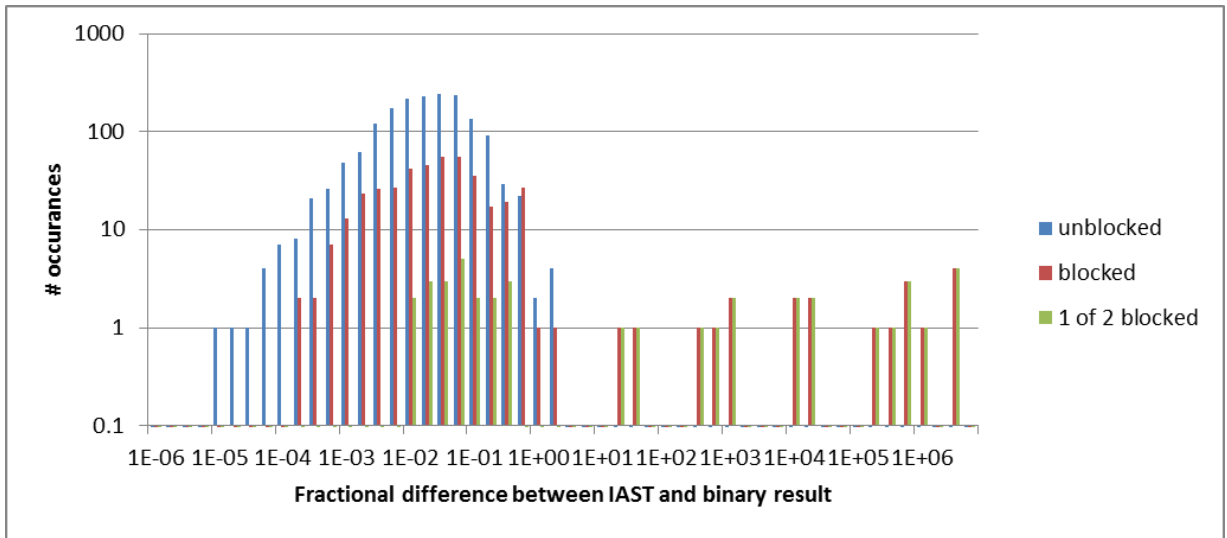


Figure 22: Correlation between the number of IAST results and the difference between IAST and binary GCMC for three cases. The definition of each case is described in the text above.

APPENDIX C: PARAMETERIZING THE SURFACE AREA CORRECTION

For the calculation of surface area,⁴¹ an appropriate value for the number of positive interactions to include needed to be determined. To accomplish this, an iterative procedure was applied wherein surface area was calculated and the correlation between surface area and Henry's constant was observed, then the number of positive interactions was adjusted to improve this correlation. A value was selected such that the favorability measure (the ratio of the Henry's constant with the ideal gas value, described in the text) was greater than 1 when the surface area was larger than 10% of the surface area of the probe molecule. This fit is illustrated in Figure 23.

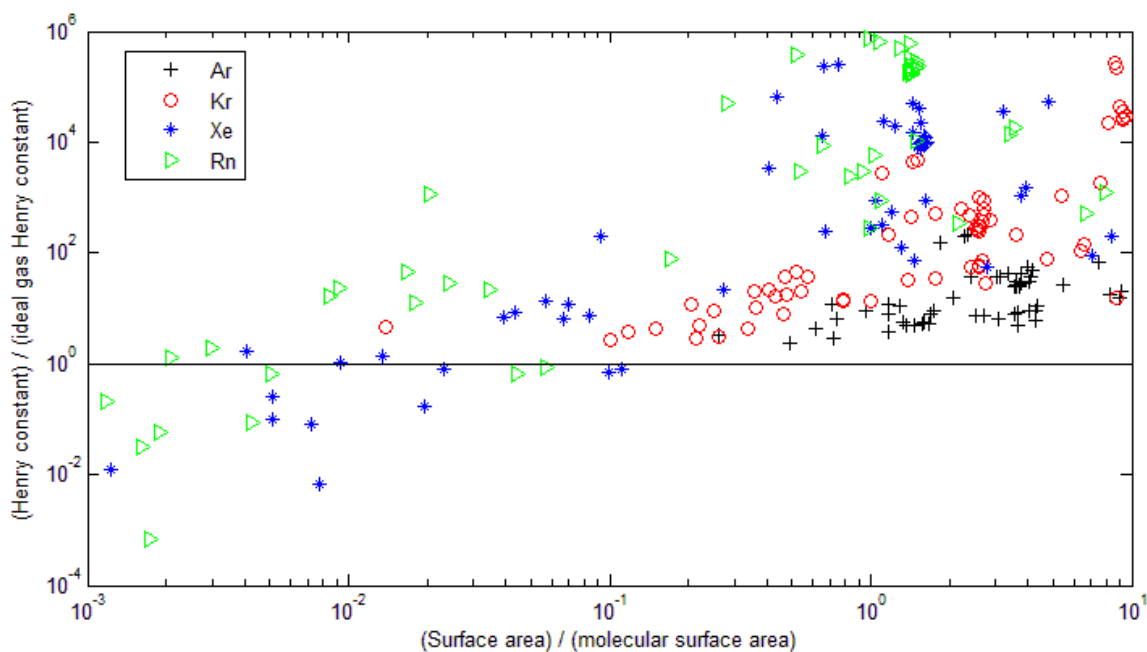


Figure 23: Correlation between the favorability measure (described in text) and normalized surface area for the MOFs used to establish the number of positive interaction to include in the formula for adjusted probe size for surface area calculations.

APPENDIX D: SCREENING DATA SUMMARY

The screening procedure described in the text resulted in a group of 70 candidate materials for 6 classes of separations. The definition of each class is defined in the text. The values of diffusivity here are the transition state theory (TST) values²⁶ calculated with a value of 1.3×10^{10} Hz, and the Henry's constant values are calculated via the Monte Carlo integral procedure and do not account for blocked regions. Though just 70 materials are presented here, these calculations were performed for 3432 materials as part of the screening process.

Table 4: The screening data for all 70 candidate structures.

Candidate	LCD (Å)	PLD (Å)	Vol (Å ³)	Diffusivity (cm ² /s)				Henry (mmol/g-atm)				Separations					
				Ar	Kr	Xe	Rn	Ar	Kr	Xe	Rn	1	2	3	4	5	6
AGESIP	3.608	2.915	6.59E+02	5.66E-08	1.15E-10	1.00E-10	1.00E-10	1.05E-01	1.44E-01	3.18E-03	1.54E-03	0	0	0	1	0	0
BACMOH10	3.601	3.079	1.15E+03	1.98E-07	2.83E-10	1.00E-10	1.00E-10	4.08E-01	1.01E+00	4.40E-02	3.95E-02	0	0	0	1	0	0
CAZGIT	4.747	3.777	4.52E+03	8.66E-06	2.53E-06	9.69E-08	1.19E-08	8.28E-01	1.16E+01	2.77E+02	8.30E+03	0	0	1	0	0	0
COKDAI	4.027	3.277	2.64E+03	3.64E-06	2.02E-07	1.43E-10	1.00E-10	1.44E-01	3.97E-01	2.21E-01	6.54E-01	0	0	0	0	1	0
DOHYIJ	3.614	3.055	1.71E+03	1.71E-07	1.80E-10	1.00E-10	1.00E-10	1.24E-01	1.78E-01	1.59E-03	6.03E-04	0	0	0	1	0	0
DOHYI01	3.65	3.189	1.71E+03	1.85E-06	1.57E-08	1.00E-10	1.00E-10	1.75E-01	3.90E-01	1.51E-02	1.30E-02	0	0	0	0	1	1
ECAVEK	4.745	3.733	1.13E+03	3.30E-05	3.39E-05	2.80E-06	7.18E-07	2.65E+00	5.98E+01	3.08E+03	1.54E+05	0	1	1	0	0	0
ECAVIO	4.784	3.776	1.13E+03	3.23E-05	3.62E-05	3.88E-06	1.12E-06	2.77E+00	6.35E+01	3.36E+03	1.69E+05	0	1	1	0	0	0
EVEGER	7.467	3.242	3.36E+03	1.79E-07	1.03E-10	1.00E-10	1.00E-10	2.23E-01	1.55E+00	2.23E+01	2.67E+02	0	0	0	1	0	0
EXUM0Z	3.814	2.859	1.21E+03	1.09E-07	1.33E-10	1.00E-10	1.00E-10	2.99E-01	2.95E-01	1.71E-04	1.66E-05	0	0	0	1	0	0
FIQYUA	4.556	3.491	1.60E+03	8.48E-06	4.26E-07	1.36E-10	1.00E-10	2.38E-01	1.62E+00	1.20E+01	1.27E+02	0	0	0	0	1	0
FOQSUA	3.369	2.906	1.30E+03	3.45E-06	2.63E-07	3.82E-10	1.05E-10	9.49E-02	6.71E-02	1.15E-04	1.43E-05	0	0	0	0	1	1
GATHAL	3.943	2.885	6.26E+03	3.41E-07	4.75E-10	1.00E-10	1.00E-10	2.41E-01	4.53E-01	2.28E-02	2.23E-02	0	0	0	1	0	0
GIQXIO	4.026	2.701	2.83E+03	2.35E-07	2.19E-10	1.00E-10	1.00E-10	1.01E-01	3.28E-01	1.33E-01	3.31E-01	0	0	0	1	0	0
GIQXUA	4.061	2.725	2.83E+03	2.47E-07	2.29E-10	1.00E-10	1.00E-10	1.05E-01	3.59E-01	1.68E-01	4.50E-01	0	0	0	1	0	0
GIQYIP	4.093	2.735	2.87E+03	2.06E-07	1.83E-10	1.00E-10	1.00E-10	1.09E-01	4.05E-01	2.81E-01	9.27E-01	0	0	0	1	0	0
GITTIN	11.263	3.545	5.15E+03	2.71E-05	6.61E-07	1.02E-10	1.00E-10	2.02E-01	6.96E-01	3.44E+00	1.87E+01	0	0	0	0	1	0
GIYSAJ	5.408	4.92	6.16E+03	3.00E-05	2.73E-05	2.46E-05	2.23E-05	9.55E-01	1.23E+01	3.98E+02	1.31E+04	0	1	1	0	0	0
GOBSUM	4.508	3.574	4.71E+03	1.11E-05	1.09E-06	3.82E-10	1.02E-10	8.58E-01	6.49E+00	2.73E+01	2.77E+02	0	0	0	0	1	0
GOLQII	3.659	3.23	1.79E+03	2.19E-06	1.98E-08	1.00E-10	1.00E-10	2.20E-01	8.50E-01	2.24E-01	5.44E-01	0	0	0	0	1	0
GOMSUW	4.489	3.802	1.12E+03	2.76E-05	3.52E-05	5.81E-06	2.10E-06	1.98E+00	3.74E+01	8.47E+02	2.68E+04	0	0	1	0	0	0

Table 4 (continued)

GUPIJEG	3.679	3.259	1.28E+03	2.18E-05	4.06E-06	2.99E-08	1.86E-09	2.47E-01	1.18E-01	2.30E-05	1.99E-06	0	0	0	0	1	1
GUPJEG01	3.649	3.237	1.27E+03	1.98E-05	3.90E-06	3.83E-08	2.65E-09	2.03E-01	7.43E-02	7.31E-06	1.18E-06	0	0	0	0	1	1
GUXQAR	3.621	2.859	3.64E+02	2.95E-07	1.28E-09	1.00E-10	1.00E-10	1.27E-01	6.95E-02	3.91E-05	3.77E-06	0	0	0	1	0	0
HAZGOF	3.932	2.85	6.23E+03	2.21E-07	2.31E-10	1.00E-10	1.00E-10	2.40E-01	4.77E-01	2.66E-02	2.74E-02	0	0	0	1	0	0
HEGNAJ	6.018	4.797	6.58E+03	4.44E-05	3.04E-05	1.91E-05	1.24E-05	5.08E-01	5.39E+00	1.70E+02	3.77E+03	0	1	0	0	0	0
HEGNIR	6.016	4.728	6.58E+03	4.53E-05	3.04E-05	1.90E-05	1.21E-05	5.28E-01	6.00E+00	2.08E+02	4.91E+03	0	1	0	0	0	0
HEGNOX	6.076	4.726	6.58E+03	4.90E-05	3.44E-05	2.23E-05	1.45E-05	5.49E-01	6.05E+00	1.97E+02	4.50E+03	0	1	0	0	0	0
HEGNUD	5.949	4.786	6.55E+03	4.36E-05	2.92E-05	1.82E-05	1.21E-05	5.33E-01	5.60E+00	1.72E+02	3.84E+03	0	1	0	0	0	0
HEGPAL	5.899	4.803	6.58E+03	4.85E-05	3.35E-05	2.08E-05	1.34E-05	5.20E-01	5.68E+00	1.87E+02	4.29E+03	0	1	0	0	0	0
HITXUE	6.996	3.349	3.33E+03	2.10E-05	1.94E-06	1.54E-10	1.00E-10	4.39E+00	5.34E+01	1.48E+03	3.59E+04	0	0	0	0	1	0
HITYEP	10.652	3.749	1.38E+04	5.40E-05	4.48E-05	2.73E-08	4.51E-10	1.38E+01	6.40E+02	1.14E+05	1.00E+06	1	1	0	0	0	0
IXISAJ	5.706	4.417	3.96E+03	3.72E-06	1.30E-06	3.33E-07	9.26E-08	1.71E+00	2.56E+01	8.67E+02	2.64E+04	0	1	1	0	0	0
JOSNAG	3.672	2.955	7.90E+02	4.05E-08	1.01E-10	1.00E-10	1.00E-10	1.26E-01	2.64E-01	3.47E-02	4.77E-02	0	0	0	1	0	0
KAHMOW	5.169	4.892	3.01E+03	3.64E-05	3.58E-05	3.55E-05	3.45E-05	1.34E+00	2.38E+01	1.11E+03	4.34E+04	0	1	1	0	0	0
KAHQUG	10.762	6.646	1.48E+04	2.08E-04	1.54E-04	9.93E-05	7.09E-05	1.83E+01	1.16E+03	2.76E+05	1.00E+06	1	1	0	0	0	0
KAHRAN	10.669	6.762	1.47E+04	2.04E-04	1.50E-04	9.55E-05	6.76E-05	2.05E+01	1.40E+03	3.36E+05	1.00E+06	1	1	0	0	0	0
KAHSES	10.906	6.795	1.51E+04	2.08E-04	1.53E-04	9.72E-05	6.88E-05	1.45E+01	8.38E+02	1.75E+05	1.00E+06	1	1	0	0	0	0
KAHSIW	10.899	6.791	1.51E+04	2.07E-04	1.52E-04	9.70E-05	6.86E-05	1.48E+01	8.59E+02	1.81E+05	1.00E+06	1	1	0	0	0	0
KAHSOC	10.812	6.834	1.51E+04	2.06E-04	1.51E-04	9.63E-05	6.80E-05	1.48E+01	8.53E+02	1.77E+05	1.00E+06	1	1	0	0	0	0
KAHSUI	10.787	6.805	1.51E+04	2.05E-04	1.50E-04	9.52E-05	6.71E-05	1.51E+01	8.76E+02	1.85E+05	1.00E+06	1	1	0	0	0	0
LEMNOH	4.016	2.974	2.16E+03	7.94E-07	7.47E-10	1.00E-10	1.00E-10	6.26E-01	2.68E+00	2.48E+00	9.76E+00	0	0	0	1	0	0
MADVUJ	5.286	4.656	1.86E+03	2.37E-05	2.20E-05	1.48E-05	1.04E-05	7.15E-01	9.16E+00	2.94E+02	7.16E+03	0	1	0	0	0	0
MADWAQ	5.135	4.44	1.81E+03	1.96E-05	1.69E-05	8.24E-06	4.77E-06	7.95E-01	1.05E+01	3.41E+02	8.64E+03	0	1	0	0	0	0
MIKJAR	5.994	4.831	6.60E+03	4.62E-05	3.16E-05	2.05E-05	1.36E-05	5.07E-01	5.25E+00	1.59E+02	3.43E+03	0	1	0	0	0	0
MIZKOW	3.757	3.277	1.78E+03	4.53E-06	1.12E-07	1.03E-10	1.00E-10	2.31E-01	7.75E-01	1.34E-01	2.59E-01	0	0	0	0	1	1
MOXNUJ	4.073	3.367	5.09E+03	5.36E-06	1.58E-07	1.05E-10	1.00E-10	2.83E-01	1.13E+00	7.85E-01	2.74E+00	0	0	0	0	1	0
NAJVUQ	10.83	6.669	1.51E+04	2.12E-04	1.57E-04	1.02E-04	7.29E-05	1.57E+01	9.13E+02	2.02E+05	1.00E+06	1	1	0	0	0	0
NIKZAJ	4.502	3.451	1.60E+03	7.13E-06	3.09E-07	1.21E-10	1.00E-10	2.06E-01	1.23E+00	6.28E+00	5.51E+01	0	0	0	0	1	0
NIKZAJ01	4.545	3.476	1.62E+03	8.54E-06	4.73E-07	1.55E-10	1.00E-10	2.09E-01	1.27E+00	7.28E+00	6.69E+01	0	0	0	0	1	0
ODONIF	3.815	3.108	8.62E+03	1.02E-06	1.08E-08	1.00E-10	1.00E-10	2.41E-01	6.42E-01	3.17E-02	3.92E-02	0	0	0	0	1	1
ODOXEK	5.205	4.243	1.70E+03	2.51E-05	1.56E-05	1.81E-06	5.08E-07	9.30E-01	1.38E+01	5.15E+02	1.63E+04	0	1	1	0	0	0
OFERUN	11.505	3.242	4.90E+03	4.72E-07	1.33E-10	1.00E-10	1.00E-10	3.43E-01	1.39E+00	8.73E+00	5.47E+01	0	0	0	1	0	0
OFORUX	5.474	4.936	2.85E+03	2.04E-05	1.63E-05	1.19E-05	9.20E-06	6.58E-01	7.89E+00	2.55E+02	6.05E+03	0	1	0	0	0	0
PAZBOH	7.786	6.7	1.56E+04	9.60E-05	4.84E-05	1.75E-05	8.02E-06	5.73E+01	6.45E+03	1.00E+06	1.00E+06	1	1	0	0	0	0
PAZBUN	7.786	6.708	1.56E+04	9.65E-05	4.87E-05	1.77E-05	8.12E-06	5.69E+01	6.35E+03	1.00E+06	1.00E+06	1	1	0	0	0	0
PENZUE	3.862	3.004	1.99E+03	1.09E-07	1.20E-10	1.00E-10	1.00E-10	5.85E-02	9.40E-02	2.47E-03	1.50E-03	0	0	0	1	0	0
QUGNOV	3.477	2.854	1.38E+03	6.31E-08	1.35E-10	1.00E-10	1.00E-10	7.36E-02	1.03E-01	9.72E-04	3.47E-04	0	0	0	1	0	0
TISGUY	4.645	3.393	4.02E+03	8.49E-06	5.90E-06	4.38E-10	1.01E-10	1.93E-01	1.03E+00	7.51E+00	8.84E+01	0	0	0	0	1	0
TONBII	4.792	4.59	1.12E+03	1.41E-05	1.37E-05	1.19E-05	1.10E-05	1.06E+00	1.61E+01	5.56E+02	1.50E+04	0	1	0	0	0	0
WASNIO	3.95	3.272	1.87E+03	8.65E-06	4.86E-07	1.88E-10	1.01E-10	1.14E+00	6.74E+00	6.06E+00	3.49E+01	0	0	0	0	1	0
WIYZOU	4.648	2.967	2.20E+03	1.80E-07	1.33E-10	1.00E-10	1.00E-10	1.47E-01	7.19E-01	3.12E+00	2.24E+01	0	0	0	1	0	0

Table 4 (continued)

WOCVUG	4.345	3.462	2.56E+03	8.60E-06	4.26E-07	1.33E-10	1.00E-10	1.01E+00	1.26E+01	9.24E+01	1.37E+03	0	0	0	0	1	0
WOPDEL	5.433	3.956	5.02E+03	6.57E-05	4.29E-05	1.87E-06	2.72E-07	1.06E+00	1.57E+01	6.62E+02	2.18E+04	0	1	1	0	0	0
XEQNIQ	7.681	6.699	1.56E+04	9.57E-05	4.81E-05	1.74E-05	7.96E-06	6.48E+01	7.57E+03	1.00E+06	1.00E+06	1	1	0	0	0	0
XOHJUA	3.484	2.953	1.69E+03	7.69E-08	1.16E-10	1.00E-10	1.00E-10	8.41E-02	8.46E-02	2.40E-04	4.68E-05	0	0	0	1	0	0
XOVPIH	3.624	2.927	7.83E+02	4.66E-08	1.01E-10	1.00E-10	1.00E-10	7.14E-02	1.21E-01	6.32E-03	5.05E-03	0	0	0	1	0	0
YAPXIX	5.159	4.885	2.97E+03	3.54E-05	3.48E-05	3.51E-05	3.40E-05	1.45E+00	2.70E+01	1.32E+03	5.45E+04	0	1	1	0	0	0
YARYOF	4.886	3.477	2.11E+03	3.03E-05	2.75E-06	9.23E-10	1.08E-10	1.72E-01	5.25E-01	1.88E+00	1.13E+01	0	0	0	0	1	0
YEYYAC	6.296	2.884	5.27E+03	1.68E-07	1.06E-10	1.00E-10	1.00E-10	5.53E-01	3.79E+00	5.34E+01	6.39E+02	0	0	0	1	0	0

APPENDIX E: BINARY GCMC DATA

Binary GCMC data was collected for comparison with IAST calculations. The binary GCMC data collected is presented in Tables 5a-c.

Table 5a: Data for GCMC isotherm calculations using a 50:50 binary mixture of Ar and Kr.

REFCODE	PAIR	S	0.01	0.055	0.1	0.55	1	5.5	10	55	100	550
AGESIP	ArandKr	Ar	7.063E-4	3.845E-3	6.982E-3	3.756E-2	6.822E-2	3.238E-1	5.164E-1	1.152E+0	1.289E+0	1.569E+0
AGESIP	ArandKr	Kr	2.369E-4	1.281E-3	2.333E-3	1.273E-2	2.302E-2	1.120E-1	1.807E-1	4.174E-1	4.728E-1	5.192E-1
BACMOH10	ArandKr	Ar	3.165E-3	1.745E-2	3.147E-2	1.657E-1	2.942E-1	1.133E+0	1.518E+0	2.138E+0	2.284E+0	2.431E+0
BACMOH10	ArandKr	Kr	1.905E-3	1.040E-2	1.848E-2	1.004E-1	1.787E-1	7.433E-1	1.008E+0	1.525E+0	1.533E+0	1.565E+0
CAZGIT	ArandKr	Ar	3.056E-2	1.560E-1	2.660E-1	8.788E-1	1.151E+0	1.694E+0	1.841E+0	2.265E+0	2.508E+0	3.897E+0
CAZGIT	ArandKr	Kr	1.023E-1	5.285E-1	8.941E-1	2.985E+0	3.868E+0	5.554E+0	5.784E+0	6.061E+0	6.073E+0	5.678E+0
COKDAI	ArandKr	Ar	2.287E-3	1.257E-2	2.290E-2	1.242E-1	2.195E-1	1.006E+0	1.561E+0	3.418E+0	4.006E+0	5.771E+0
COKDAI	ArandKr	Kr	1.521E-3	8.290E-3	1.508E-2	8.269E-2	1.473E-1	6.921E-1	1.072E+0	2.271E+0	2.566E+0	2.959E+0
DOHYIJ	ArandKr	Ar	1.986E-3	1.102E-2	2.002E-2	1.074E-1	1.914E-1	8.647E-1	1.296E+0	2.386E+0	2.601E+0	2.790E+0
DOHYIJ	ArandKr	Kr	6.835E-4	3.783E-3	6.862E-3	3.748E-2	6.832E-2	3.157E-1	4.886E-1	9.706E-1	1.021E+0	1.143E+0
DOHYIJ01	ArandKr	Ar	2.833E-3	1.550E-2	2.805E-2	1.489E-1	2.622E-1	1.045E+0	1.464E+0	2.178E+0	2.308E+0	2.490E+0
DOHYIJ01	ArandKr	Kr	1.541E-3	8.322E-3	1.502E-2	8.149E-2	1.450E-1	6.104E-1	8.689E-1	1.418E+0	1.466E+0	1.489E+0
ECAVEK	ArandKr	Ar	3.662E-2	1.468E-1	2.107E-1	3.973E-1	4.618E-1	6.201E-1	6.685E-1	8.122E-1	8.436E-1	1.078E+0
ECAVEK	ArandKr	Kr	1.995E-1	7.917E-1	1.119E+0	1.969E+0	2.169E+0	2.518E+0	2.595E+0	2.713E+0	2.746E+0	2.694E+0
ECAVIO	ArandKr	Ar	3.836E-2	1.519E-1	2.153E-1	3.966E-1	4.609E-1	6.100E-1	6.687E-1	8.334E-1	9.305E-1	1.134E+0
ECAVIO	ArandKr	Kr	2.113E-1	8.293E-1	1.166E+0	2.016E+0	2.214E+0	2.552E+0	2.612E+0	2.703E+0	2.680E+0	2.642E+0
EVEGER	ArandKr	Ar	5.303E-3	2.888E-2	5.187E-2	2.488E-1	4.058E-1	1.229E+0	1.653E+0	3.383E+0	4.341E+0	7.088E+0
EVEGER	ArandKr	Kr	8.981E-3	4.838E-2	8.670E-2	4.067E-1	6.453E-1	1.665E+0	2.038E+0	2.945E+0	3.088E+0	3.457E+0
EXUM0Z	ArandKr	Ar	2.650E-3	1.396E-2	2.553E-2	1.384E-1	2.501E-1	1.101E+0	1.626E+0	2.715E+0	2.894E+0	3.024E+0
EXUM0Z	ArandKr	Kr	6.000E-4	3.428E-3	6.161E-3	3.347E-2	5.994E-2	2.836E-1	4.261E-1	7.867E-1	8.291E-1	9.236E-1
FIQYUA	ArandKr	Ar	3.200E-3	1.741E-2	3.158E-2	1.638E-1	2.784E-1	8.668E-1	1.065E+0	1.470E+0	1.635E+0	2.436E+0
FIQYUA	ArandKr	Kr	5.267E-3	2.895E-2	5.239E-2	2.752E-1	4.766E-1	1.571E+0	1.969E+0	2.466E+0	2.499E+0	2.447E+0
FOQSUA	ArandKr	Ar	9.232E-4	5.057E-3	9.242E-3	4.931E-2	8.970E-2	4.272E-1	6.877E-1	1.751E+0	2.103E+0	2.799E+0
FOQSUA	ArandKr	Kr	1.579E-4	8.571E-4	1.571E-3	8.515E-3	1.509E-2	7.380E-2	1.184E-1	3.049E-1	3.586E-1	4.493E-1
GATHAL	ArandKr	Ar	8.362E-3	4.572E-2	8.353E-2	4.510E-1	8.131E-1	3.880E+0	6.199E+0	1.583E+1	1.973E+1	3.059E+1
GATHAL	ArandKr	Kr	3.831E-3	2.086E-2	3.784E-2	2.084E-1	3.687E-1	1.727E+0	2.617E+0	5.295E+0	5.868E+0	5.969E+0
GIQXIO	ArandKr	Ar	2.634E-3	1.466E-2	2.636E-2	1.400E-1	2.469E-1	1.076E+0	1.619E+0	3.644E+0	4.323E+0	6.055E+0
GIQXIO	ArandKr	Kr	2.065E-3	1.142E-2	2.063E-2	1.107E-1	1.941E-1	7.933E-1	1.177E+0	2.214E+0	2.453E+0	2.757E+0
GIQXUA	ArandKr	Ar	2.700E-3	1.496E-2	2.711E-2	1.449E-1	2.545E-1	1.067E+0	1.619E+0	3.633E+0	4.258E+0	6.043E+0
GIQXUA	ArandKr	Kr	2.250E-3	1.235E-2	2.253E-2	1.182E-1	2.098E-1	8.537E-1	1.222E+0	2.224E+0	2.522E+0	2.798E+0
GIQYIP	ArandKr	Ar	2.820E-3	1.530E-2	2.798E-2	1.467E-1	2.597E-1	1.084E+0	1.629E+0	3.484E+0	4.136E+0	5.911E+0
GIQYIP	ArandKr	Kr	2.512E-3	1.382E-2	2.492E-2	1.324E-1	2.307E-1	9.253E-1	1.318E+0	2.444E+0	2.660E+0	2.850E+0
GITTIN	ArandKr	Ar	5.167E-3	2.842E-2	5.169E-2	2.827E-1	5.095E-1	2.592E+0	4.295E+0	1.152E+1	1.420E+1	2.124E+1
GITTIN	ArandKr	Kr	4.336E-3	2.395E-2	4.355E-2	2.379E-1	4.329E-1	2.251E+0	3.778E+0	9.795E+0	1.141E+1	1.423E+1
GIYSAJ	ArandKr	Ar	4.050E-2	2.066E-1	3.425E-1	1.112E+0	1.517E+0	2.692E+0	3.132E+0	4.713E+0	5.599E+0	8.251E+0
GIYSAJ	ArandKr	Kr	1.265E-1	6.261E-1	1.049E+0	3.225E+0	4.093E+0	6.330E+0	6.917E+0	8.054E+0	8.173E+0	8.134E+0
GOBSUM	ArandKr	Ar	2.340E-2	1.258E-1	2.238E-1	9.982E-1	1.537E+0	3.599E+0	4.318E+0	5.873E+0	6.410E+0	7.797E+0
GOBSUM	ArandKr	Kr	4.278E-2	2.286E-1	4.096E-1	1.805E+0	2.750E+0	5.887E+0	6.764E+0	8.246E+0	8.341E+0	8.309E+0
GOLQII	ArandKr	Ar	3.811E-3	2.088E-2	3.744E-2	1.954E-1	3.378E-1	1.103E+0	1.376E+0	1.744E+0	1.828E+0	1.856E+0
GOLQII	ArandKr	Kr	3.537E-3	1.945E-2	3.537E-2	1.866E-1	3.238E-1	1.175E+0	1.486E+0	2.022E+0	2.045E+0	2.156E+0
GOMSUW	ArandKr	Ar	2.865E-2	1.267E-1	1.923E-1	4.099E-1	4.724E-1	6.200E-1	6.618E-1	8.453E-1	8.866E-1	9.569E-1
GOMSUW	ArandKr	Kr	1.287E-1	5.749E-1	8.769E-1	1.807E+0	2.049E+0	2.462E+0	2.538E+0	2.599E+0	2.632E+0	2.680E+0
GUPJEG	ArandKr	Ar	2.150E-3	1.183E-2	2.133E-2	1.162E-1	2.044E-1	9.223E-1	1.395E+0	2.870E+0	3.270E+0	3.993E+0
GUPJEG	ArandKr	Kr	2.512E-4	1.385E-3	2.457E-3	1.321E-2	2.413E-2	1.083E-1	1.671E-1	3.505E-1	3.848E-1	4.200E-1
GUPJEG01	ArandKr	Ar	1.782E-3	9.709E-3	1.761E-2	9.498E-2	1.702E-1	7.938E-1	1.249E+0	2.784E+0	3.179E+0	3.950E+0
GUPJEG01	ArandKr	Kr	1.577E-4	8.730E-4	1.553E-3	8.518E-3	1.507E-2	7.169E-2	1.149E-1	2.630E-1	3.110E-1	3.381E-1
GUXQAR	ArandKr	Ar	3.618E-4	2.013E-3	3.623E-3	1.987E-2	3.546E-2	1.715E-1	2.795E-1	7.202E-1	8.592E-1	1.192E+0
GUXQAR	ArandKr	Kr	4.821E-5	2.619E-4	4.904E-4	2.664E-3	4.670E-3	2.338E-2	3.747E-2	9.113E-2	1.060E-1	1.150E-1
HAZGOF	ArandKr	Ar	8.311E-3	4.600E-2	8.307E-2	4.457E-1	8.005E-1	3.778E+0	5.899E+0	1.458E+1	1.847E+1	2.933E+1
HAZGOF	ArandKr	Kr	3.973E-3	2.200E-2	3.924E-2	2.131E-1	3.877E-1	1.764E+0	2.665E+0	5.185E+0	5.589E+0	5.744E+0

Table 5a (continued)

HEGNAJ	ArandKr	Ar	2.592E-2	1.372E-1	2.415E-1	9.985E-1	1.459E+0	3.266E+0	4.262E+0	1.001E+1	1.290E+1	1.996E+1
HEGNAJ	ArandKr	Kr	6.164E-2	3.241E-1	5.692E-1	2.231E+0	3.147E+0	5.271E+0	5.595E+0	5.481E+0	5.297E+0	4.475E+0
HEGNIR	ArandKr	Ar	2.678E-2	1.411E-1	2.466E-1	9.719E-1	1.388E+0	2.852E+0	3.578E+0	7.474E+0	1.020E+1	1.847E+1
HEGNIR	ArandKr	Kr	7.200E-2	3.792E-1	6.559E-1	2.470E+0	3.404E+0	5.491E+0	5.849E+0	6.018E+0	5.626E+0	4.583E+0
HEGNOX	ArandKr	Ar	2.796E-2	1.470E-1	2.583E-1	1.018E+0	1.464E+0	3.097E+0	4.032E+0	9.395E+0	1.222E+1	1.878E+1
HEGNOX	ArandKr	Kr	7.381E-2	3.884E-1	6.759E-1	2.579E+0	3.555E+0	5.715E+0	6.077E+0	6.103E+0	5.962E+0	5.133E+0
HEGNUD	ArandKr	Ar	2.717E-2	1.442E-1	2.543E-1	1.057E+0	1.562E+0	3.695E+0	4.876E+0	1.181E+1	1.489E+1	2.064E+1
HEGNUD	ArandKr	Kr	6.008E-2	3.203E-1	5.577E-1	2.201E+0	3.119E+0	5.101E+0	5.435E+0	5.165E+0	4.830E+0	4.412E+0
HEGPAL	ArandKr	Ar	2.655E-2	1.399E-1	2.449E-1	9.810E-1	1.419E+0	3.103E+0	3.979E+0	9.347E+0	1.200E+1	1.934E+1
HEGPAL	ArandKr	Kr	6.751E-2	3.574E-1	6.194E-1	2.375E+0	3.321E+0	5.445E+0	5.796E+0	5.711E+0	5.499E+0	4.420E+0
HITXUE	ArandKr	Ar	9.288E-2	4.748E-1	8.063E-1	2.595E+0	3.385E+0	5.237E+0	5.673E+0	7.069E+0	7.663E+0	8.844E+0
HITXUE	ArandKr	Kr	2.716E-1	1.384E+0	2.348E+0	7.330E+0	9.194E+0	1.284E+1	1.361E+1	1.473E+1	1.477E+1	1.484E+1
HITYEP	ArandKr	Ar	1.727E-1	9.406E-1	1.681E+0	7.508E+0	1.114E+1	2.320E+1	2.707E+1	3.679E+1	4.016E+1	5.412E+1
HITYEP	ArandKr	Kr	3.511E-1	1.921E+0	3.665E+0	1.593E+1	2.324E+1	4.140E+1	4.632E+1	5.271E+1	5.346E+1	5.312E+1
IXISAJ	ArandKr	Ar	4.981E-2	2.462E-1	4.099E-1	1.286E+0	1.698E+0	2.968E+0	3.482E+0	5.376E+0	6.208E+0	9.043E+0
IXISAJ	ArandKr	Kr	1.812E-1	8.819E-1	1.446E+0	4.204E+0	5.363E+0	7.861E+0	8.367E+0	9.242E+0	9.344E+0	9.228E+0
JOSNAG	ArandKr	Ar	7.309E-4	4.031E-3	7.307E-3	3.877E-2	6.759E-2	2.825E-1	4.164E-1	9.229E-1	1.106E+0	1.652E+0
JOSNAG	ArandKr	Kr	3.766E-4	2.024E-3	6.355E-3	1.950E-2	3.417E-2	1.339E-1	1.911E-1	3.164E-1	3.495E-1	3.498E-1
KAHMOW	ArandKr	Ar	2.620E-2	1.204E-1	1.903E-1	4.569E-1	5.488E-1	9.051E-1	1.080E+0	1.967E+0	2.464E+0	4.143E+0
KAHMOW	ArandKr	Kr	1.119E-1	5.210E-1	8.161E-1	1.871E+0	2.168E+0	2.777E+0	2.972E+0	3.293E+0	3.343E+0	3.330E+0
KAHQUG	ArandKr	Ar	1.323E+0	4.431E+0	5.868E+0	1.090E+1	1.395E+1	2.842E+1	3.352E+1	4.795E+1	5.411E+1	7.006E+1
KAHQUG	ArandKr	Kr	8.812E-2	4.913E-1	8.995E-1	5.071E+0	1.977E+0	3.204E+1	3.866E+1	4.958E+1	5.131E+1	5.317E+1
KAHRAN	ArandKr	Ar	1.472E+0	4.715E+0	6.120E+0	1.114E+1	1.425E+1	2.841E+1	3.328E+1	4.788E+1	5.440E+1	6.929E+1
KAHRAN	ArandKr	Kr	9.454E-2	5.273E-1	9.630E-1	5.438E+0	9.810E+0	3.305E+1	3.943E+1	4.918E+1	5.037E+1	5.357E+1
KAHSES	ArandKr	Ar	6.246E-2	3.428E-1	6.234E-1	3.368E+0	5.965E+0	2.043E+1	2.568E+1	4.125E+1	4.712E+1	6.022E+1
KAHSES	ArandKr	Kr	8.195E-2	4.532E-1	8.245E-1	4.606E+0	8.380E+0	3.086E+1	3.817E+1	4.938E+1	5.182E+1	5.598E+1
KAHSIW	ArandKr	Ar	6.282E-2	3.437E-1	6.260E-1	3.388E+0	6.007E+0	2.038E+1	2.573E+1	4.083E+1	4.702E+1	5.926E+1
KAHSIW	ArandKr	Kr	8.278E-2	4.560E-1	8.294E-1	4.644E+0	8.438E+0	3.109E+1	3.814E+1	4.982E+1	5.162E+1	5.679E+1
KAHSOC	ArandKr	Ar	6.372E-2	3.517E-1	6.358E-1	3.447E+0	6.127E+0	2.046E+1	2.568E+1	4.145E+1	4.685E+1	6.120E+1
KAHSOC	ArandKr	Kr	8.505E-2	4.684E-1	8.530E-1	4.761E+0	8.660E+0	3.135E+1	3.845E+1	4.924E+1	5.183E+1	5.521E+1
KAHSUI	ArandKr	Ar	6.419E-2	3.529E-1	6.398E-1	3.463E+0	6.141E+0	2.053E+1	2.564E+1	4.100E+1	4.663E+1	6.072E+1
KAHSUI	ArandKr	Kr	8.532E-2	4.712E-1	8.586E-1	4.787E+0	8.695E+0	3.142E+1	3.853E+1	4.956E+1	5.221E+1	5.535E+1
LEMNOH	ArandKr	Ar	7.236E-3	3.938E-2	7.045E-2	3.470E-1	5.700E-1	1.651E+0	2.156E+0	4.001E+0	4.767E+0	7.415E+0
LEMNOH	ArandKr	Kr	7.490E-3	4.086E-2	7.249E-2	3.545E-1	5.810E-1	1.571E+0	1.909E+0	2.567E+0	2.698E+0	2.785E+0
MADVUJ	ArandKr	Ar	9.493E-3	5.003E-2	8.700E-2	3.244E-1	4.499E-1	7.874E-1	8.827E-1	1.098E+0	1.160E+0	1.161E+0
MADVUJ	ArandKr	Kr	2.932E-2	1.548E-1	2.668E-1	9.946E-1	1.363E+0	2.201E+0	2.382E+0	2.674E+0	2.705E+0	2.823E+0
MADWAQ	ArandKr	Ar	9.595E-3	5.040E-2	8.734E-2	3.296E-1	4.531E-1	7.771E-1	8.836E-1	9.607E-1	1.038E+0	1.138E+0
MADWAQ	ArandKr	Kr	3.048E-2	1.604E-1	2.788E-1	1.064E+0	1.461E+0	2.387E+0	2.565E+0	2.910E+0	2.888E+0	2.852E+0
MIKJAR	ArandKr	Ar	2.573E-2	1.367E-1	2.393E-1	9.805E-1	1.426E+0	3.211E+0	4.241E+0	9.355E+0	1.160E+1	1.564E+1
MIKJAR	ArandKr	Kr	7.005E-2	3.693E-1	6.464E-1	2.543E+0	3.585E+0	6.134E+0	6.784E+0	8.508E+0	8.752E+0	9.393E+0
MIZKOW	ArandKr	Ar	3.641E-3	1.996E-2	3.612E-2	1.890E-1	3.269E-1	1.118E+0	1.419E+0	1.922E+0	1.992E+0	2.148E+0
MIZKOW	ArandKr	Kr	2.928E-3	1.616E-2	2.888E-2	1.549E-1	2.714E-1	1.001E+0	1.342E+0	1.812E+0	1.871E+0	1.899E+0
MOXNUJ	ArandKr	Ar	6.360E-3	3.469E-2	6.298E-2	3.382E-1	6.023E-1	2.597E+0	3.765E+0	6.547E+0	6.874E+0	7.472E+0
MOXNUJ	ArandKr	Kr	6.493E-3	3.517E-2	6.319E-2	3.464E-1	6.170E-1	2.690E+0	3.973E+0	6.832E+0	7.568E+0	8.210E+0
NAJVUQ	ArandKr	Ar	6.221E-2	3.428E-1	6.223E-1	3.366E+0	5.975E+0	2.049E+1	2.589E+1	4.135E+1	4.724E+1	6.090E+1
NAJVUQ	ArandKr	Kr	8.147E-2	4.496E-1	8.175E-1	4.572E+0	8.309E+0	3.092E+1	3.807E+1	5.004E+1	5.262E+1	5.563E+1
NIKZAJ	ArandKr	Ar	2.682E-3	1.479E-2	2.669E-2	1.402E-1	2.425E-1	8.350E-1	1.069E+0	1.505E+0	1.629E+0	2.300E+0
NIKZAJ	ArandKr	Kr	3.966E-3	2.156E-2	3.904E-2	2.085E-1	3.658E-1	1.334E+0	1.730E+0	2.336E+0	2.410E+0	2.368E+0
NIKZAJ01	ArandKr	Ar	2.743E-3	1.502E-2	2.722E-2	1.423E-1	2.454E-1	8.411E-1	1.071E+0	1.520E+0	1.708E+0	2.473E+0
NIKZAJ01	ArandKr	Kr	4.064E-3	2.246E-2	4.030E-2	2.151E-1	3.753E-1	1.357E+0	1.755E+0	2.354E+0	2.391E+0	2.375E+0
ODONIF	ArandKr	Ar	1.263E-2	6.886E-2	1.224E-1	6.102E-1	1.030E+0	3.370E+0	4.403E+0	7.490E+0	8.564E+0	1.107E+1
ODONIF	ArandKr	Kr	7.931E-3	4.378E-2	7.892E-2	3.897E-1	6.557E-1	2.107E+0	2.771E+0	4.205E+0	4.328E+0	4.580E+0
ODOXEK	ArandKr	Ar	4.969E-3	2.625E-2	4.547E-2	1.768E-1	2.439E-1	4.067E-1	4.423E-1	4.642E-1	4.882E-1	5.158E-1
ODOXEK	ArandKr	Kr	1.589E-2	8.482E-2	1.477E-1	5.713E-1	8.016E-1	1.286E+0	1.371E+0	1.497E+0	1.490E+0	1.481E+0
OFERUN	ArandKr	Ar	7.034E-3	3.881E-2	7.032E-2	3.828E-1	6.888E-1	3.331E+0	5.237E+0	1.191E+1	1.430E+1	2.079E+1
OFERUN	ArandKr	Kr	6.443E-3	3.548E-2	6.464E-2	3.541E-1	6.381E-1	3.156E+0	5.034E+0	1.061E+1	1.187E+1	1.340E+1
OFORUX	ArandKr	Ar	1.279E-2	6.675E-2	1.153E-1	4.248E-1	5.732E-1	9.389E-1	1.050E+0	1.496E+0	1.802E+0	3.346E+0
OFORUX	ArandKr	Kr	3.689E-2	1.931E-1	3.354E-1	1.231E+0	1.675E+0	2.575E+0	2.716E+0	2.867E+0	2.880E+0	2.684E+0
PAZBOH	ArandKr	Ar	8.720E-2	4.793E-1	8.704E-1	4.599E+0	7.870E+0	2.140E+1	2.614E+1	4.085E+1	4.742E+1	6.581E+1
PAZBOH	ArandKr	Kr	1.313E-1	7.228E-1	1.318E+0	7.305E+0	1.289E+1	3.584E+1	4.135E+1	5.017E+1	5.120E+1	5.166E+1
PAZBUN	ArandKr	Ar	7.482E+0	8.410E+0	9.036E+0	1.529E+1	2.102E+1	4.429E+1	4.936E+1	5.809E+1	5.849E+1	6.034E+1
PAZBUN	ArandKr	Kr	3.654E-1	7.610E-1	1.180E+0	4.912E+0	8.246E+0	2.163E+1	2.678E+1	4.149E+1	4.850E+1	6.550E+1
PENZUE	ArandKr	Ar	8.497E-4	4.613E-3	8.386E-3	4.572E-2	8.401E-2	4.342E-1	7.378E-1	1.968E+0	2.258E+0	2.648E+0
PENZUE	ArandKr	Kr	3.208E-4	1.773E-3	3.200E-3	1.825E-2	3.221E-2	1.765E-1	3.101E-1	9.170E-1	1.083E+0	1.229E+0
QUGNOV	ArandKr	Ar	8.350E-4	4.564E-3	8.432E-3	4.542E-2	8.211E-2	4.255E-1	7.094E-1	2.005E+0	2.401E+0	2.863E+0
QUGNOV	ArandKr	Kr	2.792E-4	1.553E-3	2.873E-3	1.543E-2	2.792E-2	1.438E-1	2.429E-1	6.840E-1	7.917E-1	9.626E-1
TISGUY	ArandKr	Ar	4.689E-3	2.568E-2	4.628E-2	2.374E-1	4.010E-1	1.359E+0	1.891E+0	4.195E+0	5.055E+0	6.830E+0
TISGUY	ArandKr	Kr	6.029E-3	3.283E-2	5.944E-2	2.995E-1	5.060E-1	1.547E+0	1.926E+0	2.801E+0	3.058E+0	3.303E+0

Table 5a (continued)

TONBII	ArandKr	Ar	8.225E-3	4.159E-2	7.033E-2	2.214E-1	2.853E-1	4.411E-1	4.748E-1	6.109E-1	6.438E-1	8.522E-1
TONBII	ArandKr	Kr	3.011E-2	1.518E-1	2.556E-1	8.091E-1	1.029E+0	1.447E+0	1.539E+0	1.635E+0	1.662E+0	1.602E+0
WASNIO	ArandKr	Ar	1.232E-2	6.612E-2	1.177E-1	5.287E-1	8.167E-1	1.837E+0	2.109E+0	2.500E+0	2.636E+0	3.020E+0
WASNIO	ArandKr	Kr	1.754E-2	9.407E-2	1.674E-1	7.333E-1	1.125E+0	2.436E+0	2.787E+0	3.279E+0	3.262E+0	3.131E+0
WIYZOU	ArandKr	Ar	2.398E-3	1.310E-2	2.363E-2	1.236E-1	2.143E-1	8.077E-1	1.158E+0	2.450E+0	3.036E+0	4.668E+0
WIYZOU	ArandKr	Kr	2.847E-3	1.551E-2	2.799E-2	1.450E-1	2.483E-1	8.988E-1	1.232E+0	2.058E+0	2.257E+0	2.610E+0
WOCVUG	ArandKr	Ar	1.692E-2	8.701E-2	1.487E-1	5.054E-1	6.476E-1	9.238E-1	1.024E+0	1.512E+0	1.685E+0	2.427E+0
WOCVUG	ArandKr	Kr	5.019E-2	2.619E-1	4.566E-1	1.600E+0	2.086E+0	2.874E+0	2.965E+0	3.009E+0	3.050E+0	2.951E+0
WOPDEL	ArandKr	Ar	2.784E-2	1.386E-1	2.301E-1	7.153E-1	9.510E-1	1.710E+0	1.994E+0	3.038E+0	3.662E+0	5.051E+0
WOPDEL	ArandKr	Kr	9.891E-2	4.888E-1	8.070E-1	2.327E+0	2.897E+0	4.310E+0	4.674E+0	5.151E+0	5.122E+0	5.427E+0
XALDIY	ArandKr	Ar	5.426E-2	2.869E-1	4.983E-1	1.985E+0	2.851E+0	4.981E+0	5.430E+0	8.055E+0	1.014E+1	1.546E+1
XALDIY	ArandKr	Kr	9.862E-2	5.246E-1	9.374E-1	3.890E+0	5.470E+0	9.249E+0	1.007E+1	1.049E+1	9.899E+0	9.688E+0
XEQNIQ	ArandKr	Ar	8.634E-2	4.730E-1	8.585E-1	4.539E+0	7.758E+0	2.122E+1	2.588E+1	4.124E+1	4.677E+1	6.653E+1
XEQNIQ	ArandKr	Kr	1.294E-1	7.162E-1	1.300E+0	7.198E+0	1.269E+1	3.547E+1	4.094E+1	4.931E+1	5.109E+1	5.037E+1
XOHJUA	ArandKr	Ar	1.325E-3	7.199E-3	1.315E-2	7.174E-2	1.297E-1	6.323E-1	1.018E+0	2.343E+0	2.693E+0	3.043E+0
XOHJUA	ArandKr	Kr	3.089E-4	1.806E-3	3.225E-3	1.741E-2	3.229E-2	1.609E-1	2.706E-1	6.917E-1	7.299E-1	8.478E-1
XOVPIH	ArandKr	Ar	4.178E-4	2.295E-3	4.110E-3	2.214E-2	3.982E-2	1.837E-1	2.924E-1	7.612E-1	9.572E-1	1.638E+0
XOVPIH	ArandKr	Kr	1.721E-4	9.399E-4	1.690E-3	9.079E-3	1.646E-2	7.359E-2	1.135E-1	2.390E-1	2.734E-1	2.730E-1
YAPXIX	ArandKr	Ar	2.792E-2	1.285E-1	1.982E-1	4.513E-1	5.355E-1	8.603E-1	1.040E+0	1.737E+0	2.239E+0	3.980E+0
YAPXIX	ArandKr	Kr	1.272E-1	5.733E-1	8.919E-1	1.947E+0	2.236E+0	2.838E+0	3.005E+0	3.365E+0	3.344E+0	3.240E+0
YARYOF	ArandKr	Ar	2.044E-3	1.120E-2	2.041E-2	1.112E-1	2.002E-1	9.988E-1	1.651E+0	4.453E+0	5.506E+0	8.950E+0
YARYOF	ArandKr	Kr	1.539E-3	8.396E-3	1.519E-2	8.339E-2	1.503E-1	7.532E-1	1.254E+0	3.213E+0	3.693E+0	4.228E+0
YEYYAC	ArandKr	Ar	1.518E-2	8.226E-2	1.480E-1	7.243E-1	1.189E+0	3.733E+0	5.017E+0	1.009E+1	1.223E+1	1.868E+1
YEYYAC	ArandKr	Kr	2.519E-2	1.365E-1	2.442E-1	1.176E+0	1.893E+0	5.073E+0	6.290E+0	8.874E+0	9.421E+0	1.017E+1

Table 5b: Data for GCMC isotherm calculations using a 50:50 binary mixture of Kr and Xe.

REFCODE	PAIR	S	0.01	0.055	0.1	0.55	1	5.5	10	55	100	550
AGESIP	KrandXe	Kr	9.462E-4	5.112E-3	9.247E-3	5.063E-2	9.299E-2	4.602E-1	7.528E-1	1.611E+0	1.771E+0	1.945E+0
AGESIP	KrandXe	Xe	5.088E-6	2.705E-5	4.921E-5	2.675E-4	4.905E-4	2.622E-3	4.302E-3	1.047E-2	1.199E-2	1.374E-2
BACMOH10	KrandXe	Kr	7.506E-3	4.109E-2	7.552E-2	4.041E-1	7.127E-1	2.477E+0	3.036E+0	3.765E+0	3.847E+0	3.914E+0
BACMOH10	KrandXe	Xe	8.042E-5	4.359E-4	7.665E-4	4.436E-3	7.894E-3	3.090E-2	4.008E-2	5.498E-2	5.362E-2	6.788E-2
CAZGIT	KrandXe	Kr	3.146E-1	8.743E-1	1.055E+0	1.376E+0	1.383E+0	1.499E+0	1.654E+0	1.502E+0	1.360E+0	1.413E+0
CAZGIT	KrandXe	Xe	1.624E+0	4.098E+0	4.938E+0	6.167E+0	6.347E+0	6.449E+0	6.318E+0	6.498E+0	6.650E+0	6.629E+0
COKDAI	KrandXe	Kr	6.050E-3	3.378E-2	6.030E-2	3.216E-1	5.737E-1	2.353E+0	3.319E+0	5.595E+0	6.124E+0	7.217E+0
COKDAI	KrandXe	Xe	8.017E-4	4.403E-3	7.896E-3	4.247E-2	7.399E-2	2.913E-1	3.904E-1	4.951E-1	4.719E-1	4.236E-1
DOHYIJ	KrandXe	Kr	2.837E-3	1.530E-2	2.752E-2	1.503E-1	2.711E-1	1.277E+0	1.955E+0	3.466E+0	3.706E+0	3.937E+0
DOHYIJ	KrandXe	Xe	5.819E-6	3.038E-5	5.938E-5	3.347E-4	5.854E-4	3.079E-3	5.001E-3	9.508E-3	1.043E-2	1.044E-2
DOHYIJ01	KrandXe	Kr	6.217E-3	3.340E-2	6.074E-2	3.279E-1	5.793E-1	2.205E+0	2.861E+0	3.725E+0	3.831E+0	3.941E+0
DOHYIJ01	KrandXe	Xe	5.760E-5	3.055E-4	5.454E-4	3.097E-3	5.709E-3	2.394E-2	3.276E-2	4.392E-2	4.421E-2	3.834E-2
ECAVEK	KrandXe	Kr	1.616E-1	3.111E-1	3.619E-1	5.977E-1	6.393E-1	8.762E-1	8.339E-1	9.869E-1	1.019E+0	9.957E-1
ECAVEK	KrandXe	Xe	1.717E+0	1.985E+0	2.088E+0	2.214E+0	2.275E+0	2.231E+0	2.346E+0	2.315E+0	2.302E+0	2.360E+0
ECAVIO	KrandXe	Kr	1.687E-1	2.998E-1	3.788E-1	5.288E-1	6.463E-1	7.583E-1	8.739E-1	9.485E-1	1.015E+0	1.111E+0
ECAVIO	KrandXe	Xe	1.750E+0	2.064E+0	2.134E+0	2.337E+0	2.295E+0	2.384E+0	2.315E+0	2.360E+0	2.319E+0	2.275E+0
EVEGER	KrandXe	Kr	3.426E-2	1.516E-1	2.343E-1	6.111E-1	8.256E-1	1.711E+0	2.091E+0	3.139E+0	3.480E+0	6.131E+0
EVEGER	KrandXe	Xe	1.149E-1	4.969E-1	7.374E-1	1.482E+0	1.694E+0	2.239E+0	2.380E+0	2.573E+0	2.588E+0	1.706E+0
EXUM0Z	KrandXe	Kr	2.482E-3	1.344E-2	2.404E-2	1.344E-1	2.401E-1	1.238E+0	1.977E+0	3.532E+0	3.744E+0	3.948E+0
EXUM0Z	KrandXe	Xe	3.196E-7	1.790E-6	3.190E-6	2.058E-5	3.357E-5	1.931E-4	3.276E-4	6.961E-4	6.604E-4	7.836E-4
FIQYUA	KrandXe	Kr	2.094E-2	1.140E-1	2.027E-1	7.436E-1	9.319E-1	1.123E+0	1.125E+0	1.268E+0	1.197E+0	1.376E+0
FIQYUA	KrandXe	Xe	3.777E-2	2.090E-1	3.755E-1	1.570E+0	2.060E+0	2.709E+0	2.790E+0	2.720E+0	2.810E+0	2.707E+0
FOQSUA	KrandXe	Kr	6.339E-4	3.440E-3	6.227E-3	3.418E-2	6.169E-2	3.163E-1	5.335E-1	1.627E+0	2.061E+0	2.902E+0
FOQSUA	KrandXe	Xe	2.085E-7	1.311E-6	2.526E-6	1.367E-5	2.487E-5	1.241E-4	2.167E-4	6.596E-4	7.800E-4	8.817E-4
GATHAL	KrandXe	Kr	1.552E-2	8.451E-2	1.513E-1	7.993E-1	1.440E+0	6.273E+0	9.121E+0	1.658E+1	1.907E+1	2.677E+1
GATHAL	KrandXe	Xe	1.907E-4	1.016E-3	1.927E-3	9.642E-3	1.680E-2	6.839E-2	9.148E-2	1.277E-1	1.269E-1	8.973E-2
GIQXIO	KrandXe	Kr	8.430E-3	4.575E-2	8.257E-2	4.222E-1	7.083E-1	2.369E+0	3.184E+0	5.378E+0	6.115E+0	7.277E+0
GIQXIO	KrandXe	Xe	8.051E-4	4.383E-3	7.831E-3	3.991E-2	6.847E-2	2.281E-1	2.825E-1	4.578E-1	4.481E-1	4.832E-1
GIQXUA	KrandXe	Kr	9.088E-3	4.964E-2	8.889E-2	4.449E-1	7.611E-1	2.419E+0	3.149E+0	5.344E+0	6.041E+0	7.216E+0
GIQXUA	KrandXe	Xe	9.943E-4	5.503E-3	9.972E-3	4.912E-2	8.724E-2	2.653E-1	3.335E-1	4.877E-1	4.743E-1	5.098E-1
GIQYIP	KrandXe	Kr	9.992E-3	5.478E-2	9.855E-2	4.951E-1	8.287E-1	2.509E+0	3.234E+0	5.382E+0	5.980E+0	7.038E+0
GIQYIP	KrandXe	Xe	1.641E-3	8.921E-3	1.639E-2	8.259E-2	1.352E-1	3.933E-1	5.189E-1	6.873E-1	7.265E-1	7.368E-1
GITTIN	KrandXe	Kr	1.738E-2	9.586E-2	1.742E-1	9.554E-1	1.718E+0	6.076E+0	7.714E+0	1.313E+1	1.505E+1	2.370E+1
GITTIN	KrandXe	Xe	2.068E-2	1.140E-1	2.083E-1	1.168E+0	2.131E+0	7.647E+0	9.192E+0	1.052E+1	1.074E+1	9.397E+0

Table 5b (continued)

GIYSAJ	KrandXe	Kr	3.069E-1	8.660E-1	1.240E+0	2.612E+0	3.023E+0	3.788E+0	4.094E+0	4.750E+0	4.661E+0	6.188E+0
GIYSAJ	KrandXe	Xe	2.072E+0	3.630E+0	4.095E+0	5.662E+0	6.146E+0	6.975E+0	7.008E+0	7.085E+0	7.369E+0	6.922E+0
GOBSUM	KrandXe	Kr	1.675E-1	8.110E-1	1.308E+0	3.386E+0	4.215E+0	7.617E+0	8.608E+0	1.113E+1	1.141E+1	1.230E+1
GOBSUM	KrandXe	Xe	1.653E-1	7.963E-1	1.283E+0	3.100E+0	3.483E+0	3.422E+0	3.413E+0	2.935E+0	3.052E+0	3.060E+0
GOLQII	KrandXe	Kr	1.424E-2	7.771E-2	1.418E-1	7.305E-1	1.217E+0	2.903E+0	3.255E+0	3.599E+0	3.682E+0	3.695E+0
GOLQII	KrandXe	Xe	8.701E-4	4.904E-3	8.802E-3	4.878E-2	8.516E-2	2.235E-1	2.600E-1	3.103E-1	2.643E-1	2.965E-1
GOMSUV	KrandXe	Kr	2.398E-1	4.493E-1	5.247E-1	7.545E-1	8.064E-1	9.725E-1	1.139E+0	1.198E+0	1.203E+0	1.266E+0
GOMSUV	KrandXe	Xe	1.251E+0	1.799E+0	1.913E+0	2.079E+0	2.113E+0	2.145E+0	2.068E+0	2.103E+0	2.124E+0	2.094E+0
GUPJEG	KrandXe	Kr	1.001E-3	5.546E-3	9.840E-3	5.379E-2	9.867E-2	5.108E-1	8.545E-1	2.566E+0	3.124E+0	3.834E+0
GUPJEG	KrandXe	Xe	2.125E-8	2.817E-7	4.250E-7	2.395E-6	4.413E-6	2.318E-5	3.919E-5	1.320E-4	1.582E-4	2.065E-4
GUPJEG01	KrandXe	Kr	6.217E-4	3.500E-3	6.247E-3	3.443E-2	6.266E-2	3.302E-1	5.821E-1	2.131E+0	2.786E+0	3.752E+0
GUPJEG01	KrandXe	Xe	3.333E-9	8.333E-8	1.408E-7	6.296E-7	1.241E-6	6.826E-6	1.219E-5	4.876E-5	5.782E-5	8.340E-5
GUXQAR	KrandXe	Kr	1.898E-4	1.058E-3	1.901E-3	1.058E-2	1.903E-2	1.003E-1	1.745E-1	5.957E-1	7.374E-1	9.695E-1
GUXQAR	KrandXe	Xe	2.403E-8	1.242E-7	2.572E-7	1.365E-6	2.464E-6	1.324E-5	2.259E-5	8.225E-5	1.056E-4	1.509E-4
HAZGOF	KrandXe	Kr	1.588E-2	8.889E-2	1.578E-1	8.600E-1	1.507E+0	6.347E+0	9.060E+0	1.565E+1	1.752E+1	2.437E+1
HAZGOF	KrandXe	Xe	2.194E-4	1.165E-3	2.118E-3	1.119E-2	1.920E-2	7.169E-2	9.895E-2	1.292E-1	1.390E-1	1.154E-1
HEGNAJ	KrandXe	Kr	1.979E-1	5.617E-1	7.016E-1	1.022E+0	1.115E+0	1.357E+0	1.338E+0	2.288E+0	2.820E+0	4.343E+0
HEGNAJ	KrandXe	Xe	1.598E+0	4.323E+0	5.216E+0	6.924E+0	7.228E+0	7.587E+0	7.739E+0	7.401E+0	7.249E+0	6.824E+0
HEGNIR	KrandXe	Kr	2.183E-1	5.677E-1	6.917E-1	9.799E-1	1.074E+0	1.318E+0	1.526E+0	2.140E+0	2.884E+0	4.888E+0
HEGNIR	KrandXe	Xe	1.898E+0	4.642E+0	5.453E+0	7.004E+0	7.288E+0	7.615E+0	7.558E+0	7.562E+0	7.192E+0	6.377E+0
HEGNOX	KrandXe	Kr	2.298E-1	6.293E-1	7.734E-1	1.118E+0	1.169E+0	1.418E+0	1.424E+0	2.408E+0	3.379E+0	5.653E+0
HEGNOX	KrandXe	Xe	1.817E+0	4.644E+0	5.566E+0	7.084E+0	7.387E+0	7.579E+0	7.683E+0	7.317E+0	6.843E+0	6.152E+0
HEGNUD	KrandXe	Kr	1.953E-1	5.598E-1	6.842E-1	1.006E+0	1.096E+0	1.326E+0	1.418E+0	2.153E+0	2.674E+0	4.631E+0
HEGNUD	KrandXe	Xe	1.594E+0	4.352E+0	5.315E+0	6.983E+0	7.275E+0	7.612E+0	7.650E+0	7.436E+0	7.308E+0	6.630E+0
HEGPAL	KrandXe	Kr	2.099E-1	5.876E-1	7.507E-1	1.088E+0	1.148E+0	1.407E+0	1.413E+0	2.341E+0	2.529E+0	4.897E+0
HEGPAL	KrandXe	Xe	1.684E+0	4.382E+0	5.259E+0	6.984E+0	7.305E+0	7.558E+0	7.670E+0	7.311E+0	7.435E+0	6.434E+0
HITXUE	KrandXe	Kr	7.357E-1	2.224E+0	3.063E+0	6.050E+0	7.330E+0	9.593E+0	9.793E+0	1.129E+1	1.188E+1	1.359E+1
HITXUE	KrandXe	Xe	3.536E+0	6.460E+0	7.201E+0	8.828E+0	9.026E+0	9.340E+0	9.590E+0	9.093E+0	8.780E+0	8.249E+0
HITYEP	KrandXe	Kr	1.388E+0	5.572E+0	7.396E+0	1.066E+1	1.326E+1	3.901E+1	4.617E+1	5.709E+1	5.911E+1	6.688E+1
HITYEP	KrandXe	Xe	5.065E+0	2.028E+1	2.629E+1	3.563E+1	3.545E+1	3.016E+1	2.980E+1	2.752E+1	2.723E+1	2.399E+1
IXISAJ	KrandXe	Kr	4.063E-1	9.036E-1	1.108E+0	1.717E+0	1.932E+0	2.778E+0	2.927E+0	4.764E+0	5.724E+0	7.432E+0
IXISAJ	KrandXe	Xe	3.109E+0	6.069E+0	6.892E+0	8.440E+0	8.787E+0	9.125E+0	9.330E+0	9.072E+0	8.661E+0	8.188E+0
JOSNAG	KrandXe	Kr	1.490E-3	8.090E-3	1.450E-2	7.615E-2	1.310E-1	4.618E-1	6.114E-1	9.725E-1	1.079E+0	1.478E+0
JOSNAG	KrandXe	Xe	4.595E-5	2.517E-4	4.464E-4	2.448E-3	3.962E-3	1.413E-2	1.978E-2	2.592E-2	2.693E-2	2.261E-2
KAHMOW	KrandXe	Kr	1.669E-1	2.378E-1	2.685E-1	4.114E-1	4.642E-1	6.133E-1	7.042E-1	9.490E-1	9.666E-1	1.616E+0
KAHMOW	KrandXe	Xe	1.897E+0	2.645E+0	2.785E+0	3.213E+0	3.394E+0	3.744E+0	3.759E+0	3.935E+0	3.805E+0	3.561E+0
KAHQUG	KrandXe	Kr	3.545E-1	2.035E+0	3.808E+0	1.342E+1	1.651E+1	2.470E+1	2.806E+1	3.796E+1	4.935E+1	7.614E+1
KAHQUG	KrandXe	Xe	7.516E-1	4.473E+0	8.673E+0	3.238E+1	3.693E+1	4.229E+1	4.213E+1	4.087E+1	3.531E+1	2.747E+1
KAHRAN	KrandXe	Kr	3.800E-1	2.192E+0	4.092E+0	1.333E+1	1.606E+1	2.433E+1	2.755E+1	3.935E+1	4.808E+1	7.317E+1
KAHRAN	KrandXe	Xe	8.279E-1	4.994E+0	9.751E+0	3.367E+1	3.784E+1	4.244E+1	4.236E+1	3.925E+1	3.547E+1	2.807E+1
KAHSES	KrandXe	Kr	3.316E-1	1.904E+0	3.566E+0	1.334E+1	1.643E+1	2.495E+1	2.824E+1	4.290E+1	5.294E+1	8.003E+1
KAHSES	KrandXe	Xe	6.799E-1	4.015E+0	7.796E+0	3.183E+1	3.695E+1	4.259E+1	4.276E+1	3.903E+1	3.520E+1	2.690E+1
KAHSIW	KrandXe	Kr	3.340E-1	1.914E+0	3.585E+0	1.336E+1	1.649E+1	2.505E+1	2.822E+1	4.310E+1	5.177E+1	7.784E+1
KAHSIW	KrandXe	Xe	6.859E-1	4.071E+0	7.877E+0	3.207E+1	3.701E+1	4.253E+1	4.282E+1	3.877E+1	3.582E+1	2.824E+1
KAHSOC	KrandXe	Kr	3.428E-1	1.971E+0	3.697E+0	1.338E+1	1.630E+1	2.509E+1	2.793E+1	4.209E+1	5.021E+1	7.811E+1
KAHSOC	KrandXe	Xe	7.091E-1	4.250E+0	8.236E+0	3.237E+1	3.742E+1	4.243E+1	4.304E+1	3.947E+1	3.670E+1	2.797E+1
KAHSUI	KrandXe	Kr	3.447E-1	1.978E+0	3.714E+0	1.348E+1	1.649E+1	2.473E+1	2.769E+1	3.979E+1	5.126E+1	7.808E+1
KAHSUI	KrandXe	Xe	7.157E-1	4.256E+0	8.269E+0	3.234E+1	3.745E+1	4.291E+1	4.333E+1	4.101E+1	3.588E+1	2.808E+1
LEMNOH	KrandXe	Kr	2.978E-2	1.600E-1	2.809E-1	1.173E+0	1.693E+0	3.210E+0	3.701E+0	5.602E+0	6.266E+0	7.354E+0
LEMNOH	KrandXe	Xe	6.575E-3	3.502E-2	6.226E-2	2.659E-1	3.848E-1	6.440E-1	6.747E-1	5.797E-1	5.397E-1	4.622E-1
MADVUJ	KrandXe	Kr	9.157E-2	2.399E-1	2.985E-1	4.583E-1	4.936E-1	7.151E-1	7.867E-1	1.240E+0	1.362E+0	1.419E+0
MADVUJ	KrandXe	Xe	6.710E-1	1.659E+0	1.926E+0	2.377E+0	2.484E+0	2.576E+0	2.596E+0	2.469E+0	2.429E+0	2.514E+0
MADWAQ	KrandXe	Kr	9.566E-2	2.616E-1	3.218E-1	5.395E-1	6.185E-1	8.889E-1	9.408E-1	1.124E+0	1.078E+0	1.063E+0
MADWAQ	KrandXe	Xe	7.084E-1	1.735E+0	2.026E+0	2.510E+0	2.620E+0	2.796E+0	2.855E+0	2.834E+0	2.893E+0	2.932E+0
MIKJAR	KrandXe	Kr	2.363E-1	7.536E-1	9.726E-1	1.562E+0	1.765E+0	2.538E+0	3.314E+0	9.205E+0	1.217E+1	1.920E+1
MIKJAR	KrandXe	Xe	1.304E+0	3.859E+0	4.800E+0	6.435E+0	6.661E+0	6.858E+0	6.605E+0	5.173E+0	4.435E+0	2.630E+0
MIZKOW	KrandXe	Kr	1.189E-2	6.557E-2	1.173E-1	6.157E-1	1.048E+0	2.823E+0	3.204E+0	3.698E+0	3.748E+0	3.808E+0
MIZKOW	KrandXe	Xe	4.815E-4	2.656E-3	4.978E-3	2.671E-2	4.638E-2	1.380E-1	1.707E-1	1.875E-1	1.870E-1	1.797E-1
MOXNUJ	KrandXe	Kr	2.612E-2	1.411E-1	2.556E-1	1.338E+0	2.340E+0	7.593E+0	9.671E+0	1.324E+1	1.388E+1	1.441E+1
MOXNUJ	KrandXe	Xe	3.959E-3	2.193E-2	3.984E-2	2.076E-1	3.502E-1	9.969E-1	1.129E+0	1.266E+0	1.260E+0	1.407E+0
NAJVUQ	KrandXe	Kr	3.285E-1	1.881E+0	3.510E+0	1.341E+1	1.675E+1	2.536E+1	2.864E+1	4.546E+1	5.584E+1	8.098E+1
NAJVUQ	KrandXe	Xe	6.674E-1	3.943E+0	7.600E+0	3.141E+1	3.659E+1	4.243E+1	4.266E+1	3.762E+1	3.395E+1	2.696E+1
NIKZAJ	KrandXe	Kr	1.577E-2	8.584E-2	1.551E-1	6.955E-1	9.800E-1	1.421E+0	1.498E+0	1.557E+0	1.424E+0	1.543E+0
NIKZAJ	KrandXe	Xe	1.899E-2	1.062E-1	1.934E-1	9.447E-1	1.411E+0	2.234E+0	2.317E+0	2.417E+0	2.569E+0	2.507E+0
NIKZAJ01	KrandXe	Kr	1.634E-2	8.866E-2	1.584E-1	6.894E-1	9.484E-1	1.341E+0	1.387E+0	1.426E+0	1.497E+0	1.646E+0
NIKZAJ01	KrandXe	Xe	2.264E-2	1.229E-1	2.220E-1	1.082E+0	1.564E+0	2.353E+0	2.444E+0	2.535E+0	2.505E+0	2.447E+0
ODONIF	KrandXe	Kr	3.194E-2	1.743E-1	3.096E-1	1.502E+0	2.430E+0	6.609E+0	8.179E+0	1.115E+1	1.182E+1	1.359E+1
ODONIF	KrandXe	Xe	3.623E-4	1.996E-3	3.672E-3	1.965E-2	3.531E-2	1.383E-1	1.852E-1	2.868E-1	2.766E-1	2.032E-1

Table 5b (continued)

ODOXEK	KrandXe	Kr	5.193E-2	1.527E-1	1.942E-1	3.410E-1	4.139E-1	5.859E-1	6.080E-1	6.731E-1	6.467E-1	7.121E-1
ODOXEK	KrandXe	Xe	3.455E-1	8.575E-1	1.009E+0	1.221E+0	1.241E+0	1.282E+0	1.301E+0	1.306E+0	1.341E+0	1.285E+0
OFERUN	KrandXe	Kr	2.585E-2	1.422E-1	2.579E-1	1.385E+0	2.375E+0	6.604E+0	8.088E+0	1.244E+1	1.451E+1	2.205E+1
OFERUN	KrandXe	Xe	3.717E-2	2.052E-1	3.749E-1	2.041E+0	3.542E+0	8.858E+0	1.004E+1	1.116E+1	1.086E+1	8.884E+0
OFORUX	KrandXe	Kr	1.151E-1	3.044E-1	3.717E-1	5.691E-1	6.300E-1	7.208E-1	7.983E-1	7.752E-1	7.415E-1	1.273E+0
OFORUX	KrandXe	Xe	8.524E-1	2.016E+0	2.348E+0	2.936E+0	3.049E+0	3.211E+0	3.164E+0	3.249E+0	3.299E+0	3.001E+0
PAZBOH	KrandXe	Kr	5.325E-1	3.135E+0	5.656E+0	1.276E+1	1.458E+1	2.214E+1	2.545E+1	3.903E+1	4.739E+1	7.037E+1
PAZBOH	KrandXe	Xe	1.327E+0	8.415E+0	1.645E+1	3.887E+1	4.185E+1	4.392E+1	4.386E+1	4.085E+1	3.722E+1	2.857E+1
PAZBUN	KrandXe	Kr	8.448E+0	1.119E+1	1.386E+1	2.222E+1	2.433E+1	3.244E+1	3.583E+1	5.282E+1	5.921E+1	8.423E+1
PAZBUN	KrandXe	Xe	1.143E+0	7.144E+0	1.409E+1	3.664E+1	3.977E+1	4.191E+1	4.190E+1	3.646E+1	3.461E+1	2.453E+1
PENZUE	KrandXe	Kr	1.326E-3	7.160E-3	1.280E-2	7.235E-2	1.289E-1	7.341E-1	1.269E+0	3.174E+0	3.555E+0	3.894E+0
PENZUE	KrandXe	Xe	8.057E-6	4.632E-5	7.542E-5	4.194E-4	7.813E-4	4.542E-3	7.760E-3	2.106E-2	2.153E-2	2.597E-2
QUGNOV	KrandXe	Kr	1.138E-3	6.070E-3	1.110E-2	6.148E-2	1.103E-1	5.694E-1	9.476E-1	2.560E+0	3.056E+0	3.772E+0
QUGNOV	KrandXe	Xe	2.358E-6	1.431E-5	2.524E-5	1.384E-4	2.326E-4	1.109E-3	1.754E-3	3.026E-3	3.107E-3	2.733E-3
TISGUY	KrandXe	Kr	2.385E-2	1.256E-1	2.160E-1	7.647E-1	9.789E-1	1.401E+0	1.597E+0	3.459E+0	5.012E+0	8.486E+0
TISGUY	KrandXe	Xe	4.099E-2	2.143E-1	3.805E-1	1.347E+0	1.770E+0	2.456E+0	2.478E+0	2.063E+0	1.708E+0	9.167E-1
TONBII	KrandXe	Kr	7.803E-2	1.609E-1	1.870E-1	2.447E-1	2.600E-1	2.799E-1	3.635E-1	4.063E-1	4.706E-1	5.785E-1
TONBII	KrandXe	Xe	6.298E-1	1.245E+0	1.384E+0	1.614E+0	1.653E+0	1.742E+0	1.691E+0	1.747E+0	1.721E+0	1.661E+0
WASNIO	KrandXe	Kr	6.995E-2	3.552E-1	6.023E-1	2.025E+0	2.764E+0	4.479E+0	4.786E+0	5.286E+0	5.343E+0	5.292E+0
WASNIO	KrandXe	Xe	1.466E-2	7.384E-2	1.228E-1	3.701E-1	4.620E-1	6.262E-1	6.888E-1	6.125E-1	6.031E-1	7.011E-1
WIYZOU	KrandXe	Kr	1.132E-2	5.991E-2	1.059E-1	4.480E-1	6.795E-1	1.583E+0	1.952E+0	3.163E+0	3.676E+0	5.627E+0
WIYZOU	KrandXe	Xe	1.163E-2	6.123E-2	1.073E-1	4.356E-1	6.216E-1	1.114E+0	1.219E+0	1.259E+0	1.235E+0	9.740E-1
WOCVUG	KrandXe	Kr	1.899E-1	7.017E-1	9.381E-1	1.252E+0	1.351E+0	1.444E+0	1.352E+0	1.441E+0	1.561E+0	2.126E+0
WOCVUG	KrandXe	Xe	3.320E-1	1.258E+0	1.675E+0	2.432E+0	2.473E+0	2.532E+0	2.644E+0	2.630E+0	2.575E+0	2.322E+0
WOPDEL	KrandXe	Kr	2.106E-1	4.146E-1	5.053E-1	1.077E+0	1.385E+0	2.473E+0	2.784E+0	3.619E+0	3.659E+0	4.796E+0
WOPDEL	KrandXe	Xe	1.979E+0	3.213E+0	3.442E+0	3.797E+0	3.905E+0	3.953E+0	3.983E+0	4.002E+0	4.022E+0	3.439E+0
XALDIY	KrandXe	Kr	3.902E-1	1.821E+0	2.766E+0	4.915E+0	5.371E+0	5.489E+0	5.286E+0	6.252E+0	5.999E+0	7.121E+0
XALDIY	KrandXe	Xe	5.533E-1	2.675E+0	4.362E+0	8.633E+0	9.237E+0	1.030E+1	1.061E+1	9.891E+0	1.025E+1	9.838E+0
XEQNIQ	KrandXe	Kr	5.258E-1	3.094E+0	5.608E+0	1.255E+1	1.428E+1	2.133E+1	2.435E+1	3.983E+1	4.575E+1	7.284E+1
XEQNIQ	KrandXe	Xe	1.308E+0	8.352E+0	1.625E+1	3.894E+1	4.185E+1	4.415E+1	4.422E+1	3.961E+1	3.784E+1	2.681E+1
XOHJUA	KrandXe	Kr	1.291E-3	7.149E-3	1.273E-2	7.116E-2	1.284E-1	6.736E-1	1.164E+0	2.998E+0	3.446E+0	3.886E+0
XOHJUA	KrandXe	Xe	8.625E-7	4.848E-6	9.140E-6	4.882E-5	8.806E-5	4.842E-4	8.203E-4	2.634E-3	2.851E-3	3.054E-3
XOVPIH	KrandXe	Kr	6.984E-4	3.767E-3	6.850E-3	3.688E-2	6.452E-2	2.803E-1	4.155E-1	8.154E-1	9.120E-1	1.149E+0
XOVPIH	KrandXe	Xe	8.198E-6	4.480E-5	8.572E-5	4.545E-4	7.896E-4	3.396E-3	5.106E-3	1.022E-2	1.070E-2	1.104E-2
YAPXIX	KrandXe	Kr	1.676E-1	2.423E-1	2.531E-1	3.996E-1	4.339E-1	5.407E-1	6.479E-1	7.566E-1	9.935E-1	1.454E+0
YAPXIX	KrandXe	Xe	2.005E+0	2.680E+0	2.844E+0	3.269E+0	3.462E+0	3.827E+0	3.819E+0	3.910E+0	3.748E+0	3.596E+0
YARYOF	KrandXe	Kr	6.131E-3	3.372E-2	6.085E-2	3.297E-1	5.850E-1	2.339E+0	3.063E+0	4.560E+0	5.134E+0	7.216E+0
YARYOF	KrandXe	Xe	5.288E-3	2.909E-2	5.305E-2	2.876E-1	5.230E-1	2.231E+0	2.962E+0	3.887E+0	3.953E+0	3.724E+0
YEYYAC	KrandXe	Kr	9.659E-2	4.437E-1	6.991E-1	1.916E+0	2.524E+0	4.603E+0	5.575E+0	1.088E+1	1.349E+1	2.060E+1
YEYYAC	KrandXe	Xe	3.243E-1	1.435E+0	2.180E+0	4.633E+0	5.379E+0	6.755E+0	6.835E+0	5.737E+0	5.091E+0	3.374E+0

Table 5c: Data for GCMC isotherm calculations using a 50:50 binary mixture of Xe and Rn.

REFCODE	PAIR	S	0.01	0.055	0.1	0.55	1	5.5	10	55	100	550
AGESIP	XeandRd	Xe	1.930E-5	1.078E-4	1.911E-4	1.080E-3	1.980E-3	1.068E-2	1.978E-2	1.097E-1	2.059E-1	9.772E-1
AGESIP	XeandRd	Rd	2.211E-6	1.274E-5	2.206E-5	1.253E-4	2.340E-4	1.247E-3	2.339E-3	1.334E-2	2.514E-2	1.367E-1
BACMOH10	XeandRd	Xe	3.204E-4	1.711E-3	3.246E-3	1.745E-2	3.165E-2	1.791E-1	3.329E-1	1.841E+0	2.401E+0	2.977E+0
BACMOH10	XeandRd	Rd	6.842E-5	3.737E-4	6.694E-4	3.736E-3	6.806E-3	4.043E-2	7.604E-2	4.972E-1	6.937E-1	8.774E-1
CAZGIT	XeandRd	Xe	9.001E-1	9.930E-1	1.041E+0	1.082E+0	1.042E+0	8.353E-1	9.997E-1	1.039E+0	1.057E+0	1.125E+0
CAZGIT	XeandRd	Rd	6.134E+0	6.809E+0	6.844E+0	6.899E+0	6.947E+0	7.163E+0	6.999E+0	6.961E+0	6.943E+0	6.875E+0
COKDAI	XeandRd	Xe	3.185E-3	1.749E-2	3.207E-2	1.689E-1	2.978E-1	1.154E+0	1.603E+0	2.634E+0	2.943E+0	3.580E+0
COKDAI	XeandRd	Rd	2.280E-3	1.252E-2	2.216E-2	1.187E-1	2.094E-1	8.183E-1	1.124E+0	1.772E+0	1.858E+0	1.946E+0
DOHYIJ	XeandRd	Xe	2.362E-5	1.311E-4	2.359E-4	1.269E-3	2.330E-3	1.311E-2	2.463E-2	1.334E-1	2.463E-1	1.371E+0
DOHYIJ	XeandRd	Rd	2.166E-6	1.125E-5	2.214E-5	1.177E-4	2.284E-4	1.172E-3	2.222E-3	1.229E-2	2.357E-2	1.453E-1
DOHYIJ01	XeandRd	Xe	2.224E-4	1.239E-3	2.263E-3	1.209E-2	2.242E-2	1.269E-1	2.288E-1	1.348E+0	2.032E+0	2.911E+0
DOHYIJ01	XeandRd	Rd	4.344E-5	2.423E-4	4.543E-4	2.566E-3	4.611E-3	2.646E-2	5.023E-2	3.263E-1	5.330E-1	8.416E-1
ECAVEK	XeandRd	Xe	2.432E-1	3.304E-1	2.933E-1	3.391E-1	3.025E-1	2.583E-1	5.319E-1	6.264E-1	6.014E-1	6.780E-1
ECAVEK	XeandRd	Rd	2.197E+0	2.424E+0	2.555E+0	2.629E+0	2.685E+0	2.775E+0	2.547E+0	2.563E+0	2.623E+0	2.635E+0
ECAVIO	XeandRd	Xe	2.165E-1	2.497E-1	2.934E-1	3.059E-1	2.838E-1	2.436E-1	2.529E-1	4.716E-1	4.940E-1	4.925E-1
ECAVIO	XeandRd	Rd	2.337E+0	2.598E+0	2.609E+0	2.681E+0	2.716E+0	2.823E+0	2.848E+0	2.802E+0	2.807E+0	2.793E+0
EVEGER	XeandRd	Xe	2.706E-1	5.071E-1	5.844E-1	9.067E-1	1.064E+0	1.509E+0	1.668E+0	1.837E+0	1.745E+0	1.947E+0
EVEGER	XeandRd	Rd	7.796E-1	1.428E+0	1.637E+0	2.332E+0	2.612E+0	3.438E+0	3.619E+0	3.985E+0	4.149E+0	4.040E+0

Table 5c (continued)

EXUM0Z	XeandRd	Xe	1.266E-6	6.832E-6	1.368E-5	7.289E-5	1.350E-4	7.338E-4	1.365E-3	7.222E-3	1.336E-2	7.404E-2
EXUM0Z	XeandRd	Rd	1.750E-8	1.550E-7	2.846E-7	1.489E-6	2.831E-6	1.512E-5	2.962E-5	1.535E-4	2.744E-4	1.622E-3
FIQYUA	XeandRd	Xe	1.599E-1	6.372E-1	7.534E-1	8.101E-1	9.182E-1	8.959E-1	8.865E-1	8.106E-1	8.009E-1	7.979E-1
FIQYUA	XeandRd	Rd	4.385E-1	2.078E+0	2.566E+0	3.083E+0	3.020E+0	3.092E+0	3.107E+0	3.188E+0	3.198E+0	3.202E+0
FOQSUA	XeandRd	Xe	1.037E-6	5.902E-6	1.034E-5	5.541E-5	1.025E-4	5.500E-4	1.002E-3	5.449E-3	9.962E-3	5.490E-2
FOQSUA	XeandRd	Rd	1.650E-8	2.090E-7	2.930E-7	1.486E-6	3.129E-6	1.599E-5	2.783E-5	1.538E-4	2.840E-4	1.535E-3
GATHAL	XeandRd	Xe	6.999E-4	4.065E-3	7.322E-3	3.951E-2	7.394E-2	3.796E-1	6.810E-1	2.831E+0	4.100E+0	8.666E+0
GATHAL	XeandRd	Rd	1.764E-4	9.524E-4	1.710E-3	9.521E-3	1.757E-2	8.877E-2	1.598E-1	6.650E-1	9.433E-1	1.659E+0
GIQXIO	XeandRd	Xe	3.212E-3	1.707E-2	3.216E-2	1.670E-1	2.907E-1	1.110E+0	1.499E+0	2.294E+0	2.374E+0	2.767E+0
GIQXIO	XeandRd	Rd	1.925E-3	1.050E-2	1.881E-2	1.037E-1	1.800E-1	6.875E-1	9.430E-1	1.359E+0	1.473E+0	1.570E+0
GIQXUA	XeandRd	Xe	4.105E-3	2.179E-2	3.942E-2	2.097E-1	3.551E-1	1.226E+0	1.608E+0	2.195E+0	2.340E+0	2.536E+0
GIQXUA	XeandRd	Rd	2.687E-3	1.421E-2	2.601E-2	1.329E-1	2.363E-1	8.343E-1	1.062E+0	1.541E+0	1.548E+0	1.738E+0
GIQYIP	XeandRd	Xe	6.748E-3	3.679E-2	6.586E-2	3.264E-1	5.388E-1	1.452E+0	1.778E+0	2.046E+0	2.207E+0	2.690E+0
GIQYIP	XeandRd	Rd	5.373E-3	2.893E-2	5.173E-2	2.597E-1	4.363E-1	1.223E+0	1.403E+0	1.869E+0	1.839E+0	1.963E+0
GITTIN	XeandRd	Xe	8.336E-2	4.731E-1	8.832E-1	4.219E+0	5.036E+0	6.311E+0	6.789E+0	7.610E+0	7.282E+0	8.874E+0
GITTIN	XeandRd	Rd	1.108E-1	6.458E-1	1.248E+0	7.811E+0	9.990E+0	1.404E+1	1.464E+1	1.560E+1	1.635E+1	1.576E+1
GIYSAJ	XeandRd	Xe	7.832E-1	1.478E+0	1.716E+0	2.414E+0	2.293E+0	2.635E+0	2.433E+0	2.910E+0	2.844E+0	3.007E+0
GIYSAJ	XeandRd	Rd	4.192E+0	6.066E+0	6.833E+0	7.822E+0	8.284E+0	8.528E+0	8.862E+0	8.655E+0	8.787E+0	8.832E+0
GOBSUM	XeandRd	Xe	5.966E-1	1.499E+0	1.638E+0	1.794E+0	1.907E+0	2.049E+0	2.548E+0	3.783E+0	4.672E+0	5.641E+0
GOBSUM	XeandRd	Rd	1.580E+0	4.627E+0	5.367E+0	6.060E+0	6.056E+0	6.290E+0	6.379E+0	7.189E+0	6.989E+0	7.236E+0
GOLQII	XeandRd	Xe	3.547E-3	1.981E-2	3.614E-2	2.055E-1	3.889E-1	1.598E+0	1.886E+0	2.068E+0	2.345E+0	2.106E+0
GOLQII	XeandRd	Rd	2.112E-3	1.148E-2	2.164E-2	1.271E-1	2.442E-1	1.171E+0	1.472E+0	1.830E+0	1.596E+0	1.883E+0
GOMSUW	XeandRd	Xe	3.024E-1	3.007E-1	4.028E-1	4.559E-1	4.236E-1	3.964E-1	5.235E-1	5.020E-1	4.475E-1	4.832E-1
GOMSUW	XeandRd	Rd	2.182E+0	2.504E+0	2.468E+0	2.513E+0	2.568E+0	2.640E+0	2.540E+0	2.655E+0	2.761E+0	2.819E+0
GUPJEG	XeandRd	Xe	1.850E-7	9.279E-7	1.524E-6	9.206E-6	1.701E-5	9.569E-5	1.760E-4	9.460E-4	1.743E-3	9.585E-3
GUPJEG	XeandRd	Rd	3.333E-9	7.250E-8	1.083E-7	4.438E-7	7.979E-7	4.653E-6	8.210E-6	4.448E-5	8.526E-5	4.393E-4
GUPJEG01	XeandRd	Xe	6.833E-8	2.363E-7	4.429E-7	2.653E-6	4.951E-6	2.856E-5	5.143E-5	2.716E-4	5.066E-4	2.740E-3
GUPJEG01	XeandRd	Rd	1.854E-7	1.063E-6	1.914E-6	1.141E-5	1.981E-5	1.149E-4	2.017E-4	1.055E-3	2.163E-3	1.066E-2
GUXQAR	XeandRd	Xe	1.158E-7	5.604E-7	1.064E-6	5.550E-6	1.014E-5	5.553E-5	9.943E-5	5.522E-4	9.858E-4	5.400E-3
GUXQAR	XeandRd	Rd	1.111E-9	1.222E-8	1.500E-8	1.047E-7	2.315E-7	1.269E-6	2.222E-6	1.166E-5	2.138E-5	1.155E-4
HAZGOF	XeandRd	Xe	9.008E-4	4.613E-3	8.475E-3	4.616E-2	8.450E-2	4.541E-1	7.787E-1	3.047E+0	4.330E+0	8.252E+0
HAZGOF	XeandRd	Rd	2.014E-4	1.154E-3	2.071E-3	1.159E-2	2.058E-2	1.084E-1	1.945E-1	7.556E-1	1.060E+0	1.707E+0
HEGNAJ	XeandRd	Xe	1.026E+0	1.235E+0	1.280E+0	1.397E+0	1.402E+0	1.118E+0	1.570E+0	1.592E+0	1.578E+0	1.922E+0
HEGNAJ	XeandRd	Rd	6.096E+0	7.149E+0	7.334E+0	7.518E+0	7.555E+0	7.875E+0	7.428E+0	7.424E+0	7.451E+0	7.215E+0
HEGNIR	XeandRd	Xe	9.905E-1	1.161E+0	1.192E+0	1.132E+0	1.076E+0	1.213E+0	1.446E+0	1.707E+0	1.506E+0	1.044E+0
HEGNIR	XeandRd	Rd	6.225E+0	7.235E+0	7.428E+0	7.790E+0	7.879E+0	7.778E+0	7.553E+0	7.298E+0	7.517E+0	8.066E+0
HEGNOX	XeandRd	Xe	1.084E+0	1.171E+0	1.168E+0	1.397E+0	1.358E+0	9.022E-1	9.594E-1	1.194E+0	1.219E+0	1.846E+0
HEGNOX	XeandRd	Rd	6.377E+0	7.438E+0	7.611E+0	7.555E+0	7.615E+0	8.095E+0	8.040E+0	7.814E+0	7.796E+0	7.229E+0
HEGNUD	XeandRd	Xe	1.047E+0	1.240E+0	1.144E+0	1.323E+0	1.571E+0	1.531E+0	1.679E+0	1.574E+0	1.397E+0	1.647E+0
HEGNUD	XeandRd	Rd	6.151E+0	7.192E+0	7.508E+0	7.605E+0	7.390E+0	7.464E+0	7.319E+0	7.432E+0	7.617E+0	7.445E+0
HEGPAL	XeandRd	Xe	1.040E+0	1.283E+0	1.286E+0	1.292E+0	1.282E+0	1.884E+0	1.240E+0	1.227E+0	1.394E+0	1.732E+0
HEGPAL	XeandRd	Rd	6.183E+0	7.218E+0	7.415E+0	7.650E+0	7.685E+0	7.110E+0	7.758E+0	7.778E+0	7.616E+0	7.326E+0
HITXUE	XeandRd	Xe	1.480E+0	2.249E+0	2.497E+0	3.297E+0	3.393E+0	3.600E+0	4.785E+0	4.988E+0	4.703E+0	4.836E+0
HITXUE	XeandRd	Rd	8.151E+0	1.026E+1	1.127E+1	1.318E+1	1.378E+1	1.464E+1	1.377E+1	1.448E+1	1.501E+1	1.508E+1
HITYEP	XeandRd	Xe	5.425E+0	5.463E+0	5.973E+0	4.032E+0	5.659E+0	6.170E+0	5.872E+0	7.386E+0	8.989E+0	3.254E+1
HITYEP	XeandRd	Rd	4.012E+1	4.216E+1	4.181E+1	4.396E+1	4.236E+1	4.198E+1	4.247E+1	4.291E+1	4.298E+1	4.767E+1
IXISAJ	XeandRd	Xe	1.152E+0	1.412E+0	1.548E+0	1.767E+0	1.565E+0	2.095E+0	2.489E+0	2.218E+0	2.478E+0	2.477E+0
IXISAJ	XeandRd	Rd	7.790E+0	8.923E+0	9.141E+0	9.695E+0	1.011E+1	9.841E+0	9.479E+0	9.801E+0	9.568E+0	9.819E+0
JOSNAG	XeandRd	Xe	1.860E-4	1.010E-3	1.850E-3	1.016E-2	1.833E-2	9.207E-2	1.525E-1	4.577E-1	5.536E-1	7.041E-1
JOSNAG	XeandRd	Rd	6.147E-5	3.370E-4	6.279E-4	3.299E-3	6.063E-3	3.045E-2	5.021E-2	1.521E-1	1.839E-1	2.394E-1
KAHMOW	XeandRd	Xe	2.740E+0	3.131E+0	3.222E+0	3.361E+0	3.373E+0	3.417E+0	3.444E+0	3.454E+0	3.421E+0	3.621E+0
KAHMOW	XeandRd	Rd	1.284E-1	4.845E-1	6.417E-1	9.702E-1	1.052E+0	1.141E+0	1.138E+0	1.193E+0	1.243E+0	1.134E+0
KAHQUG	XeandRd	Xe	4.128E+0	1.022E+1	1.069E+1	1.208E+1	1.248E+1	1.518E+1	1.462E+1	1.407E+1	1.686E+1	1.766E+1
KAHQUG	XeandRd	Rd	1.091E+1	4.101E+1	4.436E+1	5.087E+1	5.262E+1	5.420E+1	5.556E+1	5.754E+1	5.501E+1	5.515E+1
KAHRAN	XeandRd	Xe	4.855E+0	9.613E+0	1.008E+1	1.198E+1	1.215E+1	1.335E+1	1.477E+1	1.380E+1	1.494E+1	1.422E+1
KAHRAN	XeandRd	Rd	1.418E+1	4.241E+1	4.505E+1	4.985E+1	5.171E+1	5.558E+1	5.529E+1	5.785E+1	5.686E+1	5.826E+1
KAHSES	XeandRd	Xe	3.633E+0	1.027E+1	1.064E+1	1.298E+1	1.290E+1	1.364E+1	1.453E+1	1.550E+1	1.483E+1	1.736E+1
KAHSES	XeandRd	Rd	9.112E+0	4.087E+1	4.438E+1	5.026E+1	5.253E+1	5.641E+1	5.634E+1	5.645E+1	5.756E+1	5.692E+1
KAHSIW	XeandRd	Xe	3.670E+0	1.018E+1	1.072E+1	1.232E+1	1.308E+1	1.480E+1	1.301E+1	1.256E+1	1.463E+1	1.579E+1
KAHSIW	XeandRd	Rd	9.328E+0	4.105E+1	4.432E+1	5.094E+1	5.256E+1	5.508E+1	5.778E+1	5.936E+1	5.749E+1	5.820E+1
KAHSOC	XeandRd	Xe	3.878E+0	1.007E+1	1.083E+1	1.178E+1	1.258E+1	1.372E+1	1.366E+1	1.484E+1	1.590E+1	1.566E+1
KAHSOC	XeandRd	Rd	9.954E+0	4.153E+1	4.439E+1	5.166E+1	5.295E+1	5.629E+1	5.718E+1	5.702E+1	5.629E+1	5.819E+1
KAHSUI	XeandRd	Xe	3.894E+0	1.021E+1	1.079E+1	1.177E+1	1.346E+1	1.355E+1	1.444E+1	1.539E+1	1.714E+1	1.812E+1
KAHSUI	XeandRd	Rd	9.968E+0	4.147E+1	4.465E+1	5.198E+1	5.244E+1	5.650E+1	5.644E+1	5.658E+1	5.502E+1	5.589E+1
LEMNOH	XeandRd	Xe	2.630E-2	1.393E-1	2.464E-1	9.424E-1	1.269E+0	1.810E+0	1.838E+0	2.001E+0	1.976E+0	2.332E+0
LEMNOH	XeandRd	Rd	2.474E-2	1.335E-1	2.363E-1	9.646E-1	1.296E+0	1.872E+0	1.984E+0	1.997E+0	2.070E+0	2.022E+0
MADVUJ	XeandRd	Xe	3.293E-1	3.924E-1	4.282E-1	4.862E-1	4.635E-1	5.136E-1	4.461E-1	6.440E-1	7.596E-1	8.361E-1
MADVUJ	XeandRd	Rd	2.229E+0	2.501E+0	2.554E+0	2.655E+0	2.717E+0	2.752E+0	2.847E+0	2.853E+0	2.799E+0	2.871E+0

Table 5c (continued)

MADWAQ	XeandRd	Xe	3.639E-1	4.574E-1	4.290E-1	5.076E-1	5.318E-1	8.301E-1	5.846E-1	7.343E-1	7.570E-1	7.901E-1
MADWAQ	XeandRd	Rd	2.284E+0	2.581E+0	2.725E+0	2.944E+0	3.036E+0	2.984E+0	3.325E+0	3.240E+0	3.230E+0	3.206E+0
MIKJAR	XeandRd	Xe	1.089E+0	1.291E+0	1.304E+0	1.305E+0	1.528E+0	1.669E+0	1.591E+0	8.950E-1	1.283E+0	1.286E+0
MIKJAR	XeandRd	Rd	5.723E+0	6.987E+0	7.259E+0	7.597E+0	7.411E+0	7.319E+0	7.411E+0	8.134E+0	7.767E+0	7.944E+0
MIZKOW	XeandRd	Xe	1.970E-3	1.093E-2	1.923E-2	1.069E-1	2.060E-1	1.130E+0	1.678E+0	2.297E+0	2.416E+0	2.374E+0
MIZKOW	XeandRd	Rd	9.023E-4	4.956E-3	9.228E-3	5.236E-2	9.590E-2	6.023E-1	9.750E-1	1.486E+0	1.465E+0	1.603E+0
MOXNUJ	XeandRd	Xe	1.606E-2	8.770E-2	1.573E-1	7.807E-1	1.311E+0	3.614E+0	4.507E+0	6.034E+0	6.459E+0	8.678E+0
MOXNUJ	XeandRd	Rd	1.278E-2	6.937E-2	1.268E-1	6.366E-1	1.048E+0	2.872E+0	3.320E+0	4.422E+0	4.658E+0	4.165E+0
NAJVUQ	XeandRd	Xe	3.475E+0	1.032E+1	1.127E+1	1.292E+1	1.295E+1	1.345E+1	1.349E+1	1.402E+1	1.675E+1	1.693E+1
NAJVUQ	XeandRd	Rd	8.458E+0	4.036E+1	4.382E+1	5.084E+1	5.310E+1	5.660E+1	5.720E+1	5.807E+1	5.555E+1	5.831E+1
NIKZAJ	XeandRd	Xe	7.972E-2	4.394E-1	6.717E-1	9.428E-1	1.011E+0	9.835E-1	8.574E-1	1.043E+0	9.494E-1	1.003E+0
NIKZAJ	XeandRd	Rd	1.746E-1	1.093E+0	1.783E+0	2.807E+0	2.847E+0	2.993E+0	3.131E+0	2.955E+0	3.049E+0	2.997E+0
NIKZAJ01	XeandRd	Xe	9.198E-2	4.870E-1	6.933E-1	9.174E-1	9.976E-1	9.361E-1	9.433E-1	9.120E-1	1.091E+0	1.000E+0
NIKZAJ01	XeandRd	Rd	2.122E-1	1.280E+0	1.981E+0	2.866E+0	2.884E+0	3.043E+0	3.046E+0	3.086E+0	2.907E+0	3.000E+0
ODONIF	XeandRd	Xe	1.498E-3	8.049E-3	1.482E-2	8.413E-2	1.448E-1	7.943E-1	1.412E+0	5.309E+0	6.683E+0	8.405E+0
ODONIF	XeandRd	Rd	4.468E-4	2.321E-3	4.289E-3	2.443E-2	4.408E-2	2.385E-1	4.284E-1	1.633E+0	2.178E+0	2.942E+0
ODOXEK	XeandRd	Xe	1.800E-1	2.170E-1	2.565E-1	2.935E-1	3.008E-1	3.574E-1	4.137E-1	3.894E-1	4.385E-1	3.351E-1
ODOXEK	XeandRd	Rd	1.126E+0	1.279E+0	1.283E+0	1.345E+0	1.374E+0	1.409E+0	1.388E+0	1.491E+0	1.471E+0	1.637E+0
OFERUN	XeandRd	Xe	1.506E-1	8.581E-1	1.579E+0	4.464E+0	4.970E+0	5.671E+0	6.174E+0	6.826E+0	7.265E+0	7.601E+0
OFERUN	XeandRd	Rd	2.245E-1	1.343E+0	2.617E+0	9.650E+0	1.174E+1	1.556E+1	1.566E+1	1.619E+1	1.605E+1	1.651E+1
OFORUX	XeandRd	Xe	4.180E-1	5.026E-1	5.446E-1	5.859E-1	5.776E-1	7.383E-1	5.150E-1	4.973E-1	5.888E-1	6.333E-1
OFORUX	XeandRd	Rd	2.685E+0	3.143E+0	3.233E+0	3.365E+0	3.394E+0	3.256E+0	3.483E+0	3.520E+0	3.411E+0	3.367E+0
PAZBOH	XeandRd	Xe	7.557E+0	9.181E+0	9.488E+0	1.028E+1	1.032E+1	1.214E+1	1.475E+1	1.438E+1	1.665E+1	1.809E+1
PAZBOH	XeandRd	Rd	3.198E+1	4.619E+1	4.790E+1	5.107E+1	5.214E+1	5.280E+1	5.139E+1	5.561E+1	5.477E+1	5.702E+1
PAZBUN	XeandRd	Xe	6.815E+0	9.654E+0	9.854E+0	1.108E+1	1.075E+1	1.021E+1	1.515E+1	1.535E+1	1.456E+1	1.676E+1
PAZBUN	XeandRd	Rd	2.493E+1	4.468E+1	4.684E+1	4.995E+1	5.128E+1	5.442E+1	5.051E+1	5.430E+1	5.655E+1	5.779E+1
PENZUE	XeandRd	Xe	3.324E-5	1.666E-4	3.185E-4	1.763E-3	3.226E-3	1.794E-2	3.115E-2	1.754E-1	3.138E-1	1.443E+0
PENZUE	XeandRd	Rd	4.966E-6	2.520E-5	4.781E-5	2.461E-4	4.735E-4	2.536E-3	4.582E-3	2.527E-2	4.657E-2	2.096E-1
QUGNOV	XeandRd	Xe	9.753E-6	5.194E-5	9.905E-5	5.337E-4	9.684E-4	5.607E-3	1.009E-2	5.319E-2	9.347E-2	4.164E-1
QUGNOV	XeandRd	Rd	8.622E-7	4.438E-6	8.395E-6	4.462E-5	8.516E-5	4.457E-4	8.181E-4	4.558E-3	7.904E-3	3.374E-2
TISGUY	XeandRd	Xe	1.561E-1	5.525E-1	6.762E-1	8.849E-1	9.028E-1	9.122E-1	8.587E-1	1.063E+0	7.876E-1	6.287E-1
TISGUY	XeandRd	Rd	4.519E-1	1.772E+0	2.309E+0	2.912E+0	2.983E+0	3.066E+0	3.130E+0	2.935E+0	3.212E+0	3.372E+0
TONBII	XeandRd	Xe	2.121E-1	2.018E-1	2.258E-1	2.782E-1	2.387E-1	2.424E-1	2.448E-1	3.180E-1	3.857E-1	4.382E-1
TONBII	XeandRd	Rd	1.544E+0	1.725E+0	1.731E+0	1.711E+0	1.758E+0	1.768E+0	1.769E+0	1.790E+0	1.711E+0	1.763E+0
WASNIO	XeandRd	Xe	5.703E-2	2.527E-1	3.876E-1	8.663E-1	1.114E+0	1.830E+0	2.019E+0	2.988E+0	3.099E+0	3.383E+0
WASNIO	XeandRd	Rd	8.035E-2	3.497E-1	5.279E-1	1.137E+0	1.277E+0	1.812E+0	2.062E+0	2.211E+0	2.406E+0	2.497E+0
WIYZOU	XeandRd	Xe	4.467E-2	2.028E-1	3.081E-1	6.755E-1	8.026E-1	1.267E+0	1.385E+0	1.517E+0	1.565E+0	1.580E+0
WIYZOU	XeandRd	Rd	7.713E-2	3.478E-1	5.330E-1	1.153E+0	1.342E+0	1.890E+0	2.069E+0	2.367E+0	2.379E+0	2.467E+0
WOCVUG	XeandRd	Xe	5.567E-1	7.390E-1	7.298E-1	7.033E-1	7.877E-1	8.894E-1	9.785E-1	1.074E+0	1.034E+0	1.087E+0
WOCVUG	XeandRd	Rd	2.385E+0	3.024E+0	3.135E+0	3.273E+0	3.198E+0	3.108E+0	3.019E+0	2.925E+0	2.965E+0	2.913E+0
WOPDEL	XeandRd	Xe	4.518E-1	5.354E-1	5.947E-1	9.547E-1	1.039E+0	1.313E+0	1.466E+0	1.735E+0	1.903E+0	2.318E+0
WOPDEL	XeandRd	Rd	3.511E+0	3.729E+0	3.852E+0	4.333E+0	4.633E+0	5.081E+0	5.113E+0	5.275E+0	5.248E+0	5.050E+0
XALDIY	XeandRd	Xe	1.869E+0	2.898E+0	2.492E+0	3.194E+0	3.462E+0	3.381E+0	3.329E+0	2.885E+0	3.249E+0	3.728E+0
XALDIY	XeandRd	Rd	7.167E+0	1.176E+1	1.290E+1	1.267E+1	1.246E+1	1.261E+1	1.266E+1	1.311E+1	1.275E+1	1.227E+1
XEQNIQ	XeandRd	Xe	7.497E+0	9.061E+0	9.521E+0	1.041E+1	1.098E+1	1.106E+1	1.308E+1	1.506E+1	1.552E+1	1.853E+1
XEQNIQ	XeandRd	Rd	3.217E+1	4.637E+1	4.777E+1	5.081E+1	5.108E+1	5.330E+1	5.207E+1	5.396E+1	5.492E+1	5.646E+1
XOHJUA	XeandRd	Xe	3.621E-6	1.954E-5	3.532E-5	1.901E-4	3.570E-4	1.965E-3	3.456E-3	1.923E-2	3.420E-2	1.997E-1
XOHJUA	XeandRd	Rd	1.419E-7	9.238E-7	1.569E-6	8.886E-6	1.567E-5	8.675E-5	1.629E-4	8.795E-4	1.655E-3	9.398E-3
XOVPIH	XeandRd	Xe	3.446E-5	1.835E-4	3.262E-4	1.850E-3	3.328E-3	1.826E-2	3.241E-2	1.561E-1	2.528E-1	5.929E-1
XOVPIH	XeandRd	Rd	5.935E-6	3.453E-5	6.355E-5	3.583E-4	6.568E-4	3.558E-3	6.253E-3	3.048E-2	4.903E-2	1.216E-1
YAPXIX	XeandRd	Xe	2.790E+0	3.151E+0	3.226E+0	3.360E+0	3.367E+0	3.407E+0	3.377E+0	3.455E+0	3.421E+0	3.548E+0
YAPXIX	XeandRd	Rd	1.486E-1	5.278E-1	6.967E-1	9.883E-1	1.062E+0	1.156E+0	1.207E+0	1.181E+0	1.228E+0	1.198E+0
YARYOF	XeandRd	Xe	2.125E-2	1.186E-1	2.149E-1	1.166E+0	1.780E+0	2.444E+0	2.534E+0	2.605E+0	2.553E+0	2.497E+0
YARYOF	XeandRd	Rd	3.129E-2	1.756E-1	3.228E-1	1.986E+0	3.294E+0	5.091E+0	5.204E+0	5.353E+0	5.428E+0	5.530E+0
YEYYAC	XeandRd	Xe	8.026E-1	1.598E+0	1.909E+0	2.866E+0	3.042E+0	3.198E+0	3.193E+0	3.908E+0	3.630E+0	4.694E+0
YEYYAC	XeandRd	Rd	2.332E+0	4.564E+0	5.300E+0	7.404E+0	7.876E+0	8.612E+0	8.736E+0	8.327E+0	8.788E+0	9.046E+0

APPENDIX F: PROOF IAST IS EXACT AT LOW LOADING

One of the first steps of IAST is evaluating fugacities at which the grand potential of each adsorbing phase is equal. In many other works^{17, 36b, 37} it has been shown that for IAST the grand potential is given by

$$\Psi_i = \int_0^{f_i^0} n_i^0(t) d\ln(t) \quad 8$$

where f_i^0 is the pure phase fugacity of component 'i', n_i^0 is the absorbed amount of component 'i', and 't' is simply an integration dummy variable. At low pressures, we can substitute fugacity with pressure, and we can assume that the absorbed amount can be described by the pressure and the Henry's constant, so that for a binary system in the dilute regime, we have Equation 14.

$$\Psi_i = \int_0^{f_i^0} n_i^0(t) d\ln(t) \quad 9$$

$$= \int_0^{p_i^0} n_i^0(t) d\ln(t) \quad 10$$

$$= \int_0^{p_i^0} \frac{n_i^0(p)}{p} dp \quad 11$$

$$= \int_0^{p_i^0} \frac{H_i p}{p} dp \quad 12$$

$$= \int_0^{p_i^0} H_i dp \quad 13$$

$$= H_i p_i^0 \quad 14$$

In equilibrium, the grand potential of each phase is equal, so that for our example Equations 15 and 16 describe the binary system in equilibrium.

$$H_1 p_1^0 = H_2 p_2^0 \quad 15$$

$$\frac{p_1^0}{p_2^0} = \frac{H_2}{H_1} \quad 16$$

To find the adsorption selectivity, Equation 18 is used. In this equation, x_i is given by Equation 17.

$$x_1 = \frac{P_{tot} y_1}{P_1} \quad 17$$

$$s_{1-2} = \frac{x_1/x_2}{y_1/y_2} \quad 18$$

Combining Equations 16, 17, and 18, for our system (two components in the dilute regime) we find that selectivity is simply the ratio of the Henry constants.

$$s_{1-2} = \frac{H_1}{H_2} \quad 19$$

Thus for any system where IAST applies, we can expect to find that the selectivity calculated at low pressures is simply the ratio of the Henry constants of the two competing species.

REFERENCES

1. Marshall, J.; Bird, A. C., A comparative histopathological study of argon and krypton laser irradiations of the human retina. *Br. J. Ophthalmol.* **1979**, *63* (10), 657-668.
2. Fraissard, J.; Ito, T., Xe-129 NMR study of adsorbed xenon: A new method for studying zeolites and metal-zeolites. *Zeolites* **1988**, *8* (5), 350-361.
3. Cullen, S. C.; Gross, E. G., The Anesthetic Properties of Xenon in Animals and Human Beings, with Additional Observations on Krypton. *Science* **1951**, *113* (2942), 580-582.
4. Bazan, R. E.; Bastos-Neto, M.; Moeller, A.; Dreisbach, F.; Staudt, R., Adsorption equilibria of O₂, Ar, Kr and Xe on activated carbon and zeolites: single component and mixture data. *Adsorpt.-J. Int. Adsorpt. Soc.* **2011**, *17* (2), 371-383.
5. (a) Reid, C. R.; Thomas, K. M., Adsorption Kinetics and Size Exclusion Properties of Probe Molecules for the Selective Porosity in a Carbon Molecular Sieve Used for Air Separation. *The Journal of Physical Chemistry B* **2001**, *105* (43), 10619-10629; (b) Reid, C. R.; O'Koye, I. P.; Thomas, K. M., Adsorption of gases on carbon molecular sieves used for air separation. Spherical adsorptives as probes for kinetic selectivity. *Langmuir* **1998**, *14* (9), 2415-2425.
6. (a) Ravikovitch, P. I.; Vishnyakov, A.; Russo, R.; Neimark, A. V., Unified approach to pore size characterization of microporous carbonaceous materials from N₂, Ar, and CO₂ adsorption isotherms. *Langmuir* **2000**, *16* (5), 2311-2320; (b) Groen, J. C.; Peffer, L. A. A.; Perez-Ramirez, J., Pore size determination in modified micro- and mesoporous materials. Pitfalls and limitations in gas adsorption data analysis. *Microporous Mesoporous Mat.* **2003**, *60* (1-3), 1-17; (c) Kruk, M.; Jaroniec, M., Determination of mesopore size distributions from argon adsorption data at 77 K. *J. Phys. Chem. B* **2002**, *106* (18), 4732-4739; (d) Kruk, M.; Jaroniec, M., Gas adsorption characterization of ordered organic-inorganic nanocomposite materials. *Chem. Mat.* **2001**, *13* (10), 3169-3183.
7. Saito, A.; Foley, H. C., Curvature and Parametric Sensitivity in Models for Adsorption in Micropores. *Aiche J.* **1991**, *37* (3), 429-436.
8. Munakata, K.; Fukumatsu, T.; Yamatsuki, S.; Tanaka, K.; Nishikawa, M., Adsorption equilibria of krypton, xenon, nitrogen and their mixtures on molecular sieve 5A and activated charcoal. *J. Nucl. Sci. Technol.* **1999**, *36* (9), 818-829.
9. Ianovski, D.; Munakata, K.; Kanjo, S.; Yokoyama, Y.; Koga, A.; Yamatsuki, S.; Tanaka, K.; Fukumatsu, T.; Nishikawa, M.; Igarashi, Y., Adsorption of noble gases on H-mordenite. *J. Nucl. Sci. Technol.* **2002**, *39* (11), 1213-1218.
10. Underhill, D. W., The adsorption of argon, krypton and xenon on activated charcoal. *Health Physics* **1996**, *71* (2), 160-166.
11. Koh, K.; Wong-Foy, A. G.; Matzger, A. J., A Porous Coordination Copolymer with over 5000 m²/g BET Surface Area. *Journal of the American Chemical Society* **2009**, *131* (12), 4184-4185.
12. Greathouse, J. A.; Kinnibrugh, T. L.; Allendorf, M. D., Adsorption and Separation of Noble Gases by IRMOF-1: Grand Canonical Monte Carlo Simulations. *Industrial & Engineering Chemistry Research* **2009**, *48* (7), 3425-3431.
13. (a) Keskin, S.; Van Heest, T. M.; Sholl, D. S., Can Metal-Organic Framework Materials Play a Useful Role in Large-Scale Carbon Dioxide Separations? *Chemsuschem* **2010**, *3* (8), 879-891; (b) Mueller, U.; Schubert, M.; Teich, F.; Puetter, H.; Schierle-Arndt, K.; Pastre, J., Metal-organic frameworks - prospective industrial applications. *Journal of Materials Chemistry* **2006**, *16* (7), 626-636; (c) Czaja, A. U.; Trukhan, N.; Muller, U., Industrial applications of metal-organic frameworks. *Chemical Society Reviews* **2009**, *38* (5), 1284-1293.
14. Park, K. S.; Ni, Z.; Cote, A. P.; Choi, J. Y.; Huang, R. D.; Uribe-Romo, F. J.; Chae, H. K.; O'Keeffe, M.; Yaghi, O. M., Exceptional chemical and thermal stability of zeolitic

imidazolate frameworks. *Proceedings of the National Academy of Sciences of the United States of America* **2006**, *103* (27), 10186-10191.

15. Low, J. J.; Benin, A. I.; Jakubczak, P.; Abrahamian, J. F.; Faheem, S. A.; Willis, R. R., Virtual High Throughput Screening Confirmed Experimentally: Porous Coordination Polymer Hydration. *Journal of the American Chemical Society* **2009**, *131* (43), 15834-15842.
16. Muller, U.; Hesse, M.; Putter, H.; Kamieth, M.; Schierle-Arndt, K. Adsorptive production of xenon from krypton/xenon gas mixture. 7/13/2006, 2006.
17. Ryan, P.; Farha, O. K.; Broadbelt, L. J.; Snurr, R. Q., Computational screening of metal-organic frameworks for xenon/krypton separation. *Aiche J.* **2010**.
18. Friskney, C. A.; Turnbull, J. A., The characteristics of fission gas release from uranium dioxide during irradiation. *Journal of Nuclear Materials* **1979**, *79* (1), 184-198.
19. Jameson, C. J.; Jameson, A. K.; Lim, H.-M., Competitive adsorption of xenon and krypton in zeolite NaA: ¹²⁹Xe nuclear magnetic resonance studies and grand canonical Monte Carlo simulations. *The Journal of Chemical Physics* **1997**, *107* (11), 4364-4372.
20. Thallapally, P. K.; Grate, J. W.; Motkuri, R. K., Facile xenon capture and release at room temperature using a metal-organic framework: a comparison with activated charcoal. *Chem. Commun.* **2012**, *48* (3), 347-349.
21. Frenkel, D.; Smit, B., *Understanding Molecular Simulation: From Algorithms to Applications*. 2 ed.; Academic Press: 2002; Vol. 1, p 664.
22. Pellenq, R. J. M.; Nicholson, D., Intermolecular Potential Function for the Physical Adsorption of Rare Gases in Silicalite. *Journal of Physical Chemistry* **1994**, *98* (50), 13339-13349.
23. J.J. v. L., On the thermophysical properties of liquid radon-222. *Physica B+C* **1981**, *103* (2-3), 362-364.
24. Rappe, A. K.; Casewit, C. J.; Colwell, K. S.; Goddard, W. A.; Skiff, W. M., UFF, a full periodic table force field for molecular mechanics and molecular dynamics simulations. *Journal of the American Chemical Society* **1992**, *114* (25), 10024-10035.
25. Skoulidas, A. I.; Sholl, D. S., Transport diffusivities of CH₄, CF₄, He, Ne, Ar, Xe, and SF₆ in silicalite from atomistic simulations. *J. Phys. Chem. B* **2002**, *106* (19), 5058-5067.
26. Haldoupis, E.; Nair, S.; Sholl, D. S., Efficient Calculation of Diffusion Limitations in Metal Organic Framework Materials: A Tool for Identifying Materials for Kinetic Separations. *Journal of the American Chemical Society* **2010**, *132* (21), 7528-7539.
27. Allen, F., The Cambridge Structural Database: a quarter of a million crystal structures and rising. *Acta Crystallographica Section B* **2002**, *58* (3 Part 1), 380-388.
28. Goodbody, S. J.; Watanabe, K.; MacGowan, D.; Walton, J. P. R. B.; Quirke, N., Molecular simulation of methane and butane in silicalite. *Journal of the Chemical Society, Faraday Transactions* **1991**, *87* (13), 1951-1958.
29. Keskin, S.; Sholl, D. S., Efficient Methods for Screening of Metal Organic Framework Membranes for Gas Separations Using Atomically Detailed Models. *Langmuir* **2009**, *25* (19), 11786-11795.
30. (a) Sholl, D.; Nair, S.; Hesketh, P., Unlocking the Potential of MOFs as Membranes using Coupled Modeling and Experiments National Science Foundation: Georgia Institute of Technology, Atlanta GA, 30332-0100 2009; pp 1-27; (b) Keskin, S. Accelerating development of metal organic framework membranes using atomically detailed simulations. Georgia Institute of Technology, Atlanta, 2009; (c) Adams, R.; Carson, C.; Ward, J.; Tannenbaum, R.; Koros, W., Metal organic framework mixed matrix membranes for gas separations. *Microporous Mesoporous Mat.* **2010**, *131* (1-3), 13-20.
31. Keskin, S.; Liu, J. C.; Johnson, J. K.; Sholl, D. S., Atomically detailed models of gas mixture diffusion through CuBTC membranes. *Microporous Mesoporous Mat.* **2009**, *125* (1-2), 101-106.

32. Sholl, D. S., Understanding macroscopic diffusion of adsorbed molecules in crystalline nanoporous materials via atomistic simulations. *Accounts of Chemical Research* **2006**, *39* (6), 403-411.
33. van Santen, R. A.; de Bruyn, D. P.; den Ouden, C. J. J.; Smit, B., Chapter 9 Introduction to Zeolite Theory and Modelling. In *Studies in Surface Science and Catalysis*, H. van Bekkum, E. M. F.; Jansen, J. C., Eds. Elsevier: 1991; Vol. Volume 58, pp 317-358.
34. Pan, Y.; Lai, Z., Sharp separation of C₂/C₃ hydrocarbon mixtures by zeolitic imidazolate framework-8 (ZIF-8) membranes synthesized in aqueous solutions. *Chem. Commun.* **2011**, *47* (37), 10275-10277.
35. Myers, A. L.; Prausnitz, J. M., Thermodynamics of Mixed-Gas Adsorption. *Aiche J.* **1965**, *11* (1), 121-127.
36. (a) Yang, Q. Y.; Zhong, C. L., Molecular simulation of carbon dioxide/methane/hydrogen mixture adsorption in metal-organic frameworks. *J. Phys. Chem. B* **2006**, *110* (36), 17776-17783; (b) Murthi, M.; Snurr, R. Q., Effects of Molecular Siting and Adsorbent Heterogeneity on the Ideality of Adsorption Equilibria. *Langmuir* **2004**, *20* (6), 2489-2497; (c) Babarao, R.; Hu, Z. Q.; Jiang, J. W.; Chempath, S.; Sandler, S. I., Storage and separation of CO₂ and CH₄ in silicalite, C-168 schwarzite, and IRMOF-1: A comparative study from Monte Carlo simulation. *Langmuir* **2007**, *23* (2), 659-666; (d) Chen, H.; Sholl, D. S., Examining the Accuracy of Ideal Adsorbed Solution Theory without Curve-Fitting Using Transition Matrix Monte Carlo Simulations. *Langmuir* **2007**, *23* (11), 6431-6437; (e) Keskin, S.; Liu, J. C.; Johnson, J. K.; Sholl, D. S., Testing the accuracy of correlations for multicomponent mass transport of adsorbed gases in metal-organic frameworks: Diffusion of H₂/CH₄ mixtures in CuBTC. *Langmuir* **2008**, *24* (15), 8254-8261; (f) Jorge, M.; Lamia, N.; Rodrigues, A. E., Molecular simulation of propane/propylene separation on the metal-organic framework CuBTC. *Colloid Surf. A-Physicochem. Eng. Asp.* **2010**, *357* (1-3), 27-34; (g) Liu, B.; Smit, B., Molecular Simulation Studies of Separation of CO₂/N₂, CO₂/CH₄, and CH₄/N₂ by ZIFs. *The Journal of Physical Chemistry C* **2010**, *114* (18), 8515-8522; (h) Bae, Y. S.; Mulfort, K. L.; Frost, H.; Ryan, P.; Punnathanam, S.; Broadbelt, L. J.; Hupp, J. T.; Snurr, R. Q., Separation of CO₂ from CH₄ using mixed-ligand metal-organic frameworks. *Langmuir* **2008**, *24* (16), 8592-8598.
37. Chen, H. B.; Sholl, D. S., Efficient simulation of binary adsorption isotherms using transition matrix Monte Carlo. *Langmuir* **2006**, *22* (2), 709-716.
38. Challa, S. R.; Sholl, D. S.; Johnson, J. K., Adsorption and separation of hydrogen isotopes in carbon nanotubes: Multicomponent grand canonical Monte Carlo simulations. *Journal of Chemical Physics* **2002**, *116* (2), 814-824.
39. Press, W., *Numerical recipes : the art of scientific computing*. Cambridge University Press: 2007.
40. Jee, S. E.; Sholl, D. S., Carbon Dioxide and Methane Transport in DDR Zeolite: Insights from Molecular Simulations into Carbon Dioxide Separations in Small Pore Zeolites. *Journal of the American Chemical Society* **2009**, *131* (22), 7896-7904.
41. Düren, T.; Millange, F.; Férey, G.; Walton, K. S.; Snurr, R. Q., Calculating Geometric Surface Areas as a Characterization Tool for Metal-Organic Frameworks. *The Journal of Physical Chemistry C* **2007**, *111* (42), 15350-15356.
42. Walton, K. S.; Snurr, R. Q., Applicability of the BET method for determining surface areas of microporous metal-organic frameworks. *Journal of the American Chemical Society* **2007**, *129* (27), 8552-8556.
43. Erdem-Şenatalar, A.; Tatlier, M., Effects of fractality on the accessible surface area values of zeolite adsorbents. *Chaos, Solitons & Fractals* **2000**, *11* (6), 953-960.
44. Avnir, D.; Farin, D.; Pfeifer, P., Chemistry in noninteger dimensions between two and three. II. Fractal surfaces of adsorbents. *The Journal of Chemical Physics* **1983**, *79* (7), 3566-3571.

45. Tynan, E.; Jensen, P.; Kruger, P. E.; Lees, A. C., Solvent templated synthesis of metal-organic frameworks: structural characterisation and properties of the 3D network isomers $\{[\text{Mn}(\text{dcbp})] \cdot \frac{1}{2}\text{DMF}\}_n$ and $\{[\text{Mn}(\text{dcbp})] \cdot 2\text{H}_2\text{O}\}_n$. *Chem. Commun.* **2004**, (7), 776-777.
46. Wilmer, C. E.; Leaf, M.; Lee, C. Y.; Farha, O. K.; Hauser, B. G.; Hupp, J. T.; Snurr, R. Q., Large-scale screening of hypothetical metal-organic frameworks. *Nat Chem* **2012**, 4 (2), 83-89.